ABSTRACT

LIU, HUIQING. Analysis and modeling of wave-current interaction. (Under the direction of Dr. Lian Xie).

The main task of this study focuses on studying the effect of wave-current interaction on currents, storm surge and inundation as well as effects of depth-induced wave breaking, wind field and current on waves by using numerical models. The results show that it is important to incorporate the wave-current interaction effect into coastal circulation, storm surge and inundation models. At the same time, it should consider effects of depth-induced wave breaking, wind field, currents and sea surface elevation in prediction of waves. Specially, we found that: **(1)** Depth-induced wave breaking plays an important role in wave field in shallow water areas and resolution may also impact the wave field structure. **(2)** The asymmetric structure of the wind induced wave field is created not only by the asymmetric structure of the hurricane wind field, but also by the variations in the translation speed or non-zero accelerations, of a particular hurricane. With an increasing translation speed, the significant wave height (SWH) in the front-right quadrant of the wave field increases. The results further indicate that when the translation speed reaches and passes an intrinsic critical value, the SWH in the front-right quadrant begins to decrease, while increasing in the rear-right quadrant. However, the total contribution of the hurricane translation speed to the asymmetric structure of the wave field also depends on the intensity of the hurricane. As the intensity of the hurricane wind field increases, the influence of the translation speed on the asymmetric structure of the wave field is found to decrease. Most hurricane wind models are parametric and can only generate symmetric hurricanes and consider no any background wind fields, however, actual hurricanes in nature are not symmetric and contain

environmental wind field effects. Thus, to more properly model the hurricane induced wave field, it is important to consider the asymmetric structure of the hurricane wind field, the changes in the hurricane translation time history, and the incorporation background wind field into hurricane wind field. **(3)** For SWH, it will be decreased when waves propagate in the following current direction. On the other hand, current will increase the SWH when waves propagate countercurrent direction. The effect of current on wave propagation is relative complex. The dominating mechanism affecting wave propagation direction is current (Gulf Stream) induced refraction. Depending on wind direction, it may trap some local generated waves or reflect some wave energy to open ocean. All of these mechanisms may change wave propagation direction when waves cross Gulf Stream. Therefore the change of wave propagation direction after crossing Gulf Stream depends not only on refraction, but also on others. **(4)** It is important to introduce wave-current effects into any storm surge and inundation prediction modeling system. Specially, the consideration of wave-induced wind stress, bottom shear stress, and 3-D radiation stress in storm surge and inundation modeling can significantly improve the correctness of the prediction.

Analysis and modeling of wave-current interaction

By

Huiqing Liu

A dissertation submitted to the Graduate Faculty of

North Carolina State University

In partial fulfillment of the

Requirements for the degree of

Doctor of Philosophy

Marine, Earth and Atmospheric Sciences

Raleigh, NC

2006

Approved by:

Dr. Leonard J. Pietrafesa	Dr. John M. Morrison
Dr. Gerald S. Janowitz	Dr. Lian Xie (Chair Advisory Committee)

DEDICATION

To my wife, Yao Liu. Without her love, encouragement and support, I couldn't have completed this dissertation and faced this challenge.

BIOGRAPHY

Huiqing Liu was born on the 11th of May, 1976, in AnQiu a city of Shandong province. In 1995, he was enrolled to Ocean University of Qingdao (now called Ocean University of China), where he spent seven years in the Department of Oceanography and graduated with a BS degree in 1999 and a MS degree in 2002. He joined the Department of Marine, Earth and Atmospheric Sciences of North Carolina State University in fall 2002 as a graduate student pursuing a PhD.

ACKNOWLEDGMENTS

I got much help from many great people during this work. Here, I wish to acknowledge these great people, without their help, this dissertation would not have been possible. First, I wish to express my extreme gratefulness to my advisor Dr. Lian Xie, whose knowledge, guidance and kindness gave me much help throughout my time at NCSU. His encouragement and patience led me step-by-step to complete this work. I also acknowledge the other committee members: Dr. Pietrafesa, Dr. Morrison and Dr. Janowitz for their assistance and comments to this study.

I also would like to thank my friends in the Coastal Fluid Dynamics Laboratory: Dr. Machuan Peng, Dr. Shaowu Bao, Dr. Shiqiu Peng, Dr. Tingzhuang Yan, Dr. Xiaoming Liu, Dr. Binyu Wang, Dr. Kristen Foley, Xuejin zhang, Meng, Xia and Yanyun Liu for their help and suggestions in this study. Many thanks are also given to Bob Bright, Joshua Palmer, Mike Lin and Sondra Artis for their help in my English pronunciation and writing skills.

I would also like to say thank you to my parents, Xinai Zhang and Junming Liu, and my brothers, Huidong Liu and Huisheng Liu, for your tremendous love and financial support throughout my life.

This study is supported by the Carolina Coastal Ocean Observation and Prediction System (Caro-Coops) project under NOAA Grant No. NA16RP2543 via the National Ocean Service, through Charleston Coastal Services Center. Caro-COOPS is a partnership between the University of South Carolina and North Carolina State University.

TABLE OF CONTENTS

6. FINAL REMARKS

LIST OF TABLES

LIST OF FIGURES

CHAPTER 1. INTRODUCTION

1.1 Scientific Background

Wind-generated waves are the prime energy supplier to the nearshore area, generating currents and transporting sediments, so shaping our coasts. It is logical therefore that they are a prime subject of research in physical oceanography and coastal engineering, which has led to significant advances in understanding as well as modeling capability. Prediction of wind waves in extensive areas such as oceans and shelf seas is only practically feasible in a phase-averaged sense. This has led to numerical models based on the spectral wave energy balance, with linear propagation and a set of source terms accounting for wind input, cross-spectral transfer and dissipation. The archetype model in this category is WAM [WAMDI Group, 1988; see also Komen *et al*., 1994], primarily developed for deep water, with some allowances for restricted depth. WAVEWATCH (WW) [Tolman, 1991] is a similar model, while the model SWAN, based on the same principles, is designed especially for shallow coastal regions [Booij *et al*., 1999]. The prediction skill of these models has been demonstrated in many experimental exercises. Generally the skill of wave prediction is mainly determined by wind field input as well as boundary condition, current condition and topography (depth-induced breaking). For example, when waves encounter a strong current (e.g. Gulf Stream), the changes of wave height and direction induced by current will be significant, and wind is the principal source of energy creating and driving waves. Therefore it is important to study effects of these factors on waves in order to improve the wave prediction.

Wind waves, storm surges and ocean circulation are important, mutually interacting physical processes in coastal waters. Over the past two decades, there have been a number of studies focusing on wave-current interactions [Tolman, 1990, Zhang and Li 1996, Xie et al. 2001, 2003]. It is believed that wind waves can indirectly affect the coastal ocean circulation by enhancing the wind stress [Mastenbroek et al., 1993] and by influencing the bed friction coefficients [Signell et al., 1990, Davies and Lawrence, 1995]. Xie et al. [2001, 2003] studied wave-current interactions through surface and bottom stresses and found that wind waves can play a significant role in the overall circulation in coastal regions.

The key questions here must address how these processes affect one another and how these processes can be properly coupled in numerical models. In general, these processes influence one another in several ways: (1) wind stress, which is changed by incorporating the wave effect [Donelan et al., 1993]; (2) radiation stress, which is considered to be an additional mechanical force in storm surge models [Xie et al., 2001, Mellor, 2003, Xia et al., 2004] and can be incorporated into wave models by invoking wave-action conservation [Komen et al., 1994, Lin and Huang, 1996]; (3) bottom stress, which is a function of wave-current interaction in the near bottom layer when the water depth is sufficiently shallow for wave effects to penetrate to the bottom [Signell et al., 1990]; (4) the depth variation and current conditions, which are inputted into wave models [Tolman, 1991]; (5) the Stokes' drift current induced by the non-linearity of surface waves [Huang, 1979]; and (6) wave run-up, which has an impact on storm surge and inundation prediction [Holman et al., 1985 and 1986, Hedges, 2004].

Because of the importance of these interactions, there have been several studies which have attempted to incorporate these separate but important and linked effects into coupled models. Tolman [1991] described the effects of astronomical tides and storm surges on wave modeling via the consideration of unsteady currents and varying topography. Tolman's results suggest that the effects of tides and storm surges should be considered in modeling physical waves in shelf seas. Tolman's insightful study assumed one-way coupling and did not consider the effect of wind waves on storm surge. Signell et al. [1990] studied the effect of waves on bottom shear stress and Davies and Lawrence [1995] showed that wind waves could play an important role in determining surface and near bottom currents as well as on water level variations over and along a coastal region. In the Signell et al and Davies and Lawrence studies, surface waves were considered to be a constant external input into the current model, a one-way coupling.

Xie et al. [2001, 2003] investigated the dynamic coupling between waves and currents and found that it was important to incorporate the surface wave effects into coastal circulation and storm surge modeling. The results of their study showed an improved storm surge prediction capability. However, they did not consider depth variations in their wave model, which limited the more complete application of their results. Moon [2005] also developed a wave-tide-circulation coupled system, in which the effects of wave-current interactions on surface stress, a wave breaking parameterization, and depth variations in their wave model were included. However, the effects of wave-current interaction on the bottom shear stress were not included. Moreover, all of the above mentioned storm surge models did not include the three-dimensional radiation stress in their coupled system [Mellor, 2003, Xia

et al., 2004] and did not include inundation as part of their storm surge model architecture. Flooding caused by coastal storms is an occasional threat to people living in coastal regions. So it is important to investigate the effect of wave-current interaction on coastal atmospheric storm induced storm surge and inundation.

1.2 Purposes of the Study

Ocean waves play an important role in the transfer of momentum and energy across the air-sea interface and strongly impact current, storm surge and coastal inundation flooding. Specifically, waves generated by hurricanes are relatively large and can easily reach 10-20 meters or even larger in sufficiently deep open ocean waters. Although the waves reduce their SWH when they reach the shallow water areas, they can still significantly impact the coastal zone. High waves can create hazardous conditions including debris overwash, flooding, erosion, high wave energy and turbulence in the nearshore zone, and strong currents. It is well known that hurricane waves are one of the most damaging phenomena during the passages of hurricanes. Severe wave conditions are dangerous to vessels in ocean and coastal waters, and waves can also run up over the storm surge in the coastal zone to cause more severe damage along and on the coast, for example it can overwash coastal roads and properties. So the ability to predict hurricane waves precisely is a very important challenge and is of great value to many user communities.

To predict hurricane waves, you have to quantify the sensitivity of waves to several factors, e.g. to depth-induced wave breaking (special in coastal areas), to currents and

hurricane wind fields. In order to address this issue, a suite of study topics are designed to quantify the influence of: 1) depth-induced refraction-diffraction, wave breaking and spatial resolution; 2) major western currents (e.g. Gulf Stream); 3) wind distribution, storm translation speed and intensity on ocean surface wind waves using SWAN.

As shown in the first section of this chapter and previous studies, wind waves have an important role in storm surges, inundation and ocean circulation in coastal waters. Generally, surface waves and currents influence one another in several ways: 1) wind stress, which is a function of the drag coefficient which is strongly tied to wave parameters [Donelan et al., 1993]; 2) the radiation stress, which is considered to be an additional mechanical force in storm surge models [Xie et al., 2001, Mellor, 2003, Xia et al., 2004] can be incorporated into wave models by invoking wave-action conservation [Komen et al., 1994]; 3) the bottom stress, which is a function of wave-current interaction in the near bottom layer when the water depth is sufficiently shallow for wave effects to penetrate to the bottom [Signell et al., 1990]; 4) water depth variation and current conditions, which are input parameters for the wave models [Tolman, 1991]; 5) the Stokes' drift current induced by the non-linearity of surface waves [Huang, 1979]; and 6) wave run-up, which impacts storm surge and inundation prediction [Holman et al., 1985 and 1986].

Therefore, we will develop a three-dimensional (3-D) wave-current dynamic coupled modeling system, including the effect of wave-current interaction on storm surge and inundation induced by coastal atmospheric storms via the inclusions of wave-dependent

surface wind stress, wave-current-dependent bottom shear stress, and time-dependent sea surface elevation in the wave model, and three-dimensional radiation stress.

1.3 Organization of dissertation

Investigation of depth-induced refraction-diffraction, wave breaking and nesting impacts on waves using SWAN are given in chapter 2. Chapter 3 introduces a numerical study on the effect of the GULF STREAM on waves. Sensitivity of near-shore wind waves to hurricane wind asymmetry and translation speed are investigated in chapter 4. The effect of wave-current interactions on the storm surge and inundation in CHARLESTON harbor during hurricane HUGO 1989 are presented in chapter 5. Finally, chapter 6 gives the final remarks.

CHAPTER 2. INVESTIGATION OF DEPTH-INDUCED REFRACTION-DIFFRACTION, WAVE BREAKING AND NESTING IMPACTS ON WAVES USING SWAN

2.1. Introduction

Simulation WAves Nearshore (SWAN) [Booij et al. 1999] and WAVEWATCH-III [Tolman, 2002] are the third-generation wave models, which solve the spectral action balance equation without prior assumption of spectral shape. The prediction skill of these models has been demonstrated in many experimental cases [Ris et al., 1999, Rogers et al., 2003, Hsu et al., 2005, Zijlema and Westhuysen, 2005, Tolman, 1991]. There are many factors that affect their performance in prediction, e.g. spatial resolution, dissipation and wind fields. Especially in coastal areas, depth-induced refraction-diffraction and wave breaking is important for wave prediction due to shoaling effect. In simulating hurricane induced waves, wave models frequently yield inordinately high values of wave heights in shoal areas if wave breaking effect is not taken into account in models. This is also one of driving forces to develop SWAN wave model. The main purpose of developing SWAN model is to obtain realistic estimates of wave parameters in coastal areas, lakes and estuaries from given wind, bottom and current conditions [SWAN Group, 2003]. Hence, the depth-induced refraction-diffraction [Holthuijsen et al., 2003], wave breaking [Booij et al. 1999] and nesting mechanism are all incorporated into SWAN model. The main focus of this chapter is to test these effects on waves in coastal areas by using SWAN model in order to

determine in which domain depth-induced refraction-diffraction should be considered, in which domain depth-induced wave breaking should be activated and in which domain fine grids should be selected; whereas some domain coarse grids could be ok.

Many studies have been focused on the wave breaking effect, e.g. Battjes and Janssen [1978] presented a wave breaking dissipation approach, in which the local mean rate of energy dissipation is modeled. The results of their models indicated a good agreement with field experiments. The calibration and verification of their model was conducted by Battjes and Stive [1985] using both laboratory and field data. Massel and Gourlay [2000] developed a model which predicted wave transformation and wave-induced set up on coral reefs. Two energy dissipation mechanisms had been incorporated into that model, i.e., wave breaking and bottom friction. Considering waves on shallow foreshores are subject to depth-induced breaking, Battjes and Groenendijk [2000] proposed a Composite Weibull distribution to describe the wave height distributions on shallow foreshores. Zhao, et al. [2000] developed a two-dimensional wave model which included wave breaking effects to simulate three cases. The results showed that wave height in the nearshore areas was higher obtained from Non-wave breaking than wave breaking results. As the wave breaking is one of important dissipation aspects in shallow water areas, it suggests that switching off the depth-induced breaking term is usually unwise, since that leads to unacceptably high wave heights (the computed wave heights ‘explode’ due to shoaling effects) [SWAN user manual]. At the same time, waves may be refracted and diffracted due to the presence of shoals and channels or obstacles such as islands, headlands, or break waters when they approaching a coastline [Holthuijsen et al., 2003]. Hence, it is also important to incorporate the diffraction effect into

numerical model in order to obtain realistic simulating results around coastal areas. The widely used methods accounting for diffraction effect in models are mild-slope model [Berkhoff, 1972, Ito and Tanimoto, 1972, Gao and Radder, 1998] and Bossinesq model [Madsen and Sørensen, 1992, Li and Zhan, 2001]. In SWAN model, the effects of refraction and diffraction are readily accounted by adding the diffraction-induced turning rate of the waves (obtained from mild-slope equation) to model.

So far, there are few studies which focus on investigating the effect of wave breaking dissipation on waves induced by a Hurricane, and few studies focus on examining the conditions controlling this effect on waves, i.e., did wave breaking effect play the same role on waves throughout the domain? In this chapter, we will discuss the wave breaking how to affect the wave height during hurricane passing the domain, test the effect of depth-induced refraction-diffraction incorporated into SWAN and examine the spatial resolution effect on wave field using nesting method. SWAN and WAVEWATCH-III wave models were used to simulate several real hurricane cases in our experiment in order to investigate the depth-induced wave breaking and spatial resolution impacts on waves, in which the hurricane fields were simulated by Holland hurricane model [Holland, 1980]. At the same time, several ideal experiments were conducted to examine the impacts of depth-induced refraction-diffraction presented in SWAN on waves. Wave models and hurricane model employed in this chapter are described in section 2.2. Section 2.3 introduces ideal and real hurricane experiments, model domains and buoy data stations used in this chapter. Section 2.4 provides experiment results that include ideal experiments (refraction and diffraction effect) and real hurricane

cases (wave breaking and nesting effect). Discussions and summary are presented in section 2.5.

2.2. Models description

2.2.1 SWAN

The model is based on the wave action balance equation (or energy balance in the absence of currents) with sources and sinks. In SWAN the evolution of the wave spectrum is described by the spectral action balance equation which for Cartesian coordinates is (e.g., Hasselmann et al., 1973):

$$\frac{\partial}{\partial t}N+\frac{\partial}{\partial x}C_x N+\frac{\partial}{\partial y}C_y N+\frac{\partial}{\partial \sigma}C_\sigma N+\frac{\partial}{\partial \theta}C_\theta N=\frac{S}{\sigma} \tag{2.1}$$

Where N is the action density ($N(\sigma, \theta) = E(\sigma, \theta) / \sigma$), E is the energy density spectrum and σ is the relative frequency. C_x, C_y and C_σ are propagation velocity in x-, y-, σ- and θ-space respectively. S is the source term that represents the effects of generation, dissipation and nonlinear wave-wave interactions. The governing equation is expressed in spherical coordinates is:

$$\frac{\partial}{\partial t}N+\frac{\partial}{\partial \lambda}C_\lambda N+(\cos\varphi)^{-1}\frac{\partial}{\partial \varphi}C_\varphi \cos\varphi N+\frac{\partial}{\partial \sigma}C_\sigma N+\frac{\partial}{\partial \theta}C_\theta N=\frac{S}{\sigma} \tag{2.2}$$

Where λ and φ represent longitude latitude respectively.

Depth-induced wave breaking has been considered in SWAN, which is expressed by the following formula in the source term:

$$D_{tot} = -\frac{1}{4}\alpha_{BJ} Q_b (\frac{\overline{\sigma}}{2\pi}) H_m^2$$

in wich $\alpha_{BJ} = 1$ and D_{tot} is the mean rate of energy dissipation per unit horizontal area due to wave breaking. It is based on the bore-based model of Battjes and Janssen [1978]. Q_b is the fraction of breaking waves determined by: $\frac{1-Q_b}{\ln Q_b} = -8\frac{E_{tot}}{H_m^2}$ in wich H_m is the maximum wave height that can exit at the given depth.

2.2.2 WAVEWATCH-III

WAVEWATCH-III was developed at the Marine Modeling and Analysis Branch (MMAB) of the Environmental Modeling Center (EMC) of the National Centers for Environmental Prediction (NCEP) [Tolman, 2002] in the spirit of the WAM [WAMDI group, 1998]. It is the operational ocean wave predictions model of NOAA/NCEP, in which the data assimilation is included. WAVEWATCH-III solves the spectral action density balance equation for wave number-direction spectra. The implicit assumption of this equation is that properties of medium (water depth and current) as well as the wave field itself vary on time and space scales that are much larger than the variation scales of a single wave. (http://polar.ncep.noaa.gov/waves/wavewatch/wavewatch.html) The governing equation is:

$$\frac{\partial N}{\partial t} + \nabla_x \bullet \dot{x} N + \frac{\partial}{\partial k}\dot{k} N + \frac{\partial}{\partial \theta}\dot{\theta} N = \frac{S}{\sigma} \tag{2.3}$$

$$\dot{x} = C_g + U \tag{2.4}$$

$$\dot{k} = -\frac{\partial \sigma}{\partial d}\frac{\partial d}{\partial s} - k \bullet \frac{\partial U}{\partial s} \tag{2.5}$$

$$\dot{\theta} = -\frac{1}{k}\left[\frac{\partial \sigma}{\partial d}\frac{\partial d}{\partial m} - k \bullet \frac{\partial U}{\partial m}\right] \tag{2.6}$$

K and θ are wave number and propagation direction, respectively. s is a coordinate in the direction θ and m is a coordinate perpendicular to s. The main difference between the two wave models is that parameterizations of physical processes included in WAVEWATCH-III model do not address conditions where the waves are strongly depth-limited.

2.2.3 Holland hurricane model

The wind speed is the function of radial distance from the center of the storm described as:

$$V = [AB(P_n - P_c)\exp(-A/r^B)/\rho_a r^B]^{1/2} \tag{2.7}$$

where V is wind speed at radius r, Pc is the central pressure of hurricane, P_n is the ambient pressure, ρ_a is the air density, A and B are constants. In which $P_n = 10^5$ Pa, $\rho_a = 1.2$ kg/m^3, B = 1.9 and A = $(R_{max})^B$. The value of $Rmax$ depends on the value of P_c.

2.3. Experiments and model setup

In order to examine the influence of depth-induced refraction-diffraction on waves, three ideal experiments (named case 1, 2 and 3) are conducted in this chapter. Only swell waves (avoid other effects except refraction-diffraction effect) propagate from deep water to coastal water in all of these ideal experiments. The set up of the swell waves for SWAN are: boundary condition is characterized with a Gaussian-shaped frequency energy spectrum;

width of the Gaussian frequency spectrum is 0.007 Hz; the significant wave height is 1.2 m; peak frequency is 0.071 Hz; peak wave direction is 15^0 or 45^0 in case 1 and 0^0 in case 2 and 3; the directional width is 12.4^0. All the angles used in this chapter are under Cartesian convention. The domain of these ideal experiments is 45 km in x direction and 15 km in y direction with 1 km grid size resolution of both directions. The water depth decreases from 50 m to 5 m in x direction and the water depth in y direction is uniform for case 1. There is a sub-water channel and ridge at the distance 21~26 km from coastline in case 2 and case 3 respectively. For case 2, the depth of channel is 50 meter. On the other hand, the water depth of ridge in case 3 is 8 meters.

Three real hurricane cases (Bonnie 1998, Dennis 1999 and Floyd 1999) are selected in this chapter to examine the effect of depth-induced wave breaking and the influence of spatial resolution on waves. The best tracks of these hurricanes are shown in **Fig. 2.1**. These tracks data is provided by Unisys Weather Hurricane/Tropical data center. **Figure 2.1** also describes the computational domain of these hurricane cases, which covers latitude from 25^o to 35^o north and longitude from 85^o to 70^o west. The bottom topography is derived from the ETOP5 bathymetry database. The resolution of both wave models is $1/5^o$ in both directions. The last information presented in **Fig. 2.1** is the distribution of buoy stations, in which data was used to compare with model results.

2.4. Results

2.4.1 The effect of depth-induced refraction-diffraction on waves

The effect of depth-induced refraction-diffraction plays an import role on waves propagating from deep water to shoaling water, especially when waves propagate into beach,

encounter sub-water channels or ridges. That is why these effects are incorporated into most wave models. In this section, several ideal experiments were conducted to investigate these processes represented in SWAN.

The results of the first ideal experiment (case 1) are illustrated in **Fig.** 2.2.1. In this case, swell waves propagate through a plane beach with a slope 10^{-3} in the depth range from 5 to 50 m. Two swell waves are considered in this case, one propagates with peak wave direction 45^0 and the other is 15^0. **Figure 2.2.1a** shows the variation of mean wave direction due to depth-induced refraction on the plane beach including model and analytical results. It indicates that depth refraction makes waves bend toward to the normal direction of beach (0^0) and shows a good agreement with the analytical results (symbols in **Fig. 2.2.1a**). The analytical results are calculated by using Snel's law:

$$\frac{\sin\theta}{c} = const, \qquad c = \frac{\sigma}{k} \tag{2.8}$$

Where θ is the wave direction, c is the wave phase speed, σ is the wave frequency and k is the wave number. The constant is determined from the (deep water) boundary conditions.

To illustrate the influences of depth-induced diffraction on waves, two cases (case 2 and case 3) have been considered. In case 2 (second ideal experiment), swell waves with peak wave direction 0 propagate from deep water to a plane beach (same as the first case) but with a sub-water channel. The setups of case 3 are the same as the second case except that there is a sub-water ridge not a channel in the beach. **Figure 2.2.2** presents the results of the second ideal experiments (case 2). This figure shows that diffraction-induced variations on mean wave direction (**Fig. 2.2.2a**) and wave height (**Fig. 2.2.2b**) are significant. **Figure 2.2.2a**

suggests that diffraction makes waves propagate closer to their original direction (reduced the effect of channel) during through and after passing the channel. Furthermore it increases the wave height of the back areas of channel (**Fig. 2.2.2b**). In **Fig. 2.2.3** the results of case 3 are presented. As the same anticipated, the modulation of wave propagation (**Fig. 2.2.3a)** and wave height (**Fig. 2.2.3b**) due to the diffraction is obvious. Whereas **Figure 2.2.2** and **Figure 2.2.3** indicate that the effects of diffraction are to enhance the energy penetrates into the areas behind the sub-water channel or ridge. In other words, the impacts of diffraction help reduce the influence induced by sub-water channel or ridge on waves.

2.4.2 The effect of depth-induced wave breaking on waves

To explore the depth-induced wave breaking and spatial effects on wave field, three real hurricane cases were selected as the forcing fields of SWAN and WAVEWATCH-III wave models. The best tracks of these hurricanes are shown in **Fig. 2.1** which includes Bonnie (1998), Dennis (1999) and Floyd (1999). Hurricane wind fields of each case was simulated by Holland hurricane model [Holland, 1980] and inputted into wave models. Wave fields induced by the same hurricane were simulated three times by the two wave models. The first two simulations were conducted by SWAN and the difference between them is that one switched on wave breaking term and the other switched off wave breaking term. And the last one was simulated by WAVEWATCH-III.

Figure 2.3-Figure 2.5 show the significant wave height (SWH) induced by hurricanes at different buoy stations for each hurricane case, e.g. significant wave height induced by

Bonnie are shown in **Fig. 2.3** including outputs of SWAN (switch on and off wave breaking term) and WAVEWATCH-III and observed buoy data. **Figure 2.4** and **Figure 2.5** display results of Dennis and Floyd hurricane case respectively. In view of these comparison, two wave model results display a good coincidence with buoy data no matter whether the wave breaking term on or off in SWAN at most of buoy stations for these three hurricane cases. However, it can be noted that the results of WAVEWATCH-III and SWAN (wave breaking term is off) are extremely higher than those of SWAN (including breaking term) and observed data in station **Fran Pan Shoals, NC** (**FPSN7)** for hurricane Bonnie and Floyd cases (**Fig. 2.3c and Fig. 2.5d**). The character of station **FPSN7** is that its position is 33.49N and 77.59W, which is very close to shore line, and its water depth is 20~21m. Therefore, the reason of why SWH simulated by SWAN (wave breaking term is off) and WAVEWATCH-III is poor may be that water depth of buoy station **FPSN7** is shallow enough to consider wave breaking dissipation. In other words, depth-induced wave breaking is an important dissipation mechanism in shallow water regions, which should be incorporated into wave models. Otherwise, numerical models would produce unrealistic results in these regions.

Whereas, the more interesting phenomenon is that the performances of WAVEWATCH-III and SWAN (no wave breaking term) at buoy station **FPSN7** are good for hurricane Dennis case compared to buoy data. The apparent difference among these three hurricane cases is the relative location of buoy station **FPSN7** to the best track of hurricane. It can be obviously noticed that the best track of hurricane Dennis passed through right of buoy station **FPSN7** (**Fig. 2.1**), however, buoy station **FPSN7** lies in the right area of the best tracks of hurricanes Bonnie and Floyd (**Fig. 2.1**). It implies that the SWH simulated by wave models

(depth-induced wave breaking no considered) at buoy station **FPSN7** will be extremely high when it lies in the right of the best track of hurricane, however, this phenomenon will be disappeared when buoy station **FPSN7** lies in the left of the best track of hurricane. Why? It is known that hurricane is a tropical cyclone system and its wind direction is shoreward at upper-right quadrant (along east coast of North Hemisphere). Therefore waves induced by the hurricane at this quadrant would propagate from deep water to coastal water. To the contrary, the hurricane wind direction is seaward and waves induced by the hurricane will propagate from coastal water to deep water at lower-left quadrant. It means that larger waves (SWH is high) will propagate from deep water to shallow water at the right areas of the best track of hurricane, whereas, small waves will propagate from shallow water to deep water at the left areas of the best track of hurricane. Therefore, it is obvious that the effect of depth-induced wave breaking would play a significant role in simulating waves at the right areas of the best track of hurricane and not have the same impact on waves at the left areas. To verify this explanation, an experiment had been conducted, in which the best track of Floyd was shifted to right by adding 1^{o} in west longitude named hurricane Floyd-fix for every point in order to make it pass on the right of **FPSN7**. **Figure 2.6** shows the positions of original and modified best track of Floyd (hereafter named Floyd-fix). All parameters of hurricane Floyd-fix are the same as the hurricane Floyd except the passage of the best track. The SWH induced by hurricane Floyd-fix at station **FPSN7** is presented in **Fig. 2.7**. The result indicates that there is no significantly difference between SWH simulated by SWAN (no wave breaking and including its effect) and WAVEWATCH-III. Hence, the above explanation is reasonable.

On the other hand, WAVEWATCH-III shows a better performance in station 41002 (water depth is about 3785 m) than SWAN does compared with buoy data, i.e. WAVEWATCH-III has a better performance in deep water areas than SWAN (**Fig. 2.3a, Fig. 2.4a and Fig. 2.5a**).

2.4.3 The effect of spatial resolution on waves

In order to investigate the impact of spatial resolution on wave fields, two nesting runs were conducted for the hurricane Floyd case. The first one was SWAN nested in SWAN itself run and the other one was SWAN nested in WAVEWATCH-III run. **Figure** 2.**8** shows the computational domain and the nesting windows: The outermost domain covers from 20^0 to 40^0 North and 85^0 to 60^0 West with resolution 12 minute. The mid domain is 28^0-35^0N, 82^0-70^0W with 4 minute as the spatial grid size. The inner most domain is 31^0-34^0N, 81.5^0-76.5^0W with resolution 2 minute. Time step for integration is 6 minutes. Number of frequencies of waves is 31 (0.04177~1.0 Hz) and directional resolution is 10^0 (0^0~360^0).

As was indicated in the previous section of this chapter, WAVEWATCH-III doesn't perform as well as SWAN wave model does in shallow water areas but does better in deep water (more efficient than SWAN). Hence, SWAN nested in WAVEWATCH-III run (first experiment) could be used to study the effect of boundary condition on waves, in which the mid domain and outermost domain were used. Except this experiment, SWAN nested in SWAN run was conducted in these three nesting domains to study the effect of spatial resolution on waves.

Same as the previous experiments, Hurricane Floyd was also simulated by Holland hurricane model [Holland, 1980] and Buoy data was employed to compare with model results. The results of the first nesting run are presented in **Fig. 2.9**. It shows that the significant wave height simulated in nesting run (SWAN nested in WAVEWATCH-III) is closer to WAVEWATCH-III (independent run) result during hurricane not approaching computational domain; however, it bends to SWAN (independent run) result during hurricane dominating the domain. The reason is that the wind speed is very small before the front edge of a hurricane reaches the model domain (due to no background wind field incorporated in Holland hurricane model) and wave energy is mainly transported from boundary condition (supplied by the coarse run of WAVEWATCH-III). On the other hand, wind will play much more important role in wave generation when hurricane effect reaches the domain due to the large wind speed. Thus, the significant wave height simulated in the first nesting run is mainly impacted by boundary condition when hurricane effect does not enter the domain, whereas it will be controlled by wind forces during hurricane approaching the domain. In other words, boundary conditions have little impact on waves (could be disregarded) when wind forces are strong in computational domain.

In the second nesting run experiment (SWAN nesting itself), the results are displayed in **Fig. 10**. Before describing the results, it is worthwhile to show the difference of the water depth at buoy stations among gaining from different resolution bathymetry (**Table 2.1**). It can be seen that the water depth at buoy data stations is various from grid to grid. Water depth at buoy data station 41008 is 17.20 m for the outermost grid, for the mid grid it is 17.80

m, for innermost it is 17.82 m and actual water depth is 18.0 m. The water depth bias indicated by **table 2.1** is significant among different grids and the bias of outermost is largest. Hence, the SWH values (**Fig. 2.10**) computed by the models show that the results of outermost grid are the worst compared to buoy data, mid grid and innermost grid are better. Furthermore, the results are improved more obviously from outermost to mid grid than from mid grid to innermost. It suggests that the effect of bathymetry resolution should be considered in wave prediction but not necessary to consider too fine grid resolution.

2.5. Discussions and summary

The depth-induced refraction-diffraction process presented in SWAN was tested using several ideal experiments in this chapter. The results of the beach refraction experiment indicate that depth-induced refraction has a significant impact on wave propagation; it also shows a good agreement with analytical result. At the mean time, the influence of depth-induced diffraction plays an important role in wave propagation and wave height when waves cross a sub-water channel or ridge in a beach. The results of experiments show that there is a significant impact on waves if we activating the diffraction option in the SWAN. It suggests that it is important to consider depth-induced diffraction effect to compute the wave field in some specific case.

The effect of depth-induced wave breaking is often neglected or not given regard enough by researchers in their wave simulation. Especially in hurricane cases, there are fewer studies to explore this effect. A comparison between the results of SWAN (no breaking term and

including breaking term) and WAVEWATCH-III forced by hurricane was conducted in this chapter. Three hurricane cases and one modified hurricane case were selected as examples to examine the effect of wave breaking in shallow water area. In most cases, the results in station **FPSN7** are poorer compared with observation data if the effect of wave breaking is not considered in wave models than the results that include this effect. However, the wave models exhibit no much different prediction skill at station **FPSN7** when the track of hurricanes passed through its right area. Therefore, depth-induced wave breaking is not always important in shallow water areas in hurricane-induced wave simulation case. It has more significant impact on wave field in areas which lies on the right of hurricane than those lies on the left of hurricane.

The effect of topography resolution on waves is important when bathymetry feature is complex, which need fine grid to represent it. Otherwise, it is not necessary to pick too fine grid resolution to compute wave field using nesting run. The effect of boundary condition on waves depends on the wind conditions, it is significant during weak wind conditions but it can be disregarded during peak wind conditions. That is to say, waves are mainly determined by boundary conditions during hurricanes increase phase and hurricanes play the main role in waves during hurricane peak phase.

Table 2.1 The water depth of buoy data stations get from different resolution topography. Where Bias equal water depth get from topography minus actual water depth; ∈= Bias/actual water depth.

Grid	Buoy Data Station	Water depth (m)	Bias (m)	∈ (%)
Outermost	41002	3617.06	-168.54	4.45
	41004	39.00	2.4	6.56
	41008	17.20	0.8	4.40
	Fpsn-7	19.67	-2.83	12.83
Med	41002	3635.41	-150.19	3.97
	41004	38.10	1.5	4.10
	41008	17.80	-0.2	1.11
	Fpsn-7	21.93	-0.57	2.53
Innermost	41002	NAN	NAN	NAN
	41004	38.91	2.31	6.31
	41008	17.82	-0.18	1.00
	Fpsn-7	22.39	-0.11	0.49

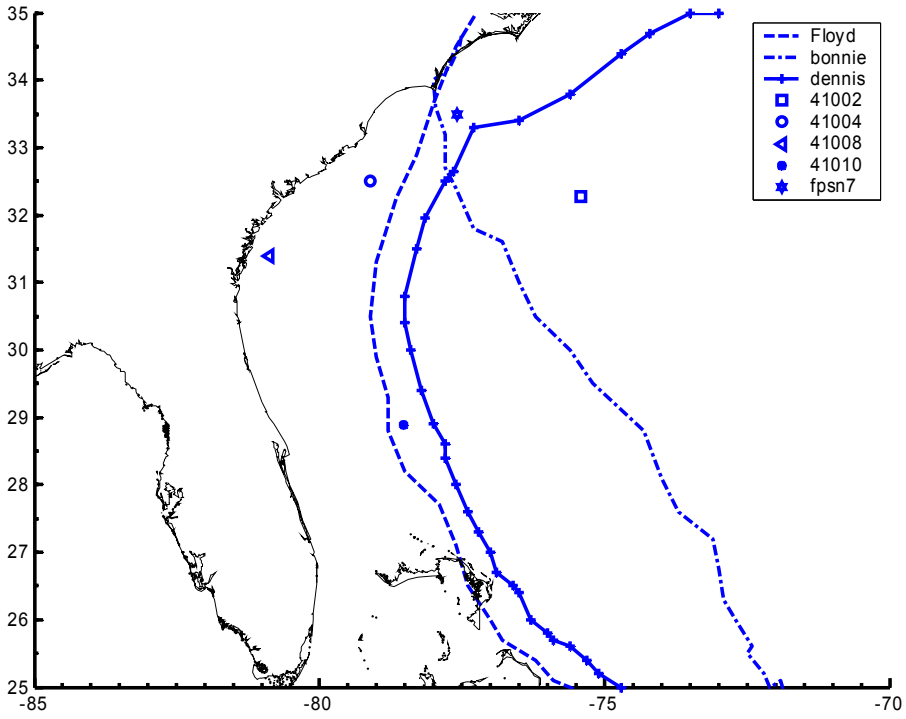

Figure 2.1. Computational domain, distribution of Buoy data stations and the best tracks of hurricane Bonnie, Dennis and Floyd.

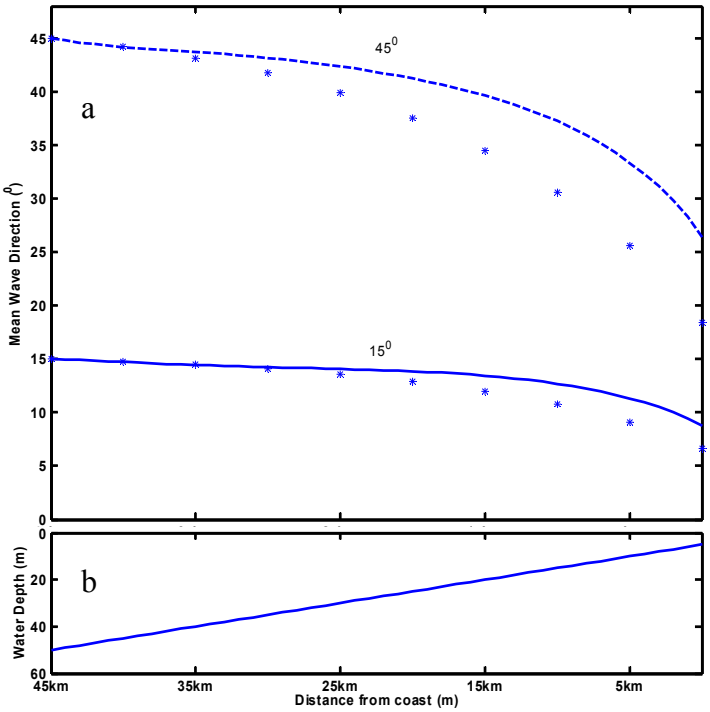

Figure 2.2.1. a) The mean wave direction along the center line from deep water to coastal line. The asterisk is the analytical solution and lines are results of SWAN. Dashed line is swell wave with peak wave direction 45^0 and solid line is swell wave with peak wave direction 15^0. b) Water depth (m) along the center line.

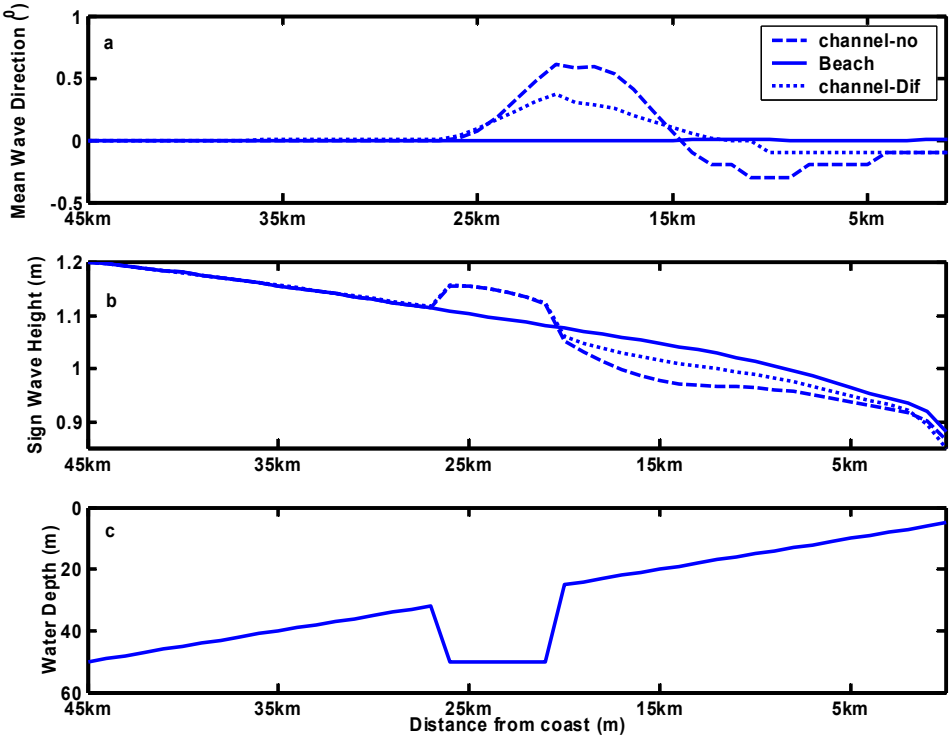

Figure 2.2.2. a) The mean wave direction and b) significant wave height along the center line from deep water to coastal line. Solid line is the result of swell wave propagates on the beach without any channels; dashed line is the result of swell wave propagates on the beach with a channel without considering diffraction effect and dotted line is considering diffraction effect. c) water depth (m) along the center line.

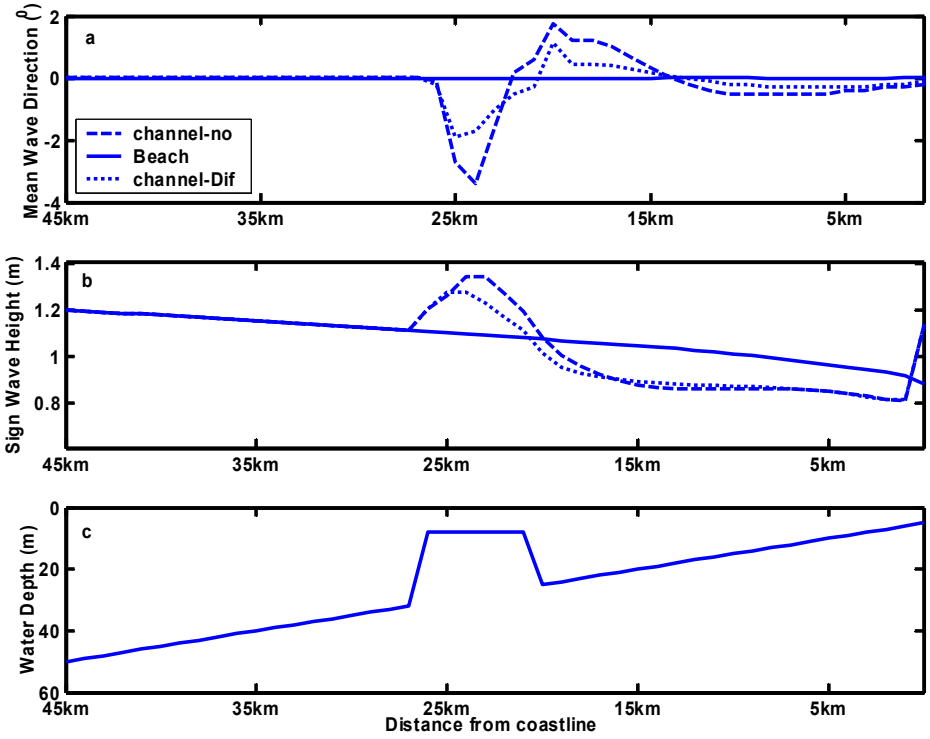

Figure 2.2.3. Same as Figure 2.2.2 but for case 3.

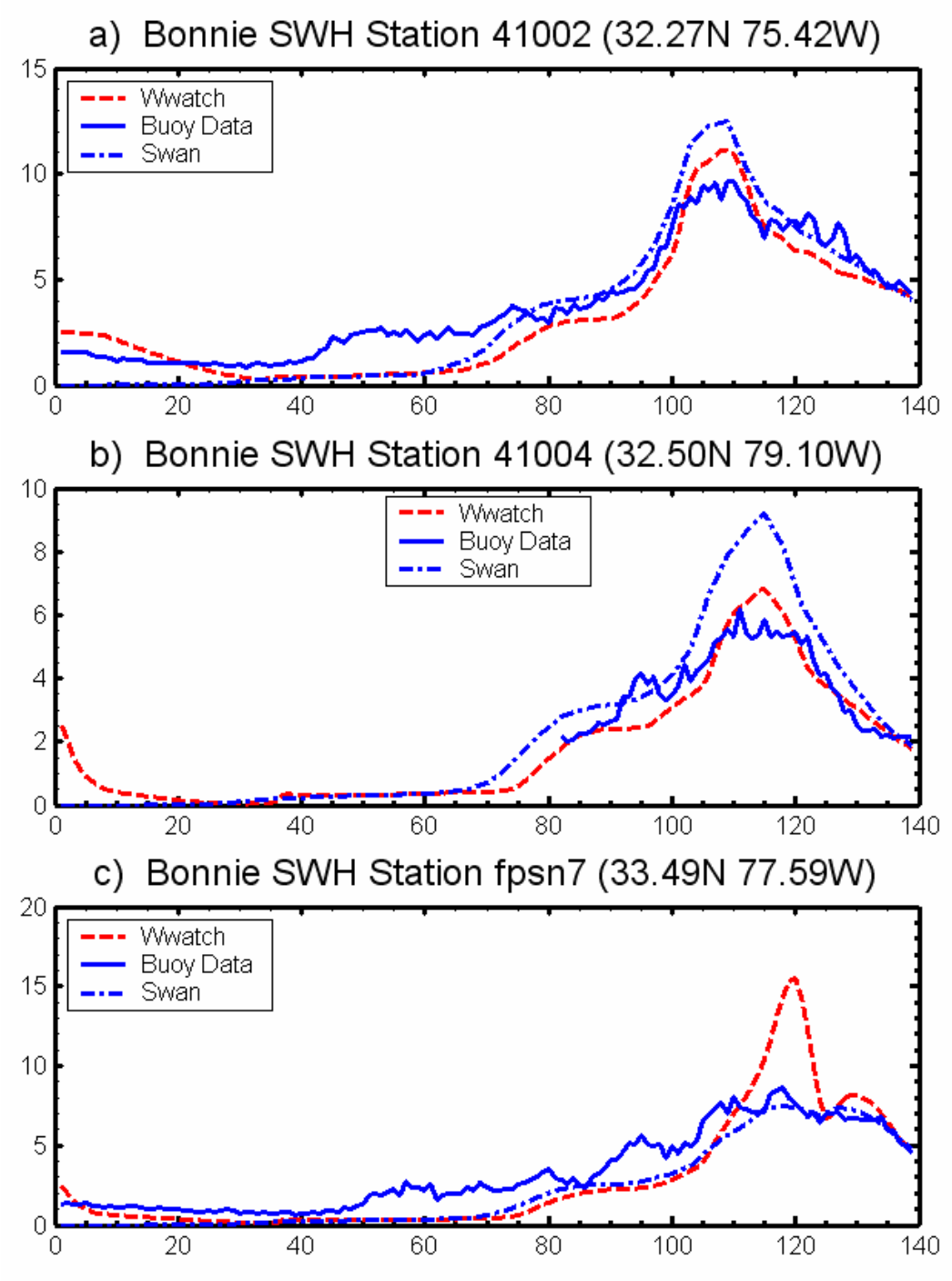

Figure 2.3.1. Significant Wave height (SWH) at buoy data stations for hurricane Bonnie. Solid line is buoy data, dashed line is WAVEWATICH-III results and dot-dashed line is SWAN results. X-axis is time (hour) and Y-axis is SWH (meter).

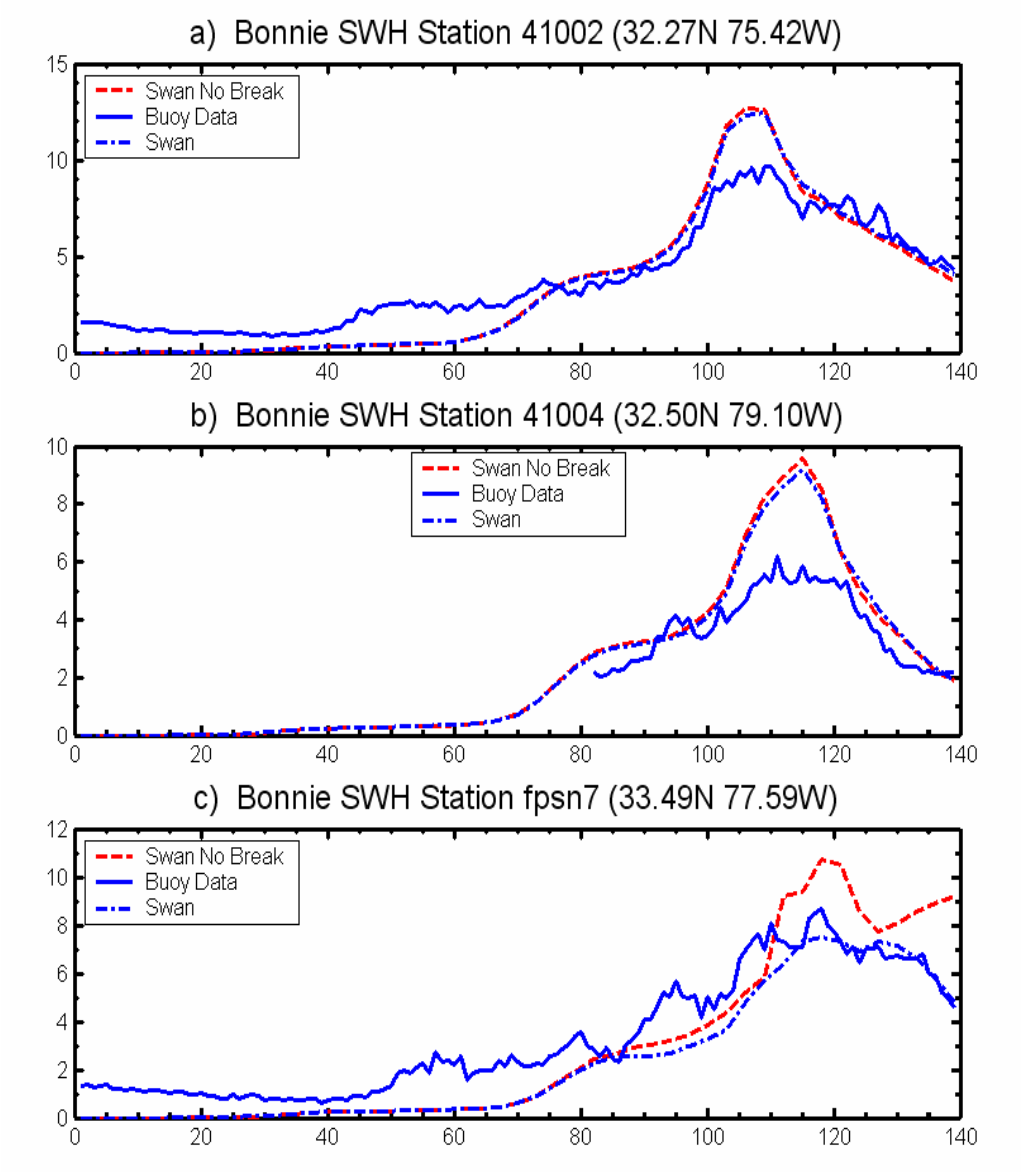

Figure 2.3.2. SWH at buoy data stations for hurricane Bonnie. Solid line is buoy data, dashed line is SWAN results and dot-dashed line is SWAN (depth-induced wave breaking not be included) results.

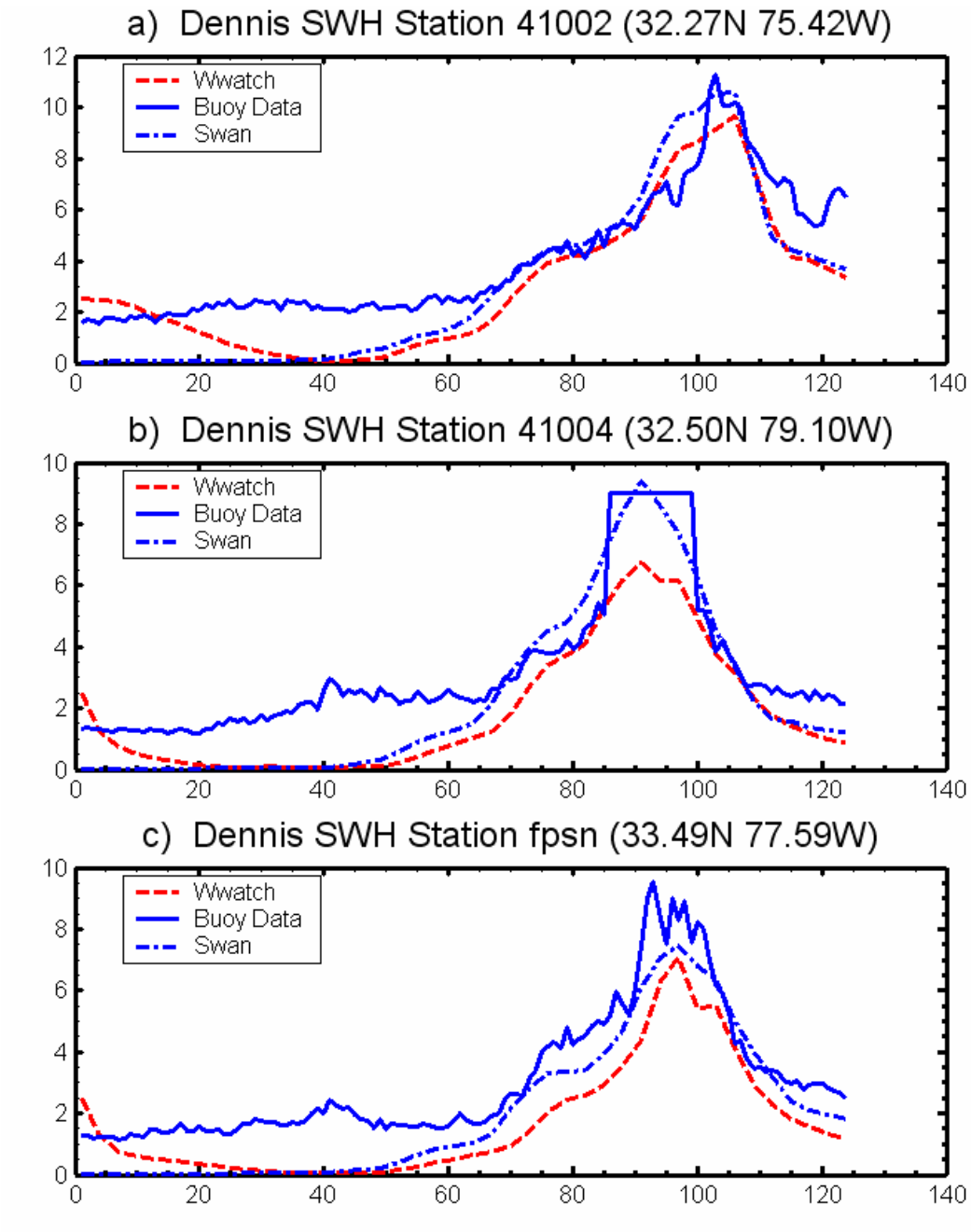

Figure 2.4.1. Same as Figure 2.3.1 but for hurricane Dennis.

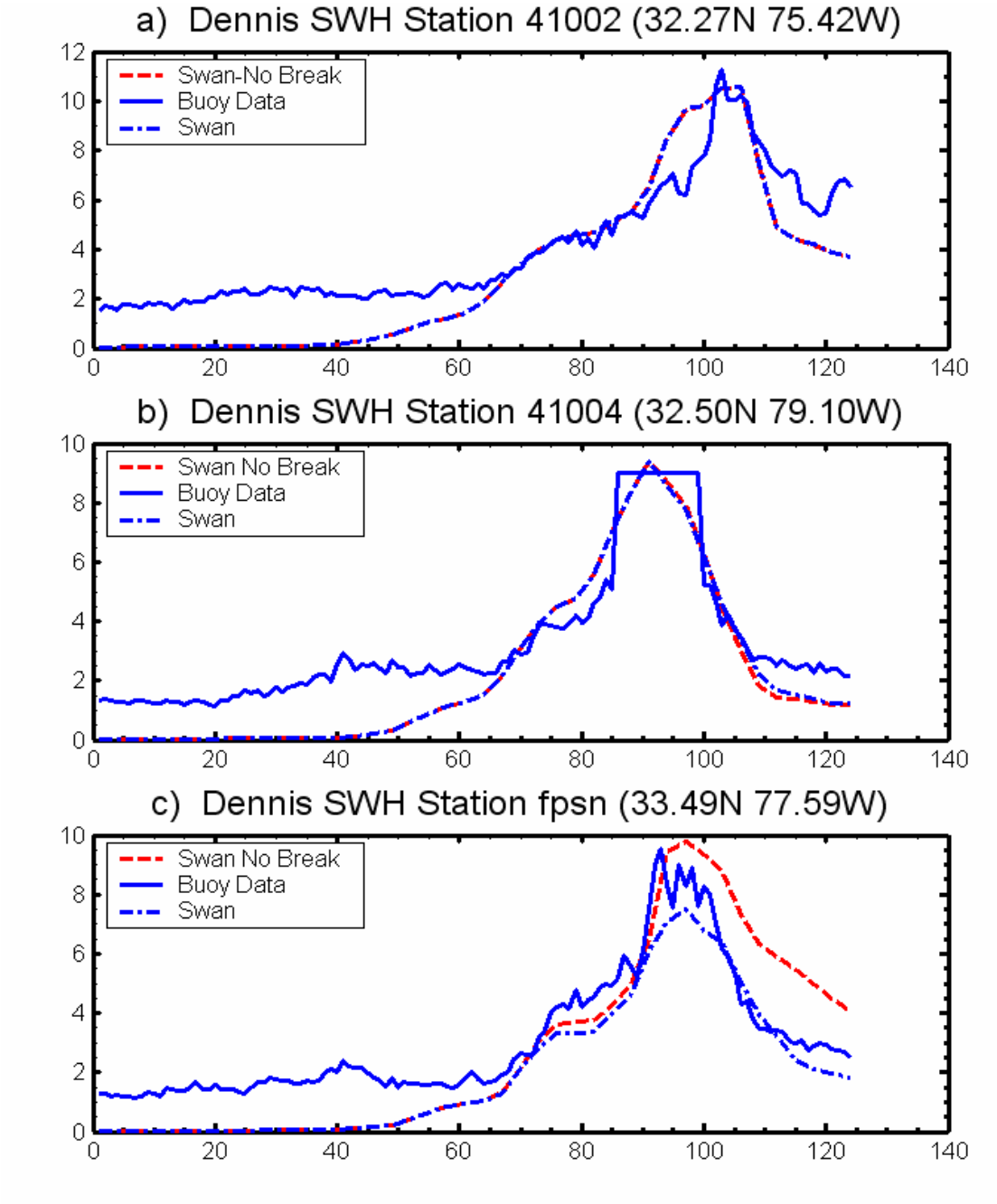

Figure 2.4.2. Same as Figure 2.3.2 but for hurricane Dennis.

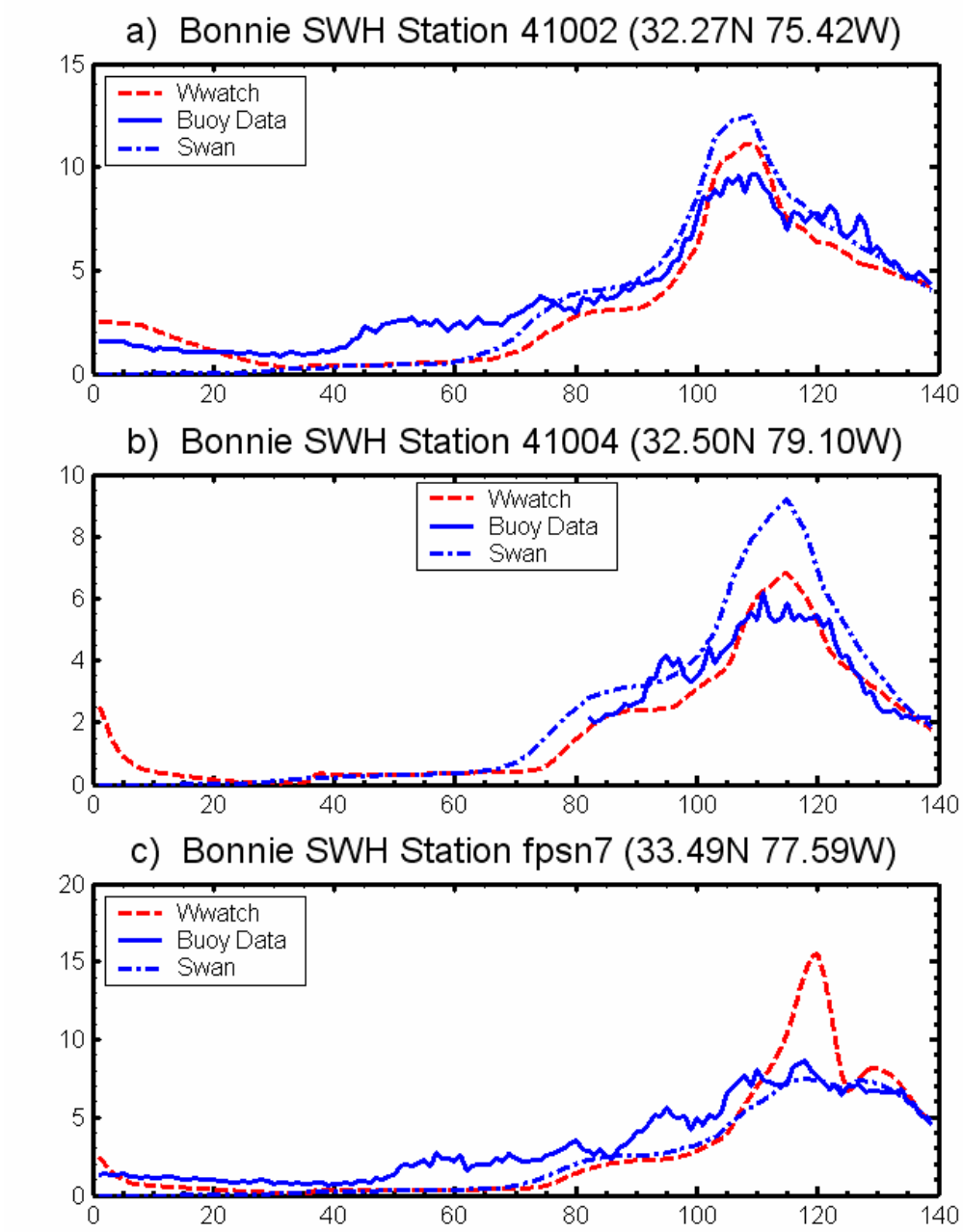

Figure 2.5.1. Same as Figure 2.3.1 but for hurricane Floyd.

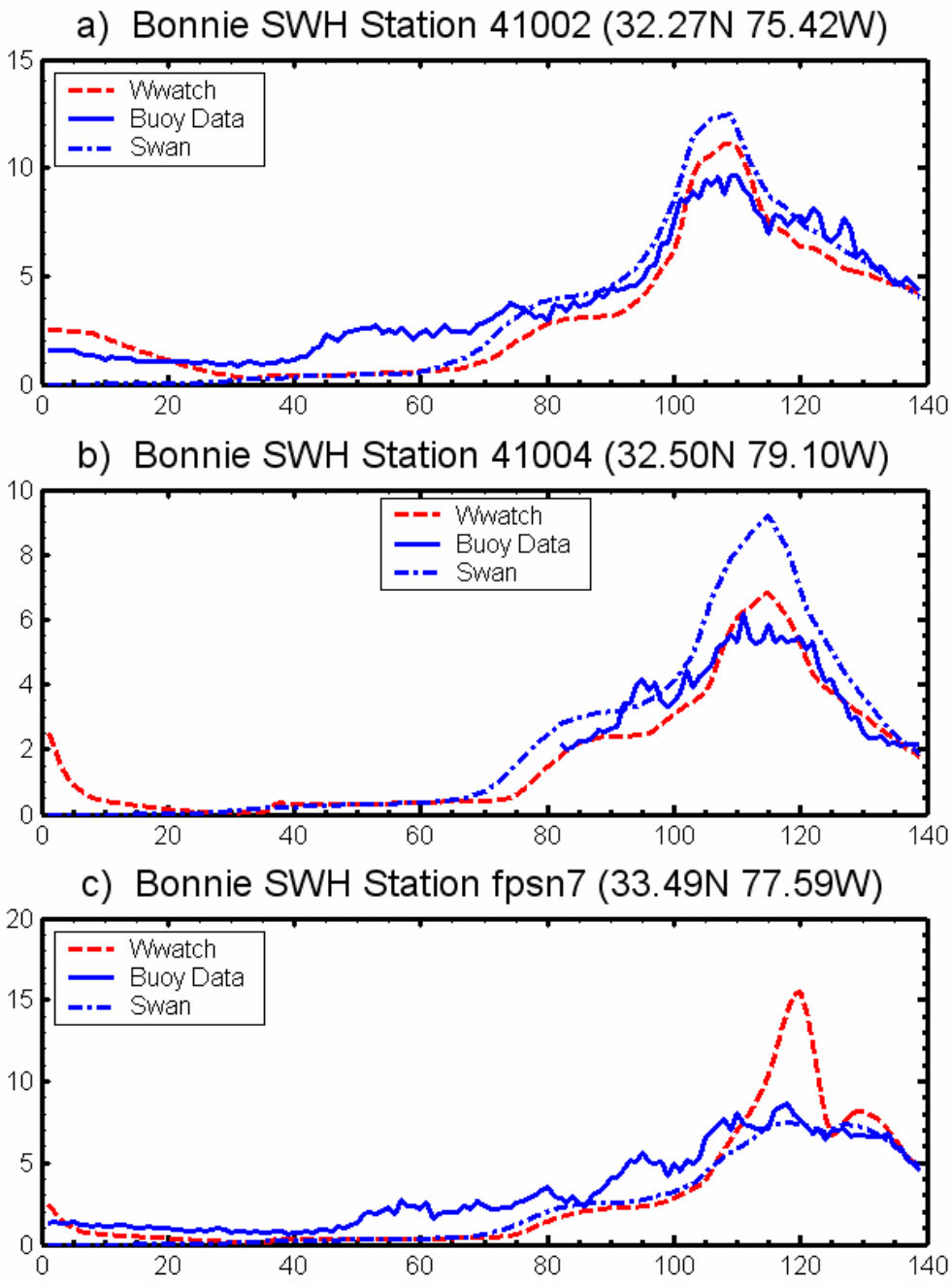

Figure 2.5.2. Same as Figure 2.3.2 but for hurricane Floyd.

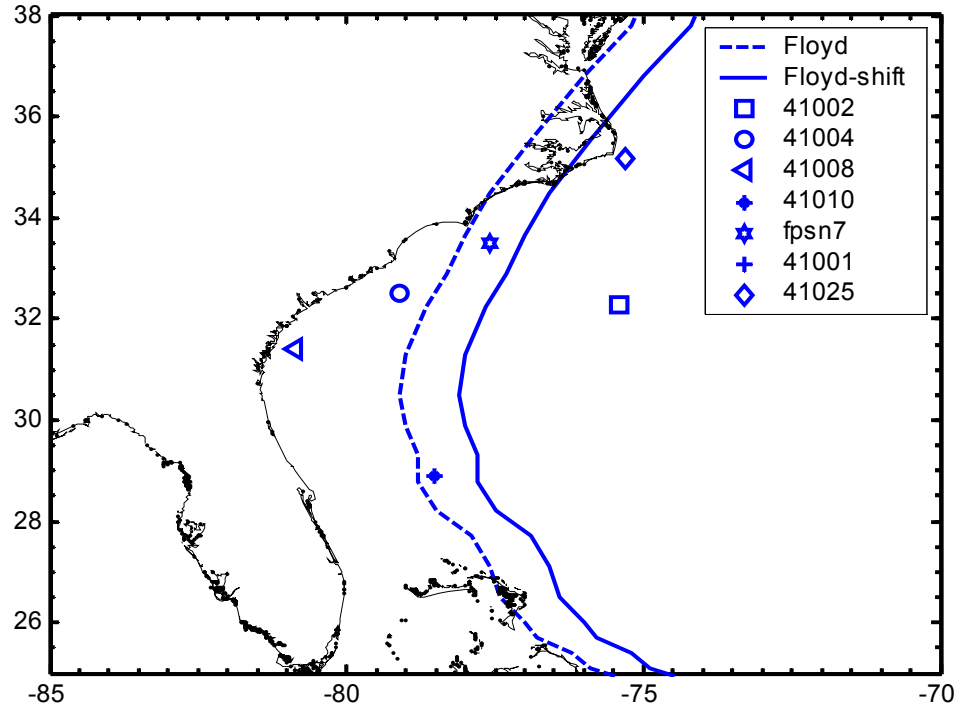

Figure 2.6. The original and shifted track of hurricane Floyd. Dashed line is original track and solid line is the shifted track, which shifted to right 1^{o}.

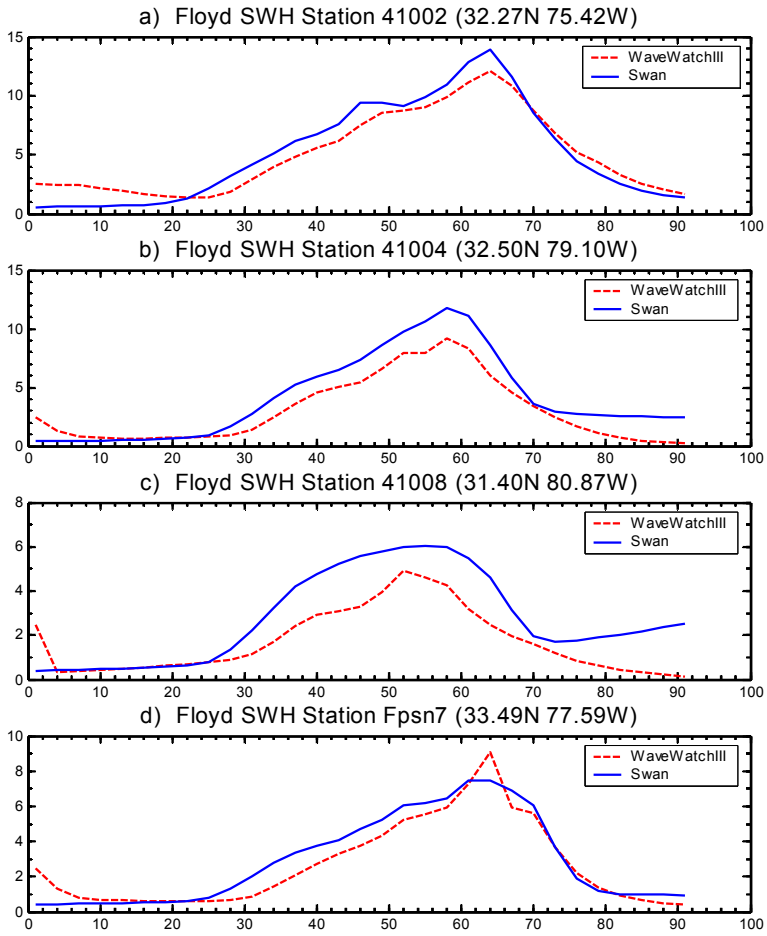

Figure 2.7. SWH at buoy data stations for modified hurricane Floyd by shifting track to right 1^{o}. Dashed line is WWATCH-III results and solid line is buoy data.

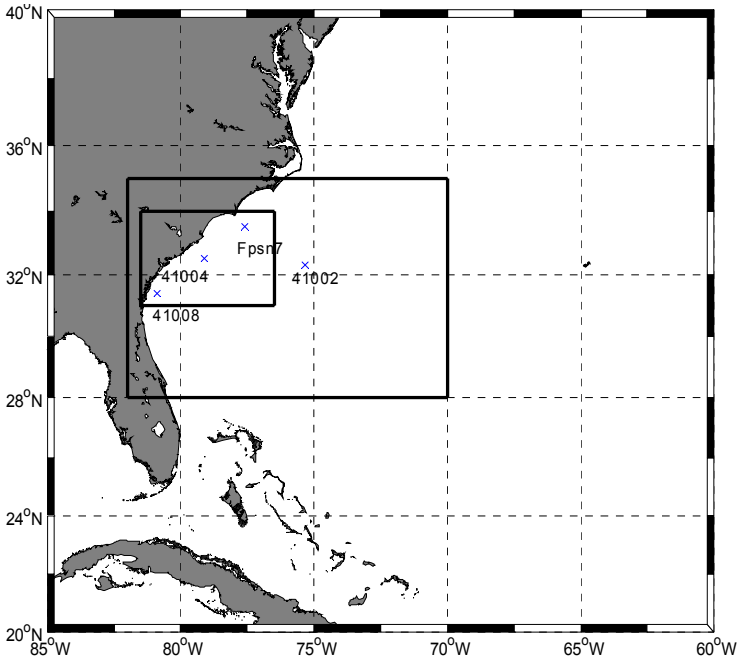

Figure 2.8. The setup of nesting domain. The outermost domain covers from 20^0 to 40^0 N and 85^0 to 60^0 W with resolution 12 minute. The mid domain is 28^0-35^0 N, 82^0-70^0W with 4 minute as the spatial grid size. The inner most domain is 31^0-34^0N, 81.5^0-76.5^0W with resolution 2 minute.

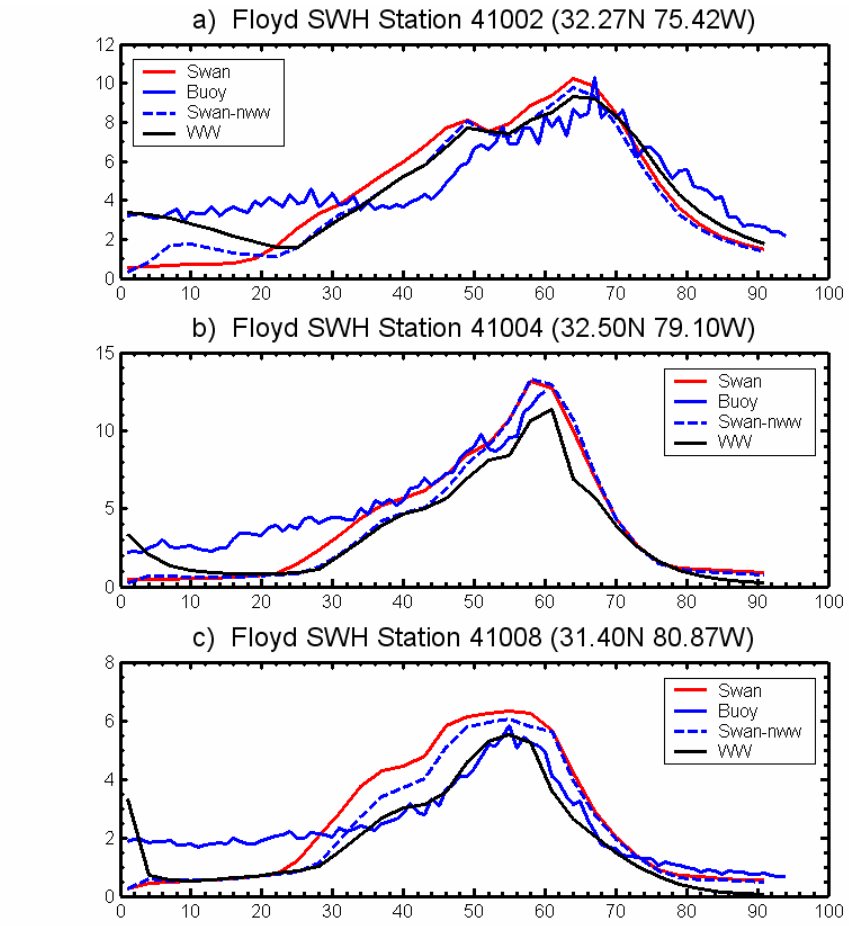

Figure 2.9. SWH at buoy data stations for hurricane Floyd. Blue solid line is buoy data, red solid line is Swan coarse run result, black solid line is WaveWatch III coarse run and blue dash line is Swan nested in WaveWatch III run.

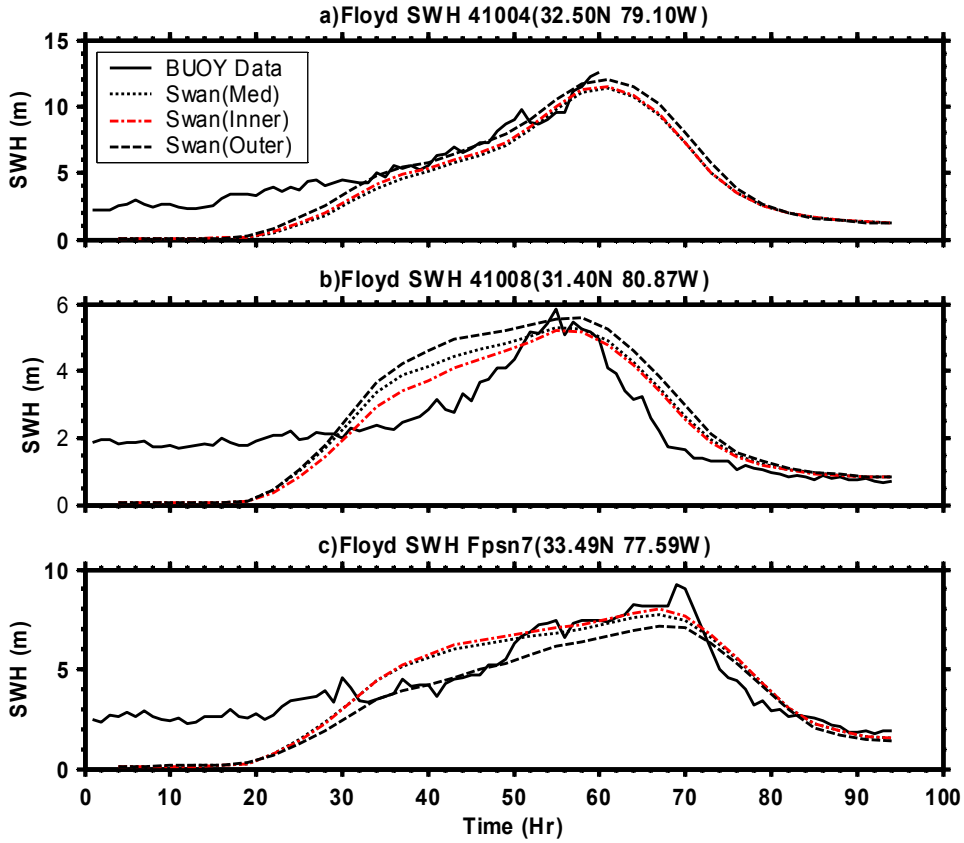

Figure 2.10. SWH at buoy data stations for hurricane Floyd. Dashed line is the results of outer domain, dotted line is med domain, dot-dashed line is inner domain and solid line is the buoy data.

References

Battjes, J.A. and H.W., Groenendijk, 2000. Wave height distributions on shallow foreshores. Coastal Eng. 40, 161-182.

Battjes, J.A. and M.J.F. Stive, 1985. Calibration and verification of a dissipation model for random breaking waves. J.Geophys. Res. 90 (c5), 9159-9167.

Battjes, J.A., J., Janssen, 1978. Energy loss and set-up due to breaking of random waves. Proc. 16th Int. Conf. Coastal Engg. ASCE, New York, pp. 569-587.

Berkhoff, J.C.W., 1972, Computation of combined refraction-diffraction. Proc. 13th Int. Conf. Coastal Eng., ASCE 1, 471-490.

Booij, N., Ris, R.C., Hothuijsen, L.H., 1999. A third-generation wave model for coastal regions: 1. Model description and validation. J. Geophys. Res. 104 (c4), 7649-7666.

Gao, Q., Radder, A.C., 1998. A refraction-diffraction model for irregular waves. Proc. 26th Int. Conf. Coastal Eng. 1, 366-379.

Hasselmann, K., T.P. Barnett, E. Bouws, H. Carlson, D.E. Cartwright, K. Enke, J.A. Ewing, H. Gienapp, D.E. Hasselmann, P. Kruseman, A. Meerburg, P. Muller, D.J. Olbers, K.

Richter, W. Sell and H. Walden, 1973. Measurements of wind-wave growth and swell decay during the Joint North Sea Wave Project (JONSWAP), Dtsch, Hydrogr.Z. Suppl., 12, A8.

Holland, G.J., 1980. An analytic Model of the wind and pressure profiles in Hurricanes. Mon. Wea. Rev., 108, 121-1218.

Holthuijsen, L.H., A. Herman and N. Booij, 2003, Phase-decoupled refraction-diffraction for spectral wave models, Coastal Engineering, 49, 291-305.

Hsu, T.-W., S.-H. Ou and J.-M. Liau, 2005, Hindcasting nearshore wind waves using a FEM code for SWAN, Coastal Engineering, 52, 177-195.

Ito, Y., tanimoto, K., 1972, A method of numerical analysis of wave propagation-application to wave diffraction and refraction. Proc. 13th Int. Conf. Coastal Eng., ASCE 1, 503-522.

Li, Y.S. and Zhan, J.M., 2001, Boussinesq-type model with boundary-fitted coordinate system. J. Waterw., Port, Coast. Ocean Eng., ASCE, New York, 127 (3), 152-160.

Madsen, P.A. and Sørensen, O.R., 1992, A new form of the Boussinesq equations with improved linear dispersion characteristics: Part2. A slowly-varying bathymetry. Coast. Eng. 18, 183-205.

Massel, S.R. and M.R. Gourlay, 2000. On the modeling of wave breaking and set-up on coral reefs. Coastal Eng. 39, 1-27.

Ris, R.C., N. Booij and L.H. Holthuijsen, 1999, A third-generation wave model for coastal regions, Part II, Verification, J.Geoph.Research C4, 104, 7667-7681.

Rogers, W.E., P.A. Hwang and D.W. Wang, 2003, Investigation of wave growth and decay in the SWAN model: three regional-scale applications, J. Phys. Oceanogr., 33, 366-389.

SWAN group, 2003. SWAN Cycle III version 40.20 USER MANUAL.

Tolman, H.L., 1991, A third-generation model for wind waves on slowly varying, unsteady and inhomogeneous depths and currents. J. Phys. Oceanogr., 21, 782-797.

Tolman, H.L., 2002. User manual and system documentation of WAVEWATCH-III version 2.22.

WAMDI group, 1998. The WAM model---a third generation ocean wave prediction model. J. Phys. Oceanogr., 1775-1810.

Zhao Liuzhi, Vijay Panchang, W. Chen, Z. Demirbilek, N. Chhabbra, 2001. Simulation of wave breaking effects in two-dimensional elliptic harbor wave models. Coastal Eng. 42, 359-373.

Zijlema, M. and A.J. van der Westhuysen, 2005, On convergence behaviour and numerical accuracy in stationary SWAN simulations of nearshore wind wave spectra, Coastal Engineering, 52, 237-256.

CHAPTER 3. A NUMERICAL STUDY ON THE EFFECT OF THE GULF STREAM ON WAVES

3.1. Introduction

The important and interesting fluid mechanical and environmental problem of the effect of currents on waves has been the subject of significant community interested as reflected in the many observing programs [e.g., Meadows et al., 1983; Mapp et al., 1985; Liu et al., 1989] and theoretical studies [e.g., Treloar, 1986; Longuet-Higgins and Stewart, 1961; Kengyon, 1971; Mathiesen, 1987]. Longuet-Higgins and Stewart [1960, 1961] developed the theory of conserved wave-current interactions. They introduced radiation stress into the governing equation. Kengyon [1971] investigated wave refraction in ocean currents by using the geometrical optics approximation, and discussed the kinematical effects of currents on waves. Mapp et al. [1985] developed a numerical model for the refraction of ocean swell by current that was tested with Seasat synthetic aperture radar (SAR) data, in which integration of the ray equation was applied in a moving medium. In 1987, Mathiesen developed another model to study wave refraction by a current whirl, which extended the study of Mapp et al. [1985]. Simons and Maciver [1998] performed experiments with regular deep-water waves propagating obliquely across a relative narrow jet-type current.

The results of previous studies of current induced changes in wave height and direction indicate that the refraction effects of deep water surface waves in major currents (Gulf

Stream) could be significant. In particular, the trapping of waves in currents and the total reflection of waves by currents is theoretically possible. Irvine and Tilley [1988] discussed the trapping of waves by straight and meandering shear currents. Holthuijsen and Tolman [1991] investigated the effects of the Gulf Stream on surface gravity waves by employing the WAVEWATCH wave model. Ocean waves were propagated across a current ring and as well as across an infinitely long and straight northward flowing Gulf Stream from the northeast (NE) and southeast (SE) directions. The results showed that refraction may trap locally generated waves in the straight Gulf Stream or it may reflect wave energy back to the open ocean depend on wind and wave conditions. However, in their research paper, they didn't investigate the condition of waves crossing the Gulf Stream from the normal direction.

The Simulating WAves Nearshore, or SWAN [Booij et al., 1999] a wave model that includes depth induced dissipation and other sophisticated physics has been extensively studied [Padilla-Hernandez and Monbaliu, 2001; Rogers et al., 2003; Holthuijsen et al., 2003; Hsu et al., 2005]. However few studies have been focused on investigating the effects of major currents on waves by employing SWAN. In the study of this chapter we repeat the Holthuijsen and Tolman [1991] experiment but we use SWAN and we also investigate the case of normal encounter of the wave field with the Gulf Stream as well as consider the case of the Hurricane Bonnie induced wave field with an idealized Gulf Stream.

A brief outline of model setups and ideal experiments conducted in this chapter are given in section 3.2. Section 3.3 presents the results of the ideal experiments to analyze the mechanism of the Gulf Stream effect on waves. A real hurricane example (1998 Bonnie) is

introduced in Section 3.4. The comparison between model results and observation data for the case of Bonnie is given in section 3.5. The last section in this chapter presents the summary and discussion.

3.2. Setups of wave model and experiments

The computational domain is from 85^0 to 70^0 (W) longitudes and from 25^0 to 35^0 (N) latitude with grid resolution 0.20. The water depth is set to 5000 m in order to avoid wave refraction due to topography. The integration time step is 6 minutes. Wave frequencies range from 0.04177 to 1.0 Hz and the directional resolution is 10° (0^0~360^0). The current fields (Gulf Stream) used in ideal experiments of this paper were simulated by X. Liu (personal communication) using the HYbrid Coordinate Ocean Model, or HYCOM ocean current model results published in Xie et al. [2006]. In Liu's study, the Gulf Stream current fields were simulated in the presence of climatological wind fields (COADS). The Gulf Stream current field varies slowly in time and the result of the 51st day of the run is selected and treated constant in time. **Figure 3.1a** shows the Gulf Stream current field of Day 51 from Liu's study.

In order to examine the influence of the Gulf Stream on waves, six ideal experiments (**Table 3.1**) are conducted in this chapter. Locally generated wind waves and waves propagating in as swell propagating in a direction counter to the direction of current constitute cases NEW and NES. The cases SEW and SES are wind waves and swell propagating in the direction of the current. Finally, the cases of wind waves and swell

encountering the Gulf Stream from the east are investigated in the cases EW and ES. Homogeneous and constant wind fields (10 m/s) were set as the wind input term of SWAN in all of wind waves cases (NEW, SEW and EW). Three directions of the wind fields were selected: one the NE wind (225^0) (case NEW); the SE wind (135^0) (case SEW); and the E wind (180^0) (case EW). The set up of the wave swell cases for SWAN are as follows: the boundary condition is characterized with a Gaussian-shaped frequency energy spectrum; the width of the Gaussian frequency spectrum is 0.007 Hz; the significant wave height is taken as 1.99 m; peak frequency is 0.071 Hz; peak wave directions are 225^0 (NES), 135^0 (SES) and 180^0 (ES); and the directional width is 12.4^0. All angles used in this paper assume a Cartesian convention.

3.3. Results

A single line (**Fig. 3.1a**) traversing the Gulf Stream was set to sample the wave character parameters to show the variation in wave fields. The line is from 80.6^0W to 79.4^0W longitudes and the latitude is 30.2^0N. The profile of the current speed (y direction) along this line is shown in **Fig. 3.1b**.

3.3.1. Case NEW

First we consider the results under the NE wind condition. **Figure 3.2a** shows the significant wave height difference between the cases of with and without the inclusion of the effect of the Gulf Stream along the line (the position is indicated in **Fig. 3.1a**). It is obvious

that the significant wave height with the Gulf Stream is much higher than is that in the case without the Gulf Stream influence. Similar results were obtained by Kenyon [1971], and Holthuijsen and Tolman [1991], etc. The results demonstrate that the current will increase the significant wave height when wave propagate in a counter-current direction. The results show good agreement with the results of previous studies [Longuet-Higgins and Stewart, 1960, 1961 and 1962; Hwang, 1983; Mapp *et al.*, 1985; Holthuijsen and Tolman, 1991; Simons and Maciver, 1998; Wolf and Prandle, 1999].

The variation of the mean wave direction crossing the Gulf Stream is shown in **Fig. 2b**. It shows that the mean wave direction bends away off the Gulf Stream normal (x-axis). However, based on the relationship between the angles of incidence and refraction, $\frac{\sin\phi_0}{\sin\phi} = \left[1 - \frac{U}{c_0}\sin\phi_0\right]$ **(A)** [Kenyon, 1971; Hwang, 1983; Sheres et al. 1985; Holthuijsen and Tolman, 1991], the mean wave direction should bend away toward the Gulf Stream normal when waves enter the Gulf Stream from the counter-current direction. In relationship (A), Φ is the angle between the wave number and the current normal and C_0 is phase speed of the waves where the current vanishes. The subscribe 0 refers to the no current condition. Therefore some effect other than the influence of the Gulf Stream current, has resulted in a refraction of the waves in this case. The effect can be seen in **Fig. 3.2c and Fig. 3.2d**. **Figures 3.2c-3.2d** illustrate the two-dimensional (frequency-direction) spectra of wind waves with a current and without a current, respectively. The location of these spectra is at 80^0 west longitude and 30.2^0 north latitude (location B in **Fig. 3.1b**). It shows that some wave energy from the south adds to the wave spectrum when waves cross the Gulf Stream. In other words,

locally wind generated waves become trapped in the Gulf Stream. Combining with those adding waves energy will shift the mean wave direction to south. In other words, the mean wave direction of incoming waves is refracted away from or off the normal of the Gulf Stream (x-axis). To confirm the above analysis, the case of swell, with the peak wave direction 225^0 interacting with the Gulf Stream is conducted in the next case study.

3.3.2. Case NES

The results of NES are shown in **Fig. 3.3**. **Figure 3.3a** shows the mean wave direction variation between considering the Gulf Stream effect and without the influence of the Gulf Stream. It demonstrates that the direction of the swell is bent toward the Gulf Stream normal (a clockwise turn) when crossing the Gulf Stream. It is a good agreement with the relationship (A) prediction. The reason for this is because there is no wind input in the case of swell. So no locally wind generated wave energy can be added to the incoming waves. In other words, current refraction is the dominant factor to influence wave propagation in this case. This can also be seen in the two-dimensional spectra of the same location as the case NEW (**Fig. 3.3b-3.3c**)**.** It is obviously that there is no additional wave energy added into the spectrum with a current (**Fig. 3.3b)** compared with the spectrum in the case without a current (**Fig. 3.3c).** Therefore waves will turn clockwise and bend toward the Gulf Stream normal under the influence of current refraction, which is the same as the prediction of equation (A).

3.3.3. Case SEW

For the SE wind case, results are illustrated in **Fig. 3.4**. The significant wave height is smaller with the effect of the Gulf Stream than those without the Gulf Stream (**Fig. 3.4a**). It indicates that a current will reduce the wave height when waves propagate in the current direction. The variation in the wave height is again in agreement with previous studies [e.g. Longuet-Higgins and stewart, 1960, 1961 and 1962; Hwang, 1983; Mapp *et al.*, 1985; Holthuijsen and Tolman, 1991; Simons and Maciver, 1998; Wolf and Prandle, 1999].

Another phenomenon can be seen from this figure is that the significant wave height on the east outside of the Gulf Stream (right section on **Fig. 3.4a**) is higher than those without considering the Gulf Stream. This may be related to the reflection of some of the wave energy by the Gulf Stream off to the open ocean. The phenomenon of reflection of waves in the following current has been noted in previous studies [Kenyon, 1971; Hwang, 1983; Holthuijsen and Tolman, 1991; etc.]. It is also illustrated in the two-dimensional wave spectra of the three locations (A, B and C in **Fig. 3.1b**) along the line (**Fig. 3.4b-3.4d**). These spectra indicate that the wave energy on the right side of the Gulf Stream (location A) is much more than those entering the Gulf Stream (location B) and on the left side of the Gulf Stream (location C). It is obvious that some wave energy (between the directions of 50^0-75^0) is added to incoming waves on the right side of the Gulf Stream (location A). On the other hand, some energy is missing from the direction of 50^0-75^0 at the location B and C. Apparently a portion of the wave energy is reflected back to the open ocean when waves enter the Gulf Stream. The effect of the Gulf Stream on wave propagation is shown in **Fig.**

3.4e. It shows that it turns the mean wave direction clockwise (bends off the Gulf Stream normal) when waves enter the Gulf Stream. It is in good agreement with the relationship (A) prediction.

3.3.4. Case SES

In addition, a swell case with the peak wave direction 135^0 is carried out in this section. The results are shown in **Fig. 3.5** and indicate that the wave direction bends away from the Gulf Stream normal (**Fig. 3.5a**). It means that the refraction of the Gulf Stream is the dominant effect for waves entering the Gulf Stream from the southeast direction. However it is not to say the effect of reflection can be neglected or is not significant. The reason why the influence of reflection on wave propagation is not as noticeable as refraction is that the reflected energy is back to the open ocean and does not enter the Gulf Stream. The phenomenon of reflection can also be seen from **Fig. 3.5b-3.5c**, which show the two-dimensional spectra of locations A and C respectively. **Figure 3.5b** (location A) illustrates that there is one more wave energy peak (between the directions of 60^0-90^0) in the spectrum incorporating the influence of the Gulf Stream than the spectrum without considering the effect of the Gulf Stream. Meanwhile, some wave energy is missing over the direction band 90^0-120^0 in the spectrum at location C (**Fig. 3.5c**) if the impact of the Gulf Stream is included. It is obvious that some wave energy is reflected back to the open ocean when swell waves propagate in a direction counter to the direction of flow of the Gulf Stream.

3.3.5. Case EW

Figure 3.6 illustrate the results of case EW, in which the wind blows toward the west. The variation of significant wave height when waves enter the Gulf Stream from the normal direction is shown in **Fig. 3.6a**. It illustrates that the influence of the Gulf Stream on significant wave height in this case is little more complex than the above two wind cases (NEW and SEW). First it reduces the significant wave height at the east side of the Gulf Stream, then it increases them in the center of the Gulf Stream, and finally reduces them again at other side of the Gulf Stream. The effect on wave propagation is shown in **Fig. 3.6b**. It can be seen from **Fig. 3.6b** that waves are turned clockwise on the eastern part of the Gulf Stream. On the other hand, the waves are bent in a southerly direction on the western part of the Gulf Stream. This effect can also be seen in the two-dimensional spectra (**Fig. 3.6c**). The main wave energy was shifted slightly to north at location A, while some wave energy was added to the spectrum from the south direction at location B and wave energy was shifted to the south at location C. It means that the mean wave direction is bent towards the north at location A (east side of the Gulf Stream), at the same time it is shifted toward the south at locations B and C (center and west side of the Gulf Stream).

3.3.6. Case ES

In this case, the experiment of swell, with the peak wave direction 180^0 crossing the Gulf Stream was conducted. Other parameters of the swell are the same as mentioned above. The results are shown in **Fig. 3.7**. **Figure 3.7a** shows the mean wave direction variation along the

traverse line. It illustrates that the Gulf Stream just simply turns the swell clockwise and is not as complex as in the case EW. The effect can also be seen from the two-dimensional spectrum (**Fig. 3.7b**). **Figure 3.7b** shows the spectrum of location B. It is obvious that the Gulf Stream makes the main wave energy distribute narrower than those without a current effect. The wave energy distribution is in the west direction (180^0). In other words, the mean wave direction is bent more closely to the west (180^0) (**Fig. 3.7a**).

3.4. Hurricane Bonnie Example

Hurricane Bonnie (1998) made landfall near Wilmington, NC and caused $360 million in insured property damage [Avila, 1998]. The best track of Bonnie is shown in **Fig. 3.8.** The data used to compare with model results in this study were obtained by the National Buoy Data Center and the NASA Goddard Space Flight Center. The NASA Scanning Radar Altimeter data (SRA) provided the first documentation of the spatial variation of the sea surface directional wave spectra throughout a hurricane passage. The buoy data station and the observation points of SRA used here are also shown in **Fig. 3.8.**

The Gulf Stream current data used in this section were simulated via a one way coupling current - wave system (coupled between HYCOM and SWAN). The forcing wind fields were used in this coupling system included two parts, one is 6-hourly ECMWF and the other is the simulated Bonnie hurricane wind field employing the Holland model [Holland, 1980]. ECMWF wind fields were used before Aug. 20 06:00 and after Aug. 30 18:00 of 1998 and the simulated Bonnie hurricane wind fields by the Holland model [Holland, 1980] were used

in between. The reason for choosing such a combination of wind fields is that hurricane Bonnie had little effect on the computed area before Aug. 20 06:00 and after Aug. 30 18:00, therefore it was deemed okay to use ECMWF wind fields to force the coupled system during this time segment. However, when hurricane Bonnie entered the computation area, the hurricane fields in the ECMWF were too weak to represent the real wind field. Therefore the hurricane wind fields simulated by the Holland model were selected as the forcing fields of the coupled system. The method of coupling between HYCOM and SWAN used in this study is the same as used by Xie, et al. [2003] in which the two models were coupled together only through the wave-induced wind stress and bottom stress. Radiation stress is not considered in this coupled system of this study.

The model domain (85.0-70.0°W, 25.0-35.0°N) and grid resolution (0.2^0 in both directions) used in this section were the same as the previous section in this paper. The bottom topography for the domain was obtained from GEODAS, version 4.0.7, @ http://www.ngdc.noaa.gov/mgg/gdas.

3.5. Results

In this section, the significant wave height and peak wave direction compared between model results and observational data in order to show the impact of Gulf Stream on waves. It is known that not only the surface current influence waves, but also the sub-surface current can also influence waves as long as the waves can reach that depth. Therefore the current field inputted to the SWAN wave model is the depth averaged (0-20 meters) current.

Under the influence of the Gulf Stream, the difference of significant wave height between models including the Gulf Stream (coupling model) and without the Gulf Stream (no coupling and only SWAN) is quite distinct. The difference of significant wave height at the NDBC buoy station is illustrated in **Fig. 3.9a**. The results indicate that the coupled model (including the Gulf Stream effect) performed better than did the SWAN model (without the Gulf Stream impact). For significant wave height, the coupled model results including the current influence are closer to the real observational data than those of the SWAN model without incorporating the effect of the current. However, the improvement in wave propagation is not as obvious as the improvement in significant wave height.

Figure 3.9b shows the mean wave propagation direction at the NDBC station 41004 (32.50 N, 79.10W). It illustrates that the total performance of the model incorporating the Gulf Stream effect (coupling model) is almost the same as the SWAN model with no Gulf Stream included. The difference of peak wave direction at the SRA sample points among two models and SRA data is illustrated in **Fig. 3.10**. It shows that the result of coupling model (including the Gulf Stream effect) is a little bit better than the result of the SWAN model (without the effect of the Gulf Stream) to the right of hurricane eye, but it is not good on the left of the hurricane eye. **Figure 3.9b** and **Figure 3.10** demonstrate that the other effects of wave-current interaction on wave propagation may be significant but are not yet incorporated into the coupling system. The other reason may be that the Gulf Stream simulated by the coupling system is not validated by real observational data which is not available.. There may be some misrepresentations of actual currents in the simulated Gulf Stream.

3.6. Summary and discussions

For Significant Wave Height: Inclusion of a current will reduce the wave height when waves propagate following the current direction due to the fact that some wave energy will be reflected back by the current to the open ocean. On the other hand, a current will increase the significant wave height when the waves propagate in a counter-current direction because there are some locally generated waves that are trapped in the current field. When waves propagate along the normal direction of the current, the effect of the current on the significant wave height will depend on the wave position in the current. In the center of the current, it will increase the significant wave height. Meanwhile, it will decrease the significant wave height on both sides of the current.

For Wave Direction: The Gulf Stream turns the mean wave direction clockwise (bends away from the Gulf Stream normal) when waves enter the Gulf Stream under a SE wind condition. This phenomenon is caused by the wave refraction of the Gulf Stream. It can be predicted by the refraction equation (A) in section 3.3. Under a NE wind condition, the Gulf Stream turns the mean wave direction away off the Gulf Stream normal. However, it is caused not by Gulf Stream refraction but by locally generated wind waves that are subsequently trapped in the Gulf Stream. If there were no such waves, the mean wave direction would be bent toward the Gulf Stream normal based on the above refraction equation. This was confirmed by the case of swell wave entering the Gulf Stream from the NE direction. That is to say, waves would be bent toward the Gulf Stream normal under a NE

wind condition, if only the refraction effect of the Gulf Stream was considered. For the easterly wind case, waves are turned clockwise on the eastern part of the Gulf Stream due to wave energy being shifted slightly to the north. On the other hand, waves are bent towards a south direction on the western part of the Gulf Stream because some wave energy was added to the spectrum from the south direction

In the example of a real hurricane, the improvement of the significant wave height prediction occurs by incorporating the Gulf Stream into the wave model. But for wave propagation, the results are not the same as for significant wave height. The reason may be that factors other than the Gulf Stream affecting wave propagation are not incorporated into our coupled system. For example, the symmetric hurricane winds simulated by the Holland hurricane model were used in this chapter. However, in general, hurricane wind fields are asymmetric. So this distortion of the real hurricane winds may affect the wave propagation direction simulation in the wave model. Another uncertainty factor is the Gulf Stream used in this study. It is simulated by the HYCOM model and may not be adequate to represent the real flow field (which cannot be confirmed due to a lack of observational data of the Gulf Stream flow field). Therefore, the impact of the Gulf Stream inputted into the wave model may have bias errors.

Table 3.1. List of Experiments

Cases	Wind Velocity (m/s)	Wind Direction (^{0})	Peak wave direction on boundary (^{0})	Significant wave height on boundary (m)
NEW	10	225	no	no
NES	no	no	225	1.99
SEW	10	135	no	no
SES	no	no	135	1.99
EW	10	180	no	no
ES	no	no	180	1.99

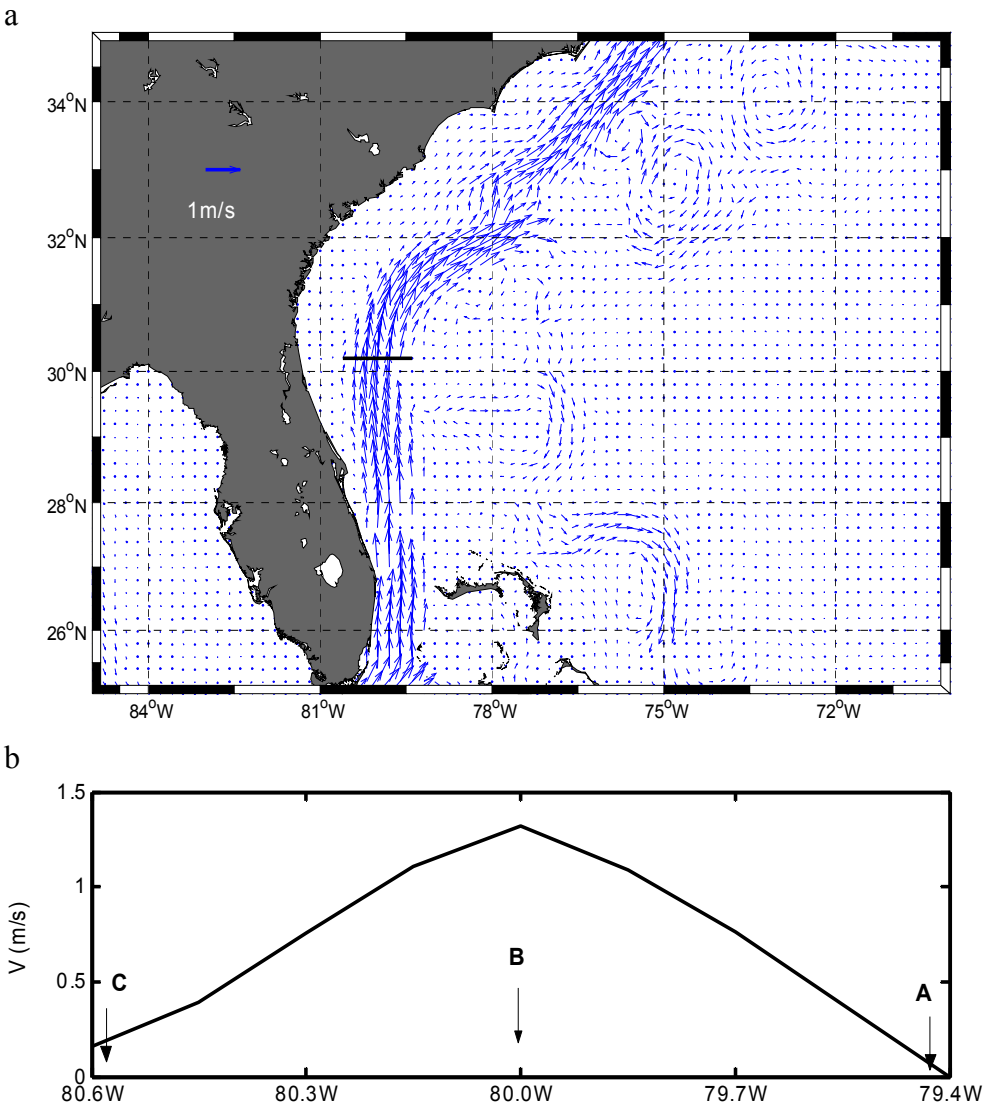

Figure 3.1 a) Computational domain and Gulf Stream current field simulated by HYCOM. One line traversing the Gulf Stream is from 80.6^0W to 79.4^0W longitude and latitude is 30.2^0N; b) The profile of current speed (y direction) along this line.

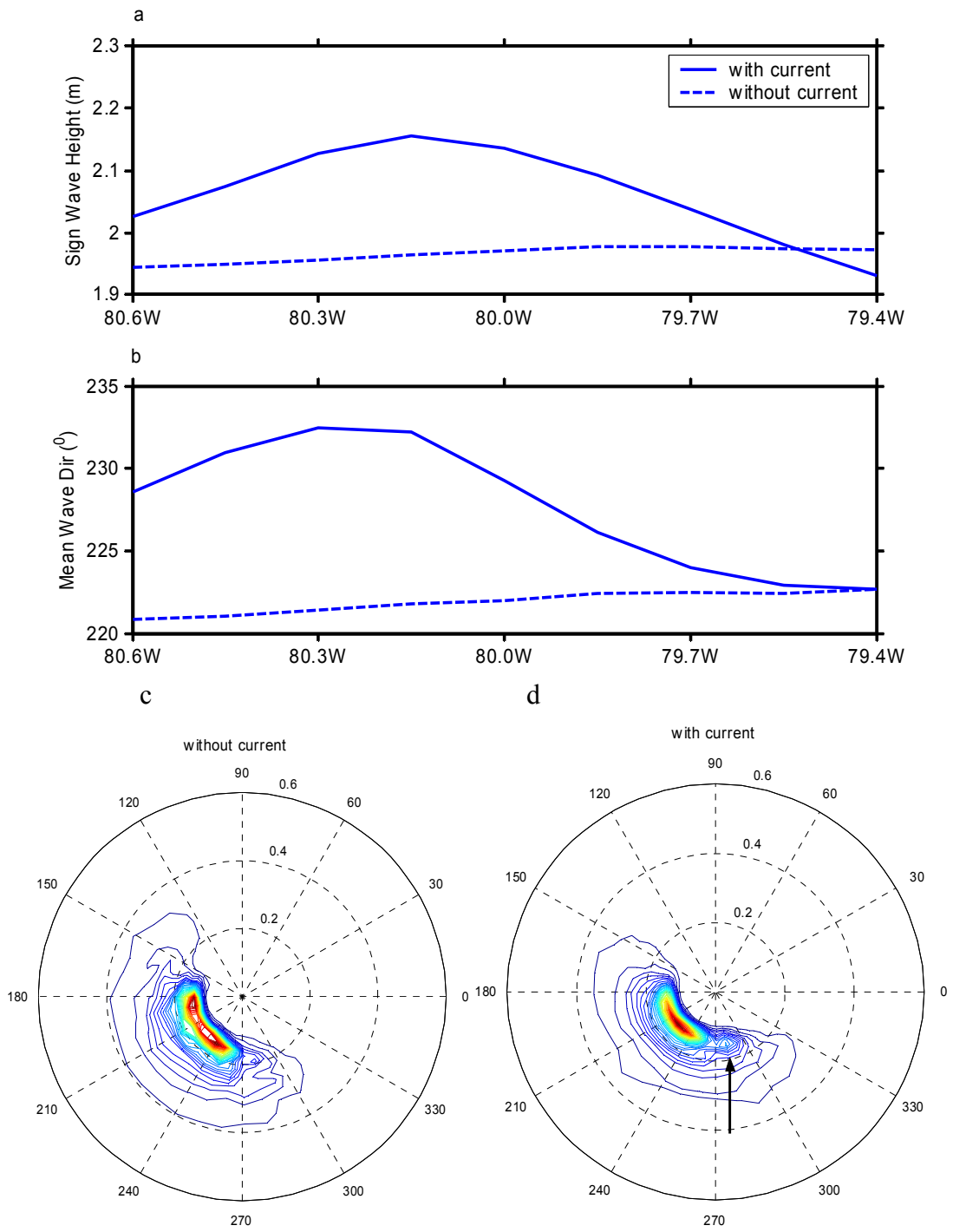

Figure 3.2 a) Significant wave height (NE wind condition) variation between including the effect of the Gulf Stream (Solid line) and without the Gulf Stream (dashed line) along the line; b) Same as a) but for mean wave direction; c) two-dimensional (frequency-direction) spectra of wind waves without current under NE wind condition. The location of this spectra is 80^0 west longitude and 30.2^0 north latitude (location B in Figure 1b); d) same as c) but including current.

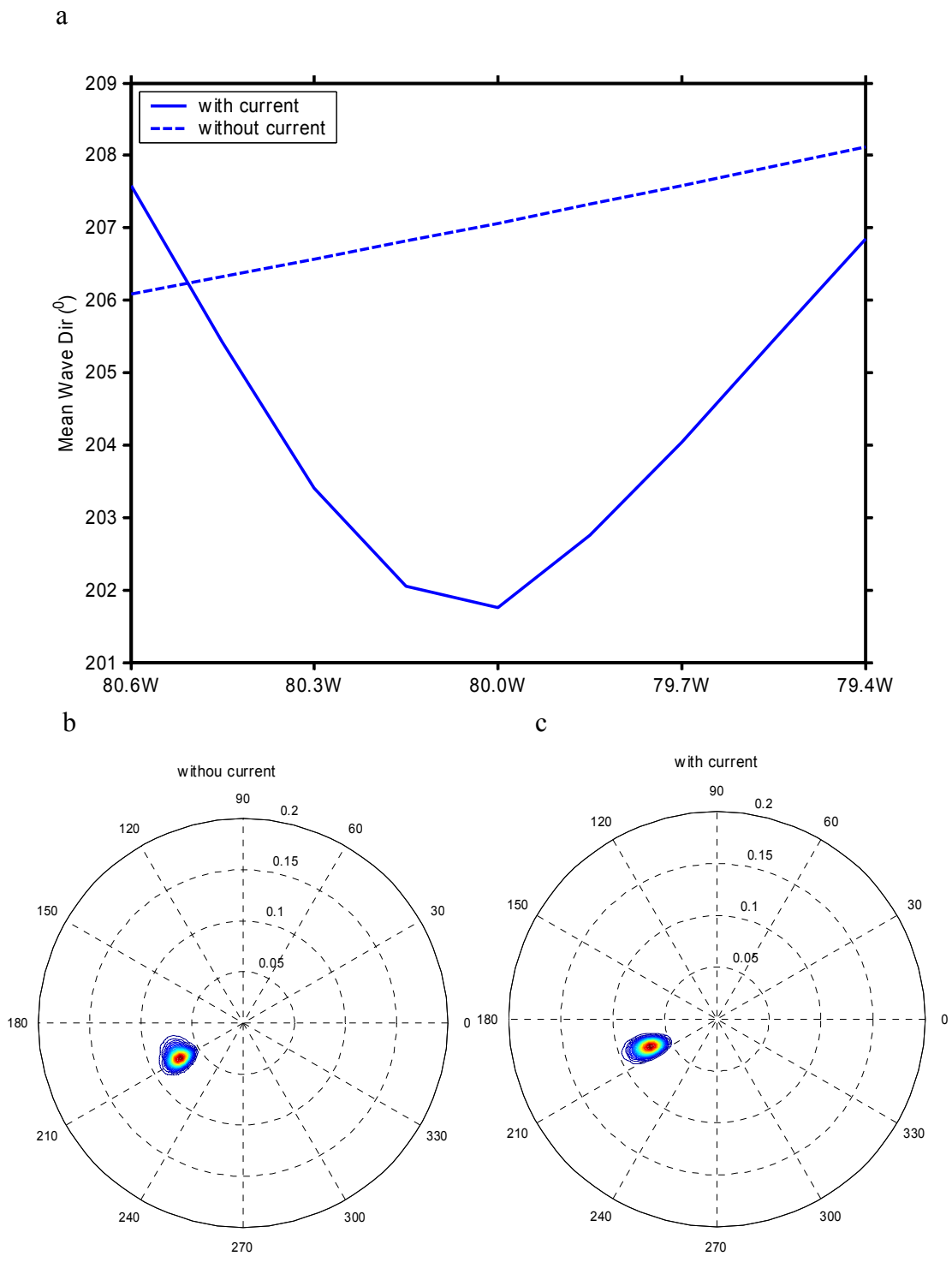

Figure 3.3 a) Same as figure 3.2b but for swell wave case; b) and c) same as figure 3.2c and 3.2d but for swell case

a

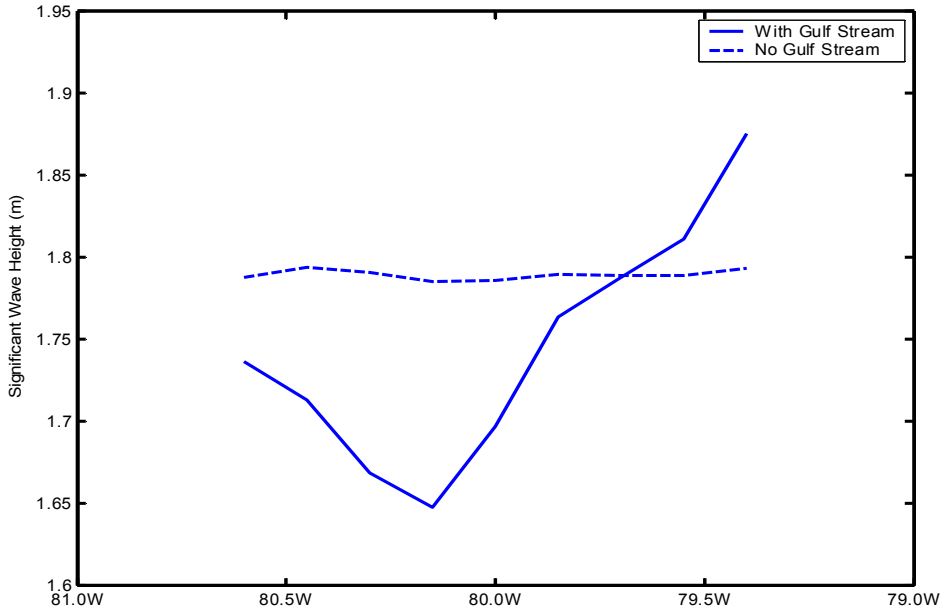

b

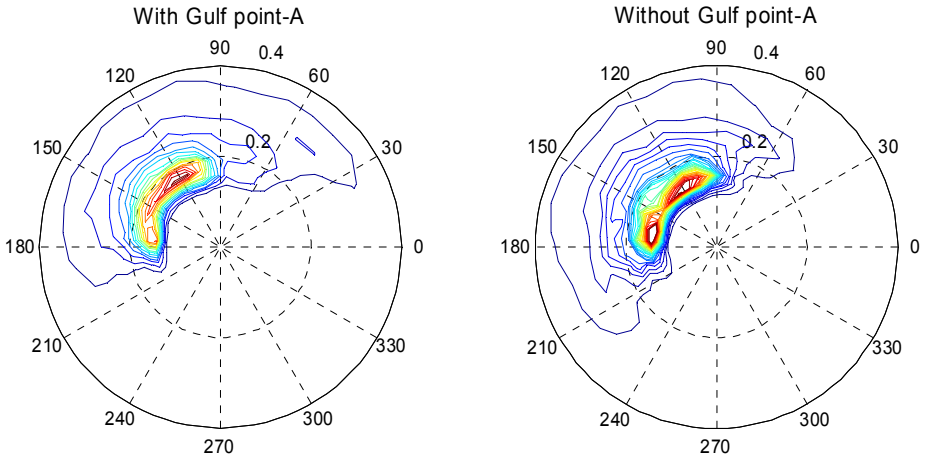

Figure 3.4 a) Same as figure 3.2a but under SE wind condition; b) two-dimensional spectra of wind waves with and without current under SE wind condition at location A (shown in Figure 3.1b); c) same as b but for location B; d) same as b but for location C; e) same as figure 3.2b but under SE wind condition

c

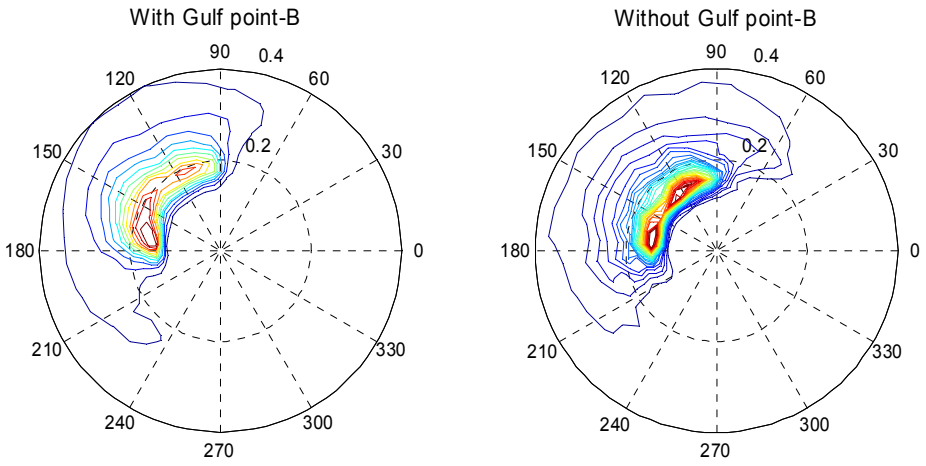

d

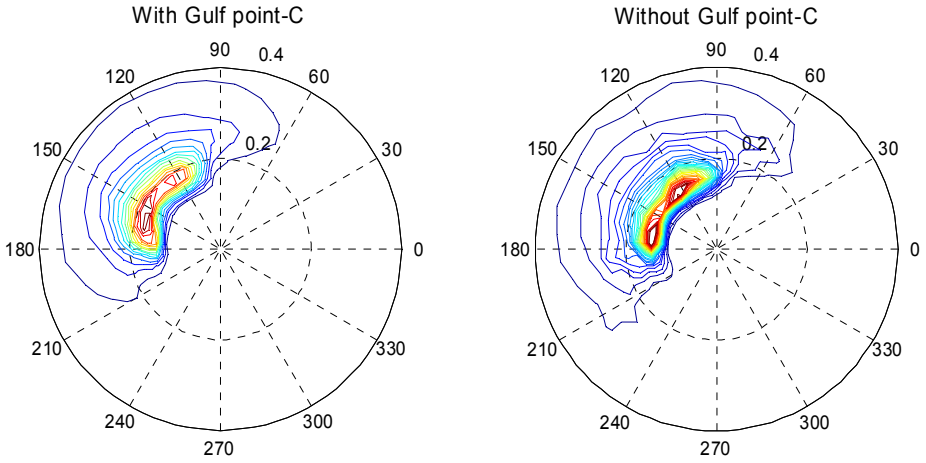

e

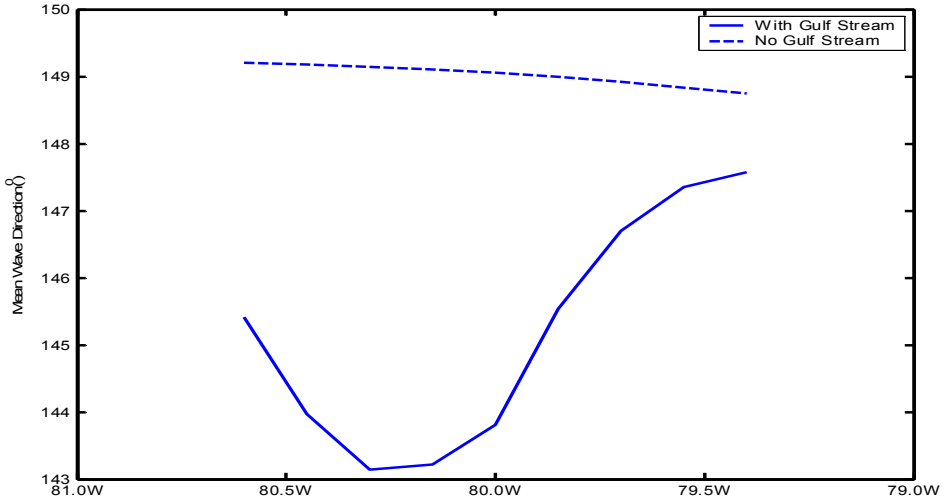

Figure 3.4 (continued)

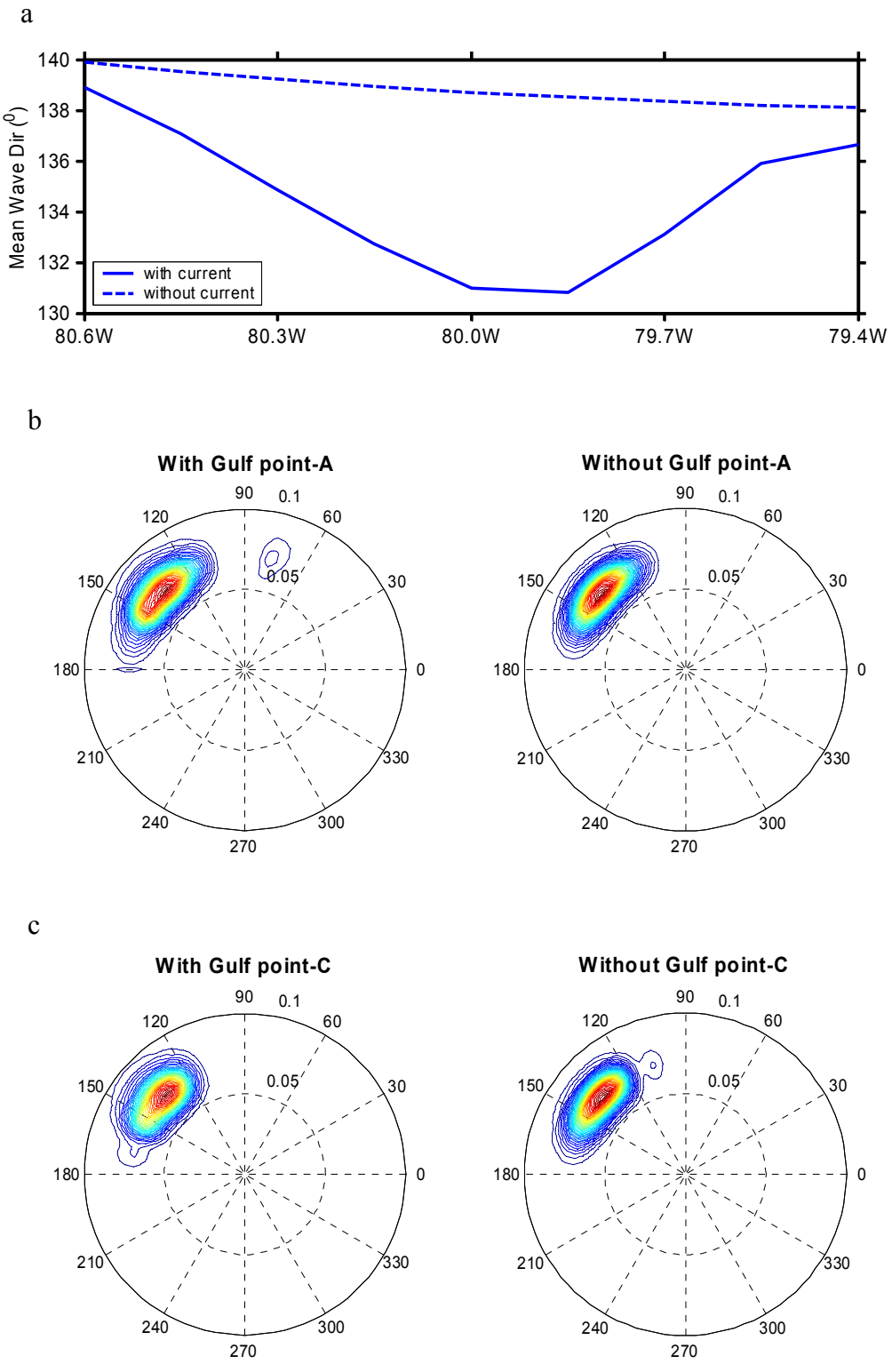

Figure 3.5 a) Same as figure 3.3a but main swell direction is SE; b) and c) same as figure 3.2b and figure 3.2d but for swell case.

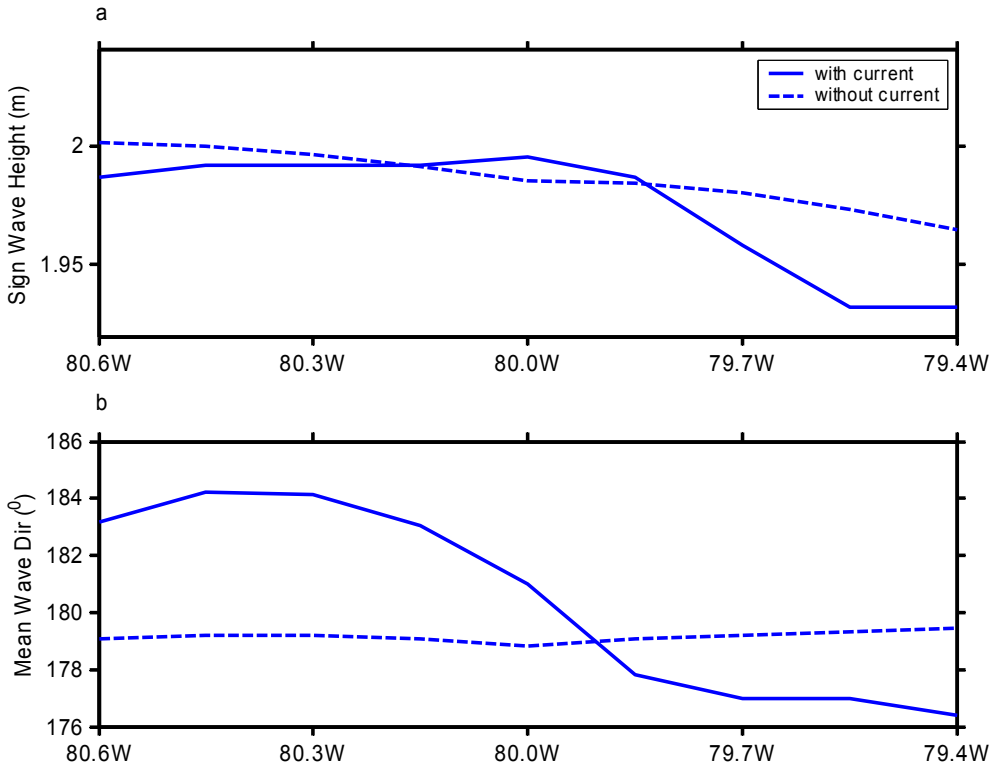

Figure 3.6 a) Same as figure 3.2a but for east wind condition; b) same as figure 3.2b but for east wind condition.

c

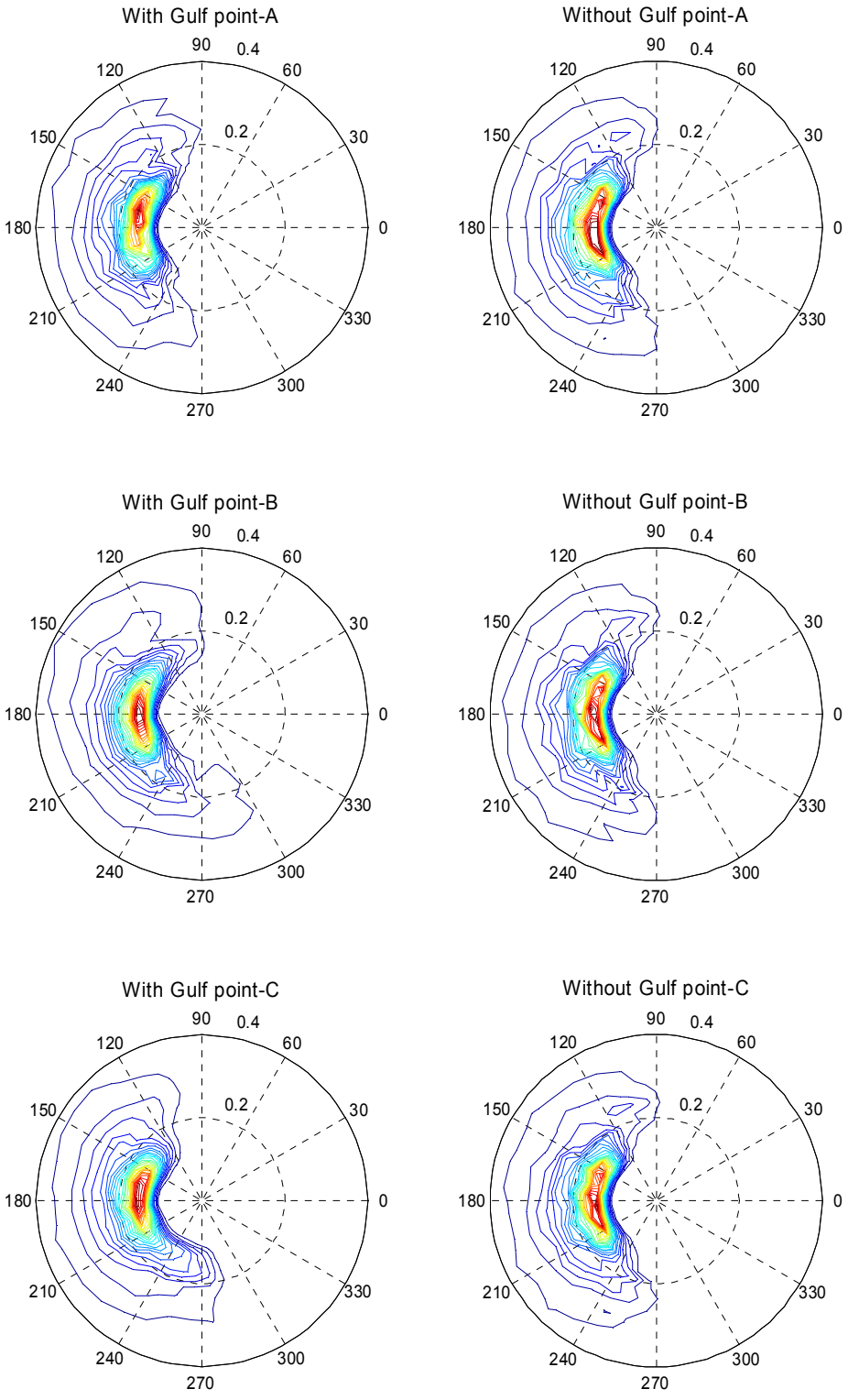

Figure 3.6 (continued)

a

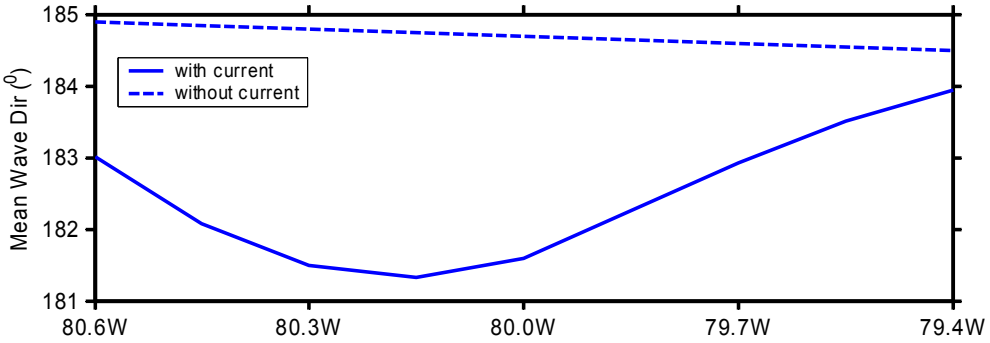

b

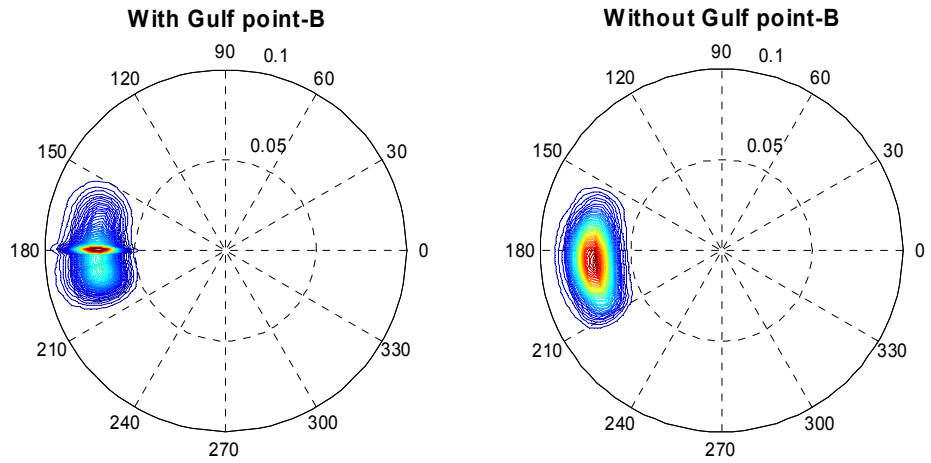

Figure 3.7 a) Same as figure 3.5a but main swell direction is east; b) same as figure 3.5b but for location B and main swell direction is east.

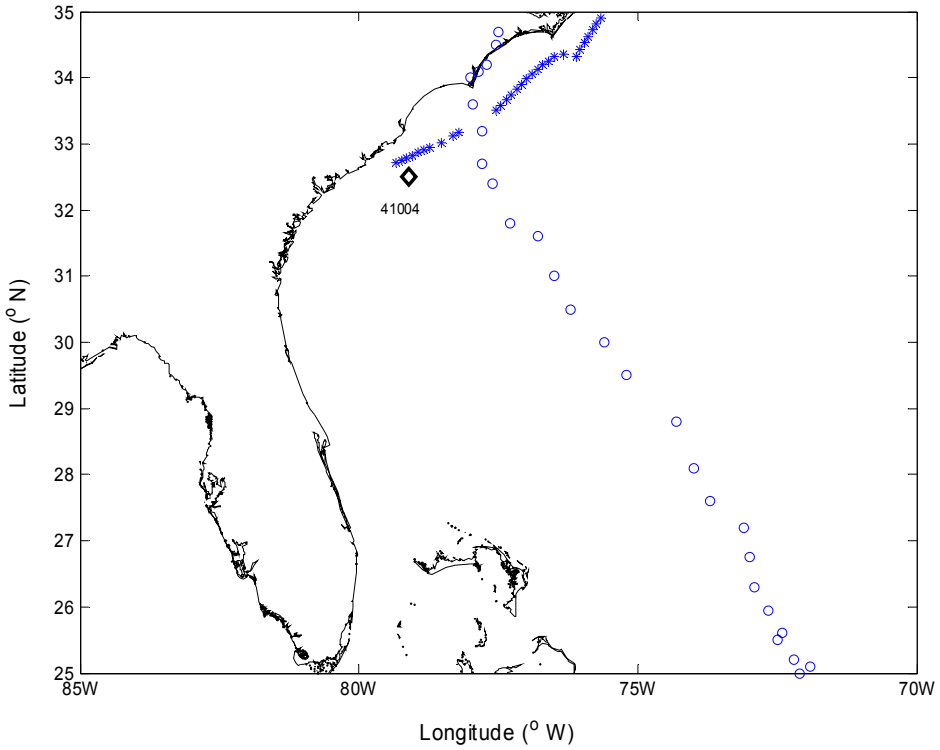

Figure 3.8 The distributions of the best track of hurricane Bonnie (1998), the buoy data station and the observation points of SRA.

a

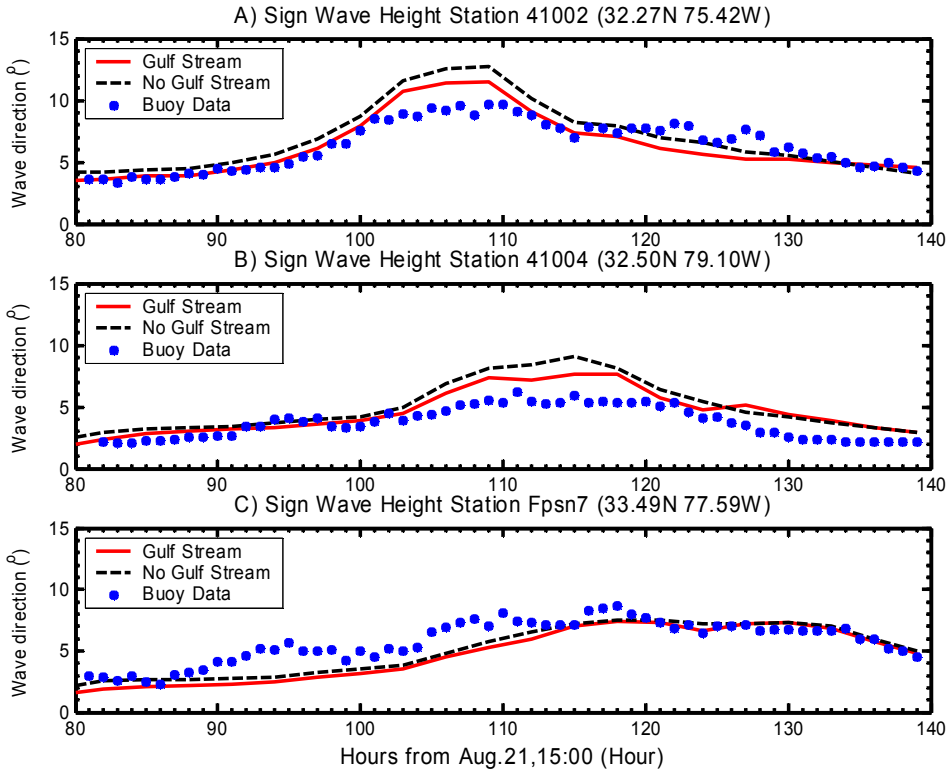

b

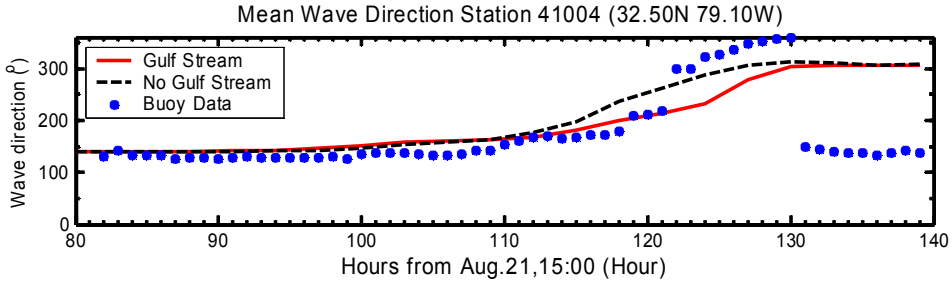

Figure 3.9 a) Significant Wave Height induced by hurricane Bonnie at buoy data station 4-1002, 41004 and Fpsn7. Solid line is the result of SWAN model including the Gulf Stream effect, dashed line is the result of SWAN model without considering the Gulf Stream effect and star point is buoy data.

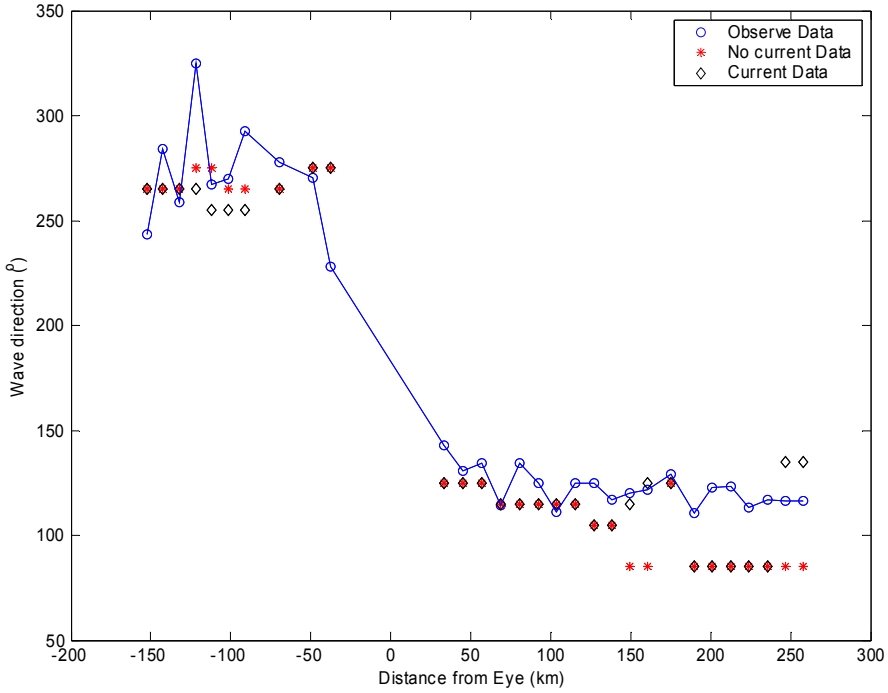

Figure 3.10 The peak wave direction along the sample SRA points under hurricane Bonnie (17:00 UTC 26 Aug. 1998). Blue circle is SRA data, red star represents model results without considering the effect of the Gulf Stream and black square represents model results considering the effect of the Gulf Stream.

References:

Booij, N., Ris, R.C., Hothuijsen, L.H., 1999. A third-generation wave model for coastal regions: 1. Model description and validation. *J. Geophys. Res.* 104 (C4), 7649-7666.

Dysthe, K. B., Refraction of gravity waves by weak current gradients, *J. Fluid Mech.*, 442, 157-159, 2001.

Holland, G.J., 1980. An analytic Model of the wind and pressure profiles in Hurricanes. *Mon. Wea. Rev.*, 108, 121-1218.

Holthuijsen, L. H. and H. L. Tolman, Effects of the Gulf Stream on ocean waves, *J. Geophys. Res.*, 96(C7), 12,775-12,771, 1991.

Holthuijsen, L.H., A. Herman and N. Booij, 2003, Phase-decoupled refraction-diffraction for spectral wave models, *Coastal Engineering*, 49, 291-305.

Hsu, T.-W., S.-H. Ou and J.-M. Liau, 2005, Hindcasting nearshore wind waves using a FEM code for SWAN, *Coastal Engineering,* 52, 177-195.

Hwang, S., The interaction of short surface gravity waves with the Gulf Stream, North Carolina State University Ph.D. dissertation, 1983.

Irvine, D. E. and D. G. Tilley, Ocean wave directional spectra and wave-current interaction in the Agulhas from the shuttle imaging radar-B synthetic aperture radar, *J. Geophys. Res.*, 93(C12), 15,389-15,401, 1988.

Kenyon, Kern E., Wave refraction in ocean currents, *Deep-Sea Res.*, 18, 1023-1034, 1971.

Liu, A. K., F. C. Jackson, E. J. Walsh and C. Y. Peng, A case study of wave-current interaction near an oceanic front, *J. Geophys. Res.*, 94(C11), 16,189-16,200, 1989.

Longuet-Higgins, M. S. and R. W. Stewart, Changes in the form of short gravity waves on long waves and tidal currents. *J. Fluid Mech.*, 8, 565-583, 1960.

Longuet-Higgins, M. S. and R. W. Stewart, Radiation stress and mass transport in gravity waves, with application to "surf-beats", *J. Fluid Mech.*, 13, 481-504, 1962.

Longuet-Higgins, M. S. and R. W. Stewart, The changes in amplitude of short gravity waves on steady non-uniform currents, *J. Fluid Mech.*, 10, 529-549, 1961.

Mapp, G. R., C. S. Welch and J. C. Munday, Wave refraction by warm core rings, *J. Geophys. Res.*, 90(C4), 7153-7162, 1985.

Mathiesen, M., Wave refraction by a current whirl, *J. Geophys. Res.*, 92(C4), 3905-3912, 1987.

Meadows, G. A., R. A. Shuchman, Y. C. Tseng and E. S. Kasischke, Seasat synthetic aperture radar observations of wave-current and wave-topographic interactions, *J. Geophys. Res.*, 88(C7), 4393-4406, 1983.

Padilla-Hernandez, R. and J. Monbaliu, 2001, Energy balance of wind waves as a function of the bottom friction formulation, *Coastal Engineering,* 43, 131-148.

Rogers, W.E., P.A. Hwang and D.W. Wang, 2003, Investigation of wave growth and decay in the SWAN model: three regional-scale applications, *J. Phys. Oceanogr.*, 33, 366-389.

Sheres, D., K. E. Kenyon, R. L. Bernstein and R. C. Beardsley, Large horizontal surface velocity shears in the ocean obtained from images of refracting swell and in situ moored current data, *J. Geophys. Res.*, 90(C3), 4934-4950, 1985.

Simons, R. R. and R. D. Maciver, Wave refraction across a current with strong horizontal shearing, *Proceedings 26th International Conference on Coastal Engineering*, Copenhagen, Denmark, June 1998. ASCE 692 – 705.

Treloar, P. D., Spectral wave refraction under the influence of depth and current, *Coastal Engineering*, 9, 439-452, 1986.

Trulsen, G. N., K. B. Dysthe and J. Trulsen, Evolution of a gravity wave spectrum through a current gradient,*J. Geophys. Res.*, 95(C12), 22,141-22,151, 1990.

Wolf, J. and D. Prandle, Some observations of wave-current interaction, *Coastal Engineering*, 37, 471-485, 1999.

Xie, L., L. J. Pietrafessa and K. Wu, A numerical study of wave-current interaction through surface and bottom stresses: Coastal ocean response to Hurricane Fran of 1996, *J. Geophys. Res.*, 108(C2), 3049-3167, 2003.

CHAPTER 4. SENSITIVITY OF NEAR-SHORE WIND WAVES TO HURRICANE WIND ASYMMETRY AND TRANSLATION SPEED

4.1. Introduction

Waves generated by hurricanes can exceed 20 meters in deep open ocean waters. Wang et al. [2005] reported that the maximum significant wave height (SWH) reached 27.7 meters during the passage of Hurricane Ivan. Although SWH is lower when waves reach shallow waters, these waves can devastate the coastal zone. It is well known that hurricane-induced waves are one of the most damaging phenomena during the passages of hurricanes. Severe wave conditions are dangerous to vessels in ocean and coastal waters, and waves can also run up over the storm surge in the coastal zone to cause more severe damage along and on the coast. So the ability to predict hurricane-induced waves precisely is a very important challenge and is of great value to many user communities. As the wind is the principal source of energy creating and driving waves, in order to forecast hurricane-induced ocean surface waves, it is necessary to establish a thorough understanding of how the wave field manifests itself in response to the spatial and temporal variation of hurricane winds.

During the 1950s, the resonance mechanism [Phillips, 1957] and the feed-back mechanism [Miles, 1957] of how wind energy is transferred to waves were developed. Most of the present community wave models [e.g., WAM by the WAMDI Group, 1988; and

SWAN by Booij et al., 1999] still use the concepts introduced by the pioneering works of Phillips and Miles as the mechanisms of wind energy input into ocean surface waves. These two wave models have been verified and used to forecast waves, hind cast waves and in wave-current interaction analyses over many oceans around the world [WAMDI Group, 1988; Komen et al., 1994; Xie et al., 2001; Booij et al., 1999; and Ris et al., 1999].

There have been a number of past studies on the response of wind waves to tropical cyclones including data analysis and numeric model studies. Wright et al. [2001] and Walsh et al. [2002] provided all quadrants of sea surface directional wave spectrum in the open water (Aug. 24, 1998) and at landfall (Aug. 26, 1998) during hurricane Bonnie using the NASA airborne scanning radar altimeter data. They found that the dominant waves generally propagated at significant angles to the downwind direction, and developed a simple model to predict the dominant wave propagation direction. Recently, Young [2006] studied the directional wave spectrum during the passage of several hurricanes using wave buoy observations and showed that in almost all quadrants of the storm, the dominant waves are remotely generated swells. In the meantime, Ou et al. [2002] used SWAN to simulate typhoon-induced waves in the coastal waters of Taiwan. Their results showed that waves under typhoon forcing can be reasonably well simulated by the SWAN wave model. Moon et al. [2003] simulated the surface wave spectra under hurricane wind forcing using a high resolution WAVEWATCH III model [Tolman, 1991]. They showed that numerical simulation results agree reasonably well with observational data. Furthermore, they also analyzed the effect of hurricane translation speed on the wave spectra. However, their study focused on the analysis of a specific case. Moon et al. [2004] investigated the effect of sea

surface waves on air-sea momentum flux during the passages of tropical cyclones. A remaining issue which has received little attention in the past is the sensitivity of surface wind waves to the spatial and temporal variations of tropical cyclone winds. In order to address this issue, a suite of numerical experiments are designed to quantify the influence of wind distribution, storm translation speed and intensity on ocean surface wind waves using SWAN. Additionally, two historical hurricane cases (Hurricane Bonnie, 1998 and Floyd, 1999) are studied to quantify the effects of actual hurricane structure and background wind field on waves. A brief description of the SWAN model and parameteric hurricane wind models are given in subsection 4.2. Subsection 4.3 describes the model experiments. Results are presented in subsection 4.4, followed by discussions and conclusions of this chapter.

4.2. Model Description

4.2.1 The SWAN Wave Model

The SWAN model is based on the wave action balance equation (or energy balance in the absence of currents) with sources and sinks. In SWAN the evolution of the wave spectrum is described by the spectral action balance equation, which for Cartesian coordinates [e.g., Hasselmann et al., 1973] is:

$$\frac{\partial}{\partial t}N + \frac{\partial}{\partial x}C_x N + \frac{\partial}{\partial y}C_y N + \frac{\partial}{\partial \sigma}C_\sigma N + \frac{\partial}{\partial \theta}C_\theta N = \frac{S}{\sigma} \tag{4.1}$$

Where N is the action density $(N(\sigma, \theta) = E(\sigma, \theta)/\sigma)$, E is the energy density spectrum and σ is the relative frequency. C_x, C_y and C_σ are propagation velocities in x-, y-, σ- and θ-space

respectively. S is the source term that represents the effects of generation, dissipation and nonlinear wave-wave interactions. The governing equation is expressed in spherical coordinates is:

$$\frac{\partial}{\partial t}N + \frac{\partial}{\partial \lambda}C_{\lambda}N + (\cos\varphi)^{-1}\frac{\partial}{\partial \varphi}C_{\varphi}\cos\varphi N + \frac{\partial}{\partial \sigma}C_{\sigma}N + \frac{\partial}{\partial \theta}C_{\theta}N = \frac{S}{\sigma} \tag{4.2}$$

Where λ and φ represent longitude latitude respectively.

Depth-induced wave breaking is an integral part of SWAN, and is expressed by the following formula in the source term:

$$D_{tot} = -\frac{1}{4}\alpha_{BJ}Q_b(\frac{\overline{\sigma}}{2\pi})H_m^2$$

In which $\alpha_{BJ} = 1$ and D_{tot} is the mean rate of energy dissipation per unit horizontal area due to wave breaking. It is based on the bore-based model of Battjes and Janssen [1978]. Q_b is the fraction of breaking waves determined by: $\frac{1-Q_b}{\ln Q_b} = -8\frac{E_{tot}}{H_m^2}$ where H_m is the maximum wave height that can exit at the given depth. The depth-induced wave breaking process is included in SWAN, which implies that the computations are more realistic in shallow water.

4.2.2 Hurricane Models

Two hurricane wind models are employed in this chapter to simulate hurricanes, one is the symmetric Holland [1980] model (hereafter referred to as H1980) and the other is asymmetric Holland-NCSU model [Xie et al. 2006] (referred to as HN2006 hereafter). In

H1980 , the wind speed as a function of radial distance from the center of the storm is described as

$$V_a = [AB(P_n - P_c)\exp(-A/r^B)/\rho_a r^B]^{1/2} \tag{4.3}$$

where V_a is wind speed at radius r, P_c is the central pressure, P_n is the ambient pressure, and A, B are scaling parameters ($A = (R_{\max})^B$). Wind field parameters used in equation (4.3) were obtained from the National Hurricane Center (NHC), National Oceanic and Atmospheric Administration (NOAA).

The other hurricane wind field used in this study is obtained by combining an asymmetric hurricane wind field produced by HN2006 with the background wind field. In the asymmetric hurricane wind model R_{max} in Equation (4.3) was modified to be a polynomial function of the azimuthal angle θ:

$$R_{\max}(\theta) = P_1\theta^{n-1} + P_2\theta^{n-2} + \ldots + P_{n-1}\theta + P_n \tag{4.4}$$

B and R_{max} in Equation (4.3) are then optimized using available observational data, wind analysis or forecast guidance. The background wind field was obtained by removing the hurricane vortexes in the Eta Data Assimilation System (EDAS) data, which are often coarse and weak, using a cylindrical filtering operator [Kurihara et al. 1993]. Then the optimized asymmetric hurricane wind field described above was incorporated into the background wind field to produce the total wind field [Bao et al., 2006].

4.3. Experimental Designs

Four experiments are designed to investigate the effect of Hurricane translation speed, intensity and structure on the wave field. The experiments are listed in **Table 4.1**. Hurricane wind fields for these experiments are simulated by H1980 for symmetric wind cases and by HN2006 for the asymmetric hurricane cases as well as for Hurricane Bonnie in 1998 and Floyd in 1999. For symmetric hurricane experiments, an idealized domain and bathymetry are assumed, which is 1500 km in the x direction and 3000 km in the y direction. The water depth is set to a constant 5000 m for convenience. The moving direction of the hurricanes is from south to north. The domain for the asymmetric hurricane experiments will be shown in the next subsection.

In Exp. A, fifteen hurricane cases are used to explore the effect of the hurricane translation speed on waves. All fifteen hurricanes have the identical intensity (same central pressure) but travel at different translation speeds. The effect of hurricane intensity on waves is investigated in Exp. B, as the hurricane translation speed is set to 0 and different central pressures are assumed. Next, the combined effects of hurricane intensity and translation speeds on waves are examined in Exp. C. Finally, the effects of hurricane wind field structure and background wind field on waves are investigated in Exp. D which includes real hurricane cases of Hurricane Bonnie [1998] and Floyd [1999]. The observed hurricane translation speed and center pressure are used in these two cases. Hurricanes in Exp. A, B and C have the same Radius of Maximum Wind (RMW).

4.4. Results and explanations

4.4.1. The effect of hurricane translation speed on waves

The distributions of SWH driven by symmetric hurricanes with different translation speeds (Exp. A) are shown in **Fig. 4.1**. **Figure 4.1** also displays the SWH differences between each case and the SWH generated by a static hurricane. These SWHs are plotted at locations within a distance of 300km from the center of the hurricane. **Figure 4.1** shows that the SWH in the front-right quadrant of the storm track increases, while that in the rear-left quadrant becomes decreases, with increasing hurricane translation speed. This result is consistent with the findings of Moon et al. [2004]. From these figures, it is implied that hurricane translation speed can cause the asymmetric structure of waves regardless of whether the hurricane is symmetric or asymmetric.

It is worth noting that, initially the hurricane translation speed increases from 0 to 12 m/s, the SWH in the front-right quadrant of the storm track also increases, but when the translation speed exceeds 13 m/s, the SWH begin to decrease. To illustrate this trend, the SWH values of waves generated by hurricanes moving with different translation speeds for a point in the first quadrant one RMW from the storm center (Point A in **Fig. 4.2**), and a point located in the third quadrant, also one RMW away from the storm center (Point B in **Fig. 4.2**) are plotted in **Fig. 4.3**. Note that Point A is located at 45^{o} (fron-right), while Point B is 235^{o} (rear-left) of the storm. It can be seen that the SWH at Point A monotonically increases with the translation speed from 0 to 12 m/s, but begins to drop when the translation speed exceeds

13 m/s. This phenomenon can be explained by the following resonance theory proposed by King and Shemdin [1978], [Young 1988, Bowyer and MacAfee 2000, Moon et al. 2003]: waves to the right of the hurricane track are exposed to the prolonged forcing of winds, and as the hurricane translation speed becomes comparable to the group speed of the dominant waves, those waves essentially become trapped within the hurricane and there appears to be resonance between swells produced previously by the hurricane and the locally generated wind waves. **Figure 4.4** shows one dimensional directional spectrum at Point A. It can also be seen from **Figs. 4.4a-g** that wave energy increases with increasing translation speed. However, it shows the presence of only one spectrum energy peak, which is located near 100°, because the direction of swells (**Fig**. **4.6**) is similar with the direction of local wind-generated waves at Point A. The notion that waves in the forward quadrants of storm are being dominated by swell is also verified by observational data [Wright, et al., 2001 and Young, 2006]. Alternatively, as the hurricane translation speed becomes greater than the group speed of the dominant waves, the waves to the right of the hurricane track are less likely to be trapped within the influence of the hurricane. Hence, swells at location produced previously can not reach the same location when the hurricane reaches that location. In other words, there is no resonance effect at the front-right quadrant of the hurricane, and as a result, wave energy starts to decrease at Point A (**Fig**. **4.4h**).

The situation at Point B is exactly the opposite. At the beginning, the SWH at the rear-left of hurricane decreases monotonically with increasing hurricane translation speed (**Fig. 4.3b**). However, it will start to increase when the translation speed reaches at about 7m/s. Furthermore, the SWH at Point B generated by the hurricane with translation speed at (or in

excess of) 11 m/s will be higher than that induced by a static hurricane (**Fig**. **4.3b**). In contrary, SWH to the left of the hurricane track are reduced as hurricane translation speed increases at the beginning. **Figure 4.5** shows the one dimensional directional spectrum of Point B. It can be seen from **Figs. 4.5a-d** that the major wave spectrum energy is located between 270^0 and 360^0, which is the same as the local wind direction. In other words, SWH is mainly contributed from locally-generated wind waves because the waves are not trapped when the storm translation speed is below of the group speed of the dominant waves. Therefore, SWH of locally-generated wind waves are reduced at the beginning (**Figs. 4.5a-d**) due to reduced forcing time as the waves propagate against the hurricane moving direction. However, as the hurricane translation speed becomes greater than the group speed of the dominant waves, the waves to the left of the hurricane track are more likely to be trapped in the hurricane region. Same as the above explanation, this is caused by the resonance between the swells and the locally generated wind waves. It can be explained by using **Figs. 4.5e-h**. There is another part of energy, which is located between 100^0 and 140^0, added to the wave spectrum. It is obviously that this part of wave energy does not come from local wind generated waves, but comes from swells transported from some distance. Therefore, the SWH at Point B increases as the hurricane translation speed increases to a critical value 7-8 m/s in the case considered here.

The reason why the two critical values of Point A and Point B are different can be explained by using **Fig. 4.6**. **Figure 4.6** shows a schematic picture of swell (of Point A and Point B) propagating in the direction tangential to the circle defined by the RMW at an earlier position of the storm. This schematic picture is based on the assumption that the swell

is generated from the earlier position of the storm and the propagation direction of the swell at each point is determined by the waves propagating in the direction tangential to circle of RMW at the earlier position of the storm (**Fig. 4.6**) [Moon et al. 2003]. It is obvious that the swell propagating speed in the north direction (storm propagating direction) of Point B is slower than that of Point A, in which we assume all the swells haves the same propagating velocity. Therefore, the locally-generated wind waves would catch up with the swells at Point B sooner than those at Point A.

4.4.2. The effect of hurricane intensity of waves

In Exp. B, three static hurricanes with different center pressure (intensity) were used to investigate the effect of hurricane intensity on waves. One is a strong hurricane whose central pressure is 953 hpa (Maximum Wind Velocity, MWV is 44m/s), the second is a moderate hurricane whose central pressure is 963 hpa (MWV=39 m/s) and the third is a weak hurricane whose central pressure is 973 hpa (MWV=34 m/s). The SWH at locations A and B, as indicated in **Fig. 4.2**, is shown in **Fig. 4.7** for the three different hurricane cases. It is obvious that the SWH at two of the points indicated in **Fig. 4.2** increases with hurricane intensity and the intensity of hurricane does not the asymmetric structure of waves.

The question is what would the combined effects of hurricane intensity and translation speed be on the SWH of the wave field? The answer is simple when the hurricane is static. However, if the hurricane is moving, then the question becomes: is there any relationship

between the effect of intensity and that of the storm translation speed? This question will be addressed in the next section.

4.4.3. The effect of the combining the hurricane intensity and translation speed on waves

In this part, we will examine how waves can vary with varying hurricane intensity and translation speed. Different hurricanes with translation speeds at 0, 1, 2, 3, 4 and 5 (m/s), each of which has different central pressures, were used in Exp. C (**Table 4.1**). We now examine whether or not the effect of the hurricane translation speed on waves depends on hurricane intensity. The normalized SWH difference (NSD) between C2 (C3, C4, C5 or C6) and C1 at locations A and B is defined as

$$NSD = \frac{SWH_{ci} - SWH_{c1}}{SWH_{c1}} \times 100\%$$

It was used to represent the impact of hurricane translation speed on waves where SWH_{ci} represents the SWH in experiments C2, C3 C4, C5 or C6 and SWH_{c1} represents the SWH in Exp. C1. **Figure 4.8** shows that the NSD at locations A and B (refer to **Fig. 4.2**) varies with different intensity and translation speed. It is obvious that NSD decreases with increasing the intensity of hurricanes at location a (**Fig. 4.8a**) and at location b (**Fig. 4.8b**). The results imply that the effect of the hurricane translation speed on waves decreases with increasing intensity of the hurricane. The percentage of increasing at front-right of hurricanes is reduced and meanwhile the percentage of decreasing at rear-left of hurricanes increased. In other

words, its impact on the asymmetry of the wave field decreases with increasing intensity of the hurricane.

The mechanism used in subsection 4.4.1 can also be applied here to explain this phenomenon. The influence of hurricane translation speed on waves is mainly due to the possibility of interaction (resonance) between local wind-generated waves and swells induced by previous wind. The locally generated waves will be large and dominate for an intense hurricane, and the relative effect of swells would be less important than under the situation of a weak hurricane.

4.4.4. The effect of the hurricane wind field structure on the waves

Actual hurricanes in nature are usually not symmetric in either wind speed or shape. In all previous experiments (A, B, C), symmetric hurricanes are used. In this subsection, the effect of an asymmetric hurricane wind field on hurricane-induced wave field will be examined. It is important to quantify the effect of wind asymmetry on surface wind waves in order to provide either a justification for the current practice of using symmetric hurricane wind model for wave forecasting, or recommend the use of asymmetric wind model. To evaluate the effects of wind asymmetry on waves, two hurricane wind models are employed to simulate Hurricane Bonnie's (1998) wind field. One is assumed to be symmetric, as simulated by the H1980, and the other to be asymmetric as simulated by HN2006. These simulations are referred to as Exp. D. The hurricane central pressure, translation speed and RMW are obtained from the NOAA "best track" database.

As Exp. D assumes an actual hurricane forcing, the domain is different from that used for the idealized cases in Exps. A, B, and C. **Figure 4.9** shows the model domain, extending latitudinally from 25^{o} to 35^{o} north and longitudinally from 85^{o} to 70^{o} west. Bottom topography is derived from the ETOP5 bathymetry database. The tracks of Bonnie and Floyd, which were used in the experiment, are also shown in **Fig. 4.9**. The track data is provided by the NOAA "best track" database. **Figure 4.9** also shows the distribution of buoy stations, whose data was used to compare with the model results.

Figure 4.10 displays the distribution of two hurricane wind fields and the difference between them at 18:00 of Aug. 25 1998 in the model domain. It is obvious that wind speeds to the front right of the hurricane track in the asymmetric hurricane are higher than those in the symmetric hurricane. Meanwhile, wind speeds to the rear left of the hurricane track in the asymmetric hurricane are weaker than those in the symmetric hurricane. Intuitively, this asymmetric wind speeds distribution would cause the waves to be stronger in the front right areas and weaker in rear left areas than those generated by the symmetric hurricane. The distribution of SWH generated by these two hurricane wind fields and the difference between them are shown in **Figs. 4.11a-c**, respectively. It is apparent that the differences among them mainly appear in the front right and rear left quadrants. The SWH generated by the asymmetric hurricane are higher than that induced by the symmetric hurricane in front right areas. In contrast, the SWH are lower in the rear left areas. These differences evidently reflect the asymmetry of the wind speeds. In other words, more wind speed asymmetry causes more asymmetric structure of waves.

The above analysis clearly indicates the influence of asymmetric hurricane wind structure on waves. Presumably, the asymmetric hurricane wind model (HN2006) should produce more accurate wave forecasts. To assess the performance of the wave model driven by the asymmetric, as opposed to the symmetric, hurricane winds, the SWH generated by the two hurricane wind fields and the SWH obtained from the observational data at the different buoy stations are compared (**Fig. 4.12**). The comparison shows that the SWH generated by the asymmetric hurricane (HN2006) resembles more closely to the buoy data than do that generated by the symmetric hurricane (H1980), especially at the Fpsn7 station (shown in **Fig.4.9**), which is located on the right side of Bonnie's track. The wind speed at station Fpsn7 is stronger than that at a point the same distance to the left of Bonnie's track. The SWH simulated by the asymmetric wind field agrees very well with the observational data. Compared to the results from the asymmetric wind model, the SWH produced by the symmetric wind field shows a much larger difference from the observations taken at station Fpsn7, clearly indicating an under-prediction.

4.4.5. The effect of background wind field on waves

In this subsection, the effect of background wind field on waves will be investigated by using hurricane Floyd (1998) as an example. Two hurricane wind models are employed to simulate Hurricane Floyd's (1998) wind field. One is symmetric as simulated by the H1980, and the other is asymmetric as simulated by HN2006, but also incorporates the background

wind field. The domain and settings of the parameters used in SWAN wave model are the same as in Section 4.4.4.

In general, parametric hurricane wind models such as H1980 or HN2006 do not include environmental wind field. Thus, the simulated wind field will be zero before the front edge of a hurricane reaches the model domain. The actual wind field, however, won't be zero even if its effect doesn't reach the domain because of the presence of an environmental wind field. This phenomenon can be obviously seen from **Fig. 4.13**. It shows the wind speed simulated by two hurricane wind models as compared to the observed wind speeds at different buoy stations. The wind speed simulated by H1980 is almost zero at the beginning (spin-up) (**Fig. 4.13**), but the actual wind speed measured by the buoy is clearly not zero. The waves driven by winds simulated by H1980 is close to zero which is clearly unrealistic before the storm winds enter the domain (**Fig. 4.14**). On the other hand, the wind speed modeled by HN2006 with a merged background wind field is much closer to the observations during the early hours (**Fig. 4.13**). **Figure 4.14** also shows the SWH generated by the two hurricane wind fields and the SWH obtained from the observational data at different buoy stations. These figures show that the SWH produced by the merged hurricane and background wind field is much more realistic than that generated by H1980 alone, particularly during the early hours.

4.5. Discussion and conclusions

In this chapter, the effect of hurricane wind distribution, translation speed, intensity, and

background wind field on sea surface wind waves was examined by using the SWAN wave model.

The results suggest that the hurricane translation speed makes a significant contribution to the asymmetric structure of the waves. Furthermore, the translation speed can enhance the value of the SWH in the front-right quadrant of the hurricane track because of the resonance effect. This effect is significant when the hurricane translation speed increases to become comparable to the group speed of the dominant waves; but weak when the hurricane translation speed is much larger or less than the group speed of the dominant waves. On the other hand, it can reduce the value of the SWH in the rear-left quadrant of the hurricane track because of a lessening of the wind forcing time and effective fetch. However, it will gain some wave energy when the hurricane translation speed increases to the level that is comparable to the group speed of the dominant waves.

The effect of hurricane intensity on waves is found to be such that SWH increases with increasing wind speed. On the other hand, the hurricane translation speed causes less asymmetry for more intense hurricanes than for weaker storms. Another factor affecting the structure of the wind waves is the asymmetric distribution of hurricane winds. Considering the actual asymmetric structure of a hurricane can considerably alter the SWH distribution produced by the hurricane and improve the skill of wind wave prediction. The effect of background wind field on waves can be significant before the effect of hurricanes reaches the forecast domain. Thus, the prediction of the wave SWH can be improved by merging the environmental wind field into the hurricane wind field.

Table 4.1 Experimental designs

Expt name		HTS(m/s)	Center Pressure (intensity)(hpa)	Structure
A		From 0 to 14 Interval=1m/s	963	Symmetric
B		0	953 963 973	Symmetric
C	C1	0	953 963 973	Symmetric
	C2	1	953 963 973	
	C3	2	953 963 973	
	C4	3	953 963 973	
	C5	4	953 963 973	
	C6	5	953 963 973	
D		Varying	Varying	Symmetric Asymmetric

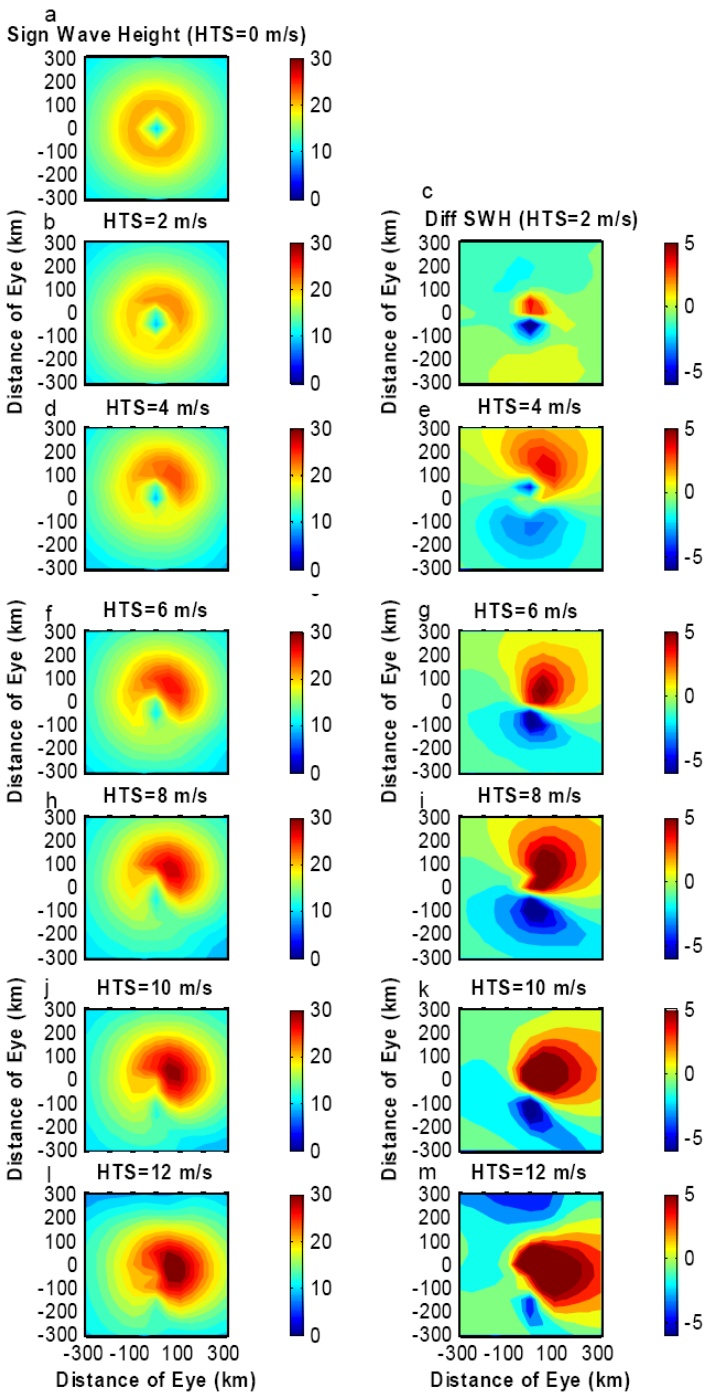

Figure 4.1 The distribution of significant wave height (SWH) driven by static symmetric hurricanes (a) and symmetric hurricanes with different translation speeds b) 2 m/s; d) 4 m/s; f) 6 m/s; h) 8 m/s; j) 10 m/s; i) 12 m/s and different SWH differences between them and these generated by the static hurricane c) 2 m/s; e) 4 m/s; g) 6 m/s; i) 8 m/s; l) 10 m/s; m) 12 m/s.

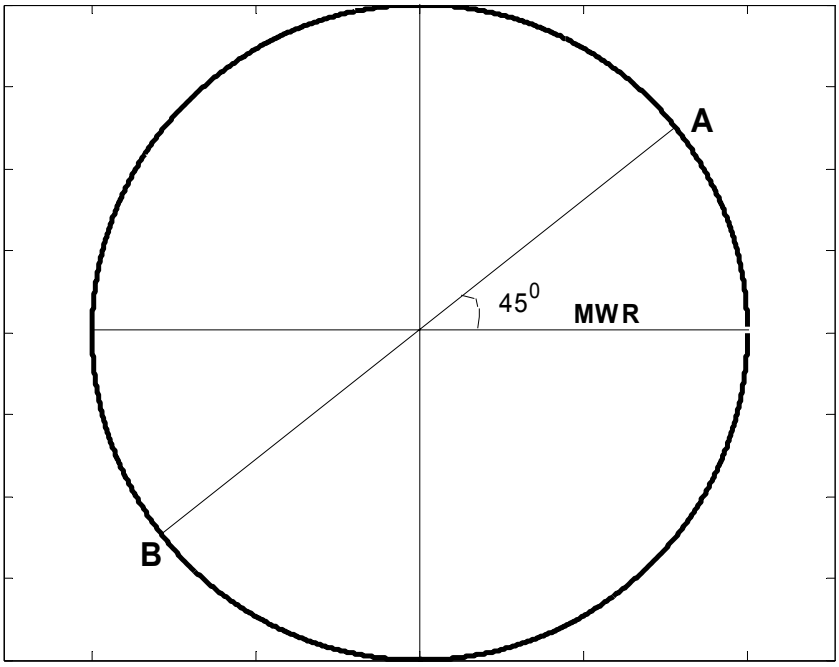

Figure 4.2 The locations of two points. Point ‘A’ locates in the first quadrant one RMW from the storm center, while point ‘B’ locates in the third quadrant, also one RMW away from the storm center.

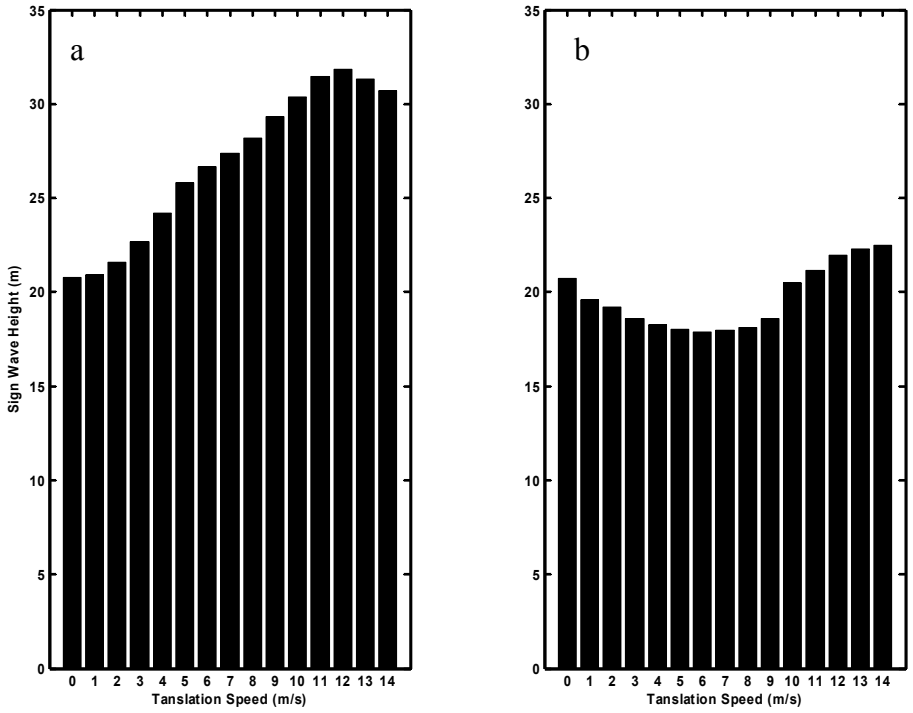

Figure 4.3 SWH values of waves generated by symmetric hurricanes moving with different translation speeds of location 'A' a) and location 'B' b) (shown in Figure 2) at MWRs.

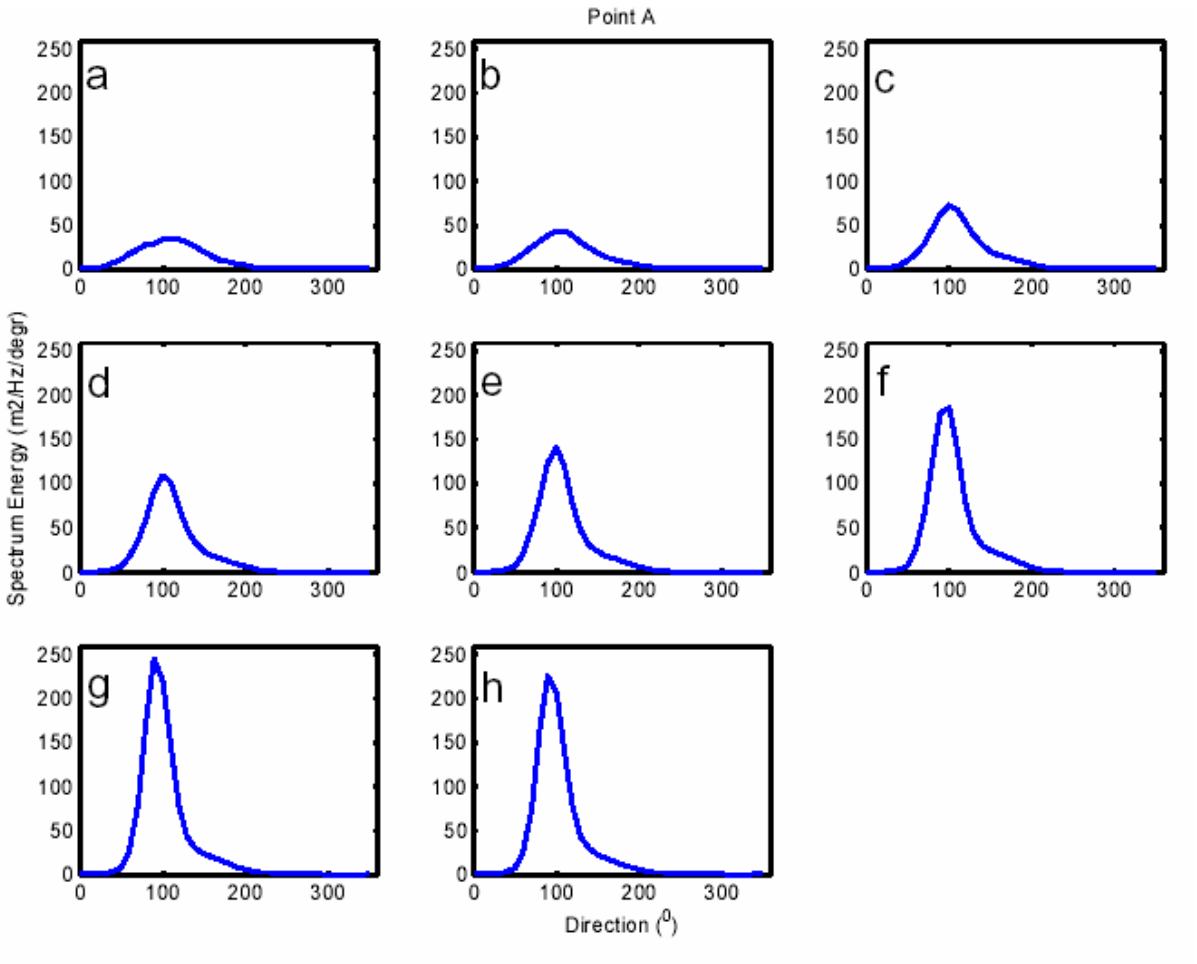

Figure 4.4 One dimensional directional wave spectrum at Point A, which were generated by symmetric hurricanes moving with different translation speeds: a) 0 m/s; b) 2 m/s; c) 4 m/s; d) 6 m/s; e) 8 m/s; f) 10 m/s; g) 12 m/s and h) 14 m/s.

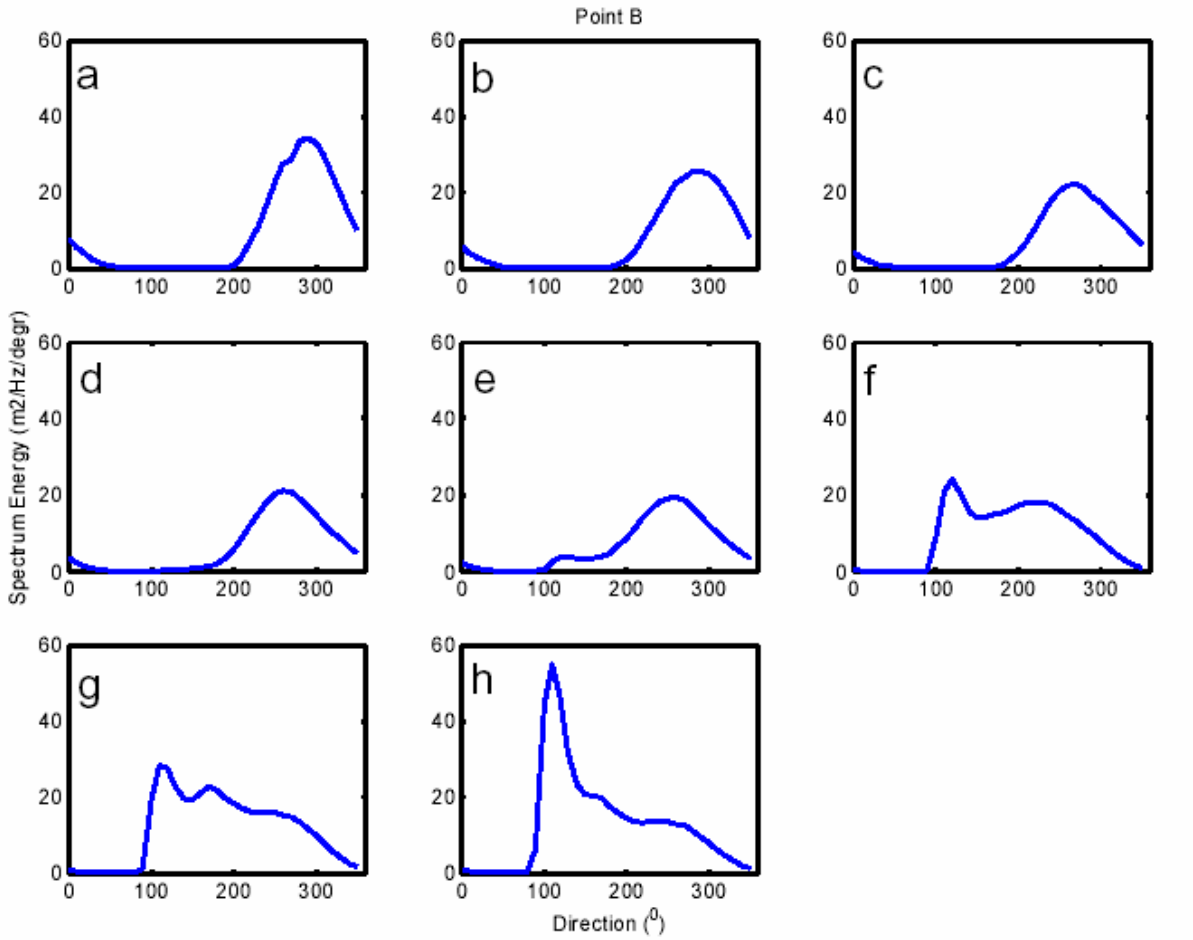

Figure 4.5 Same as Figure 4.4 except for Point B.

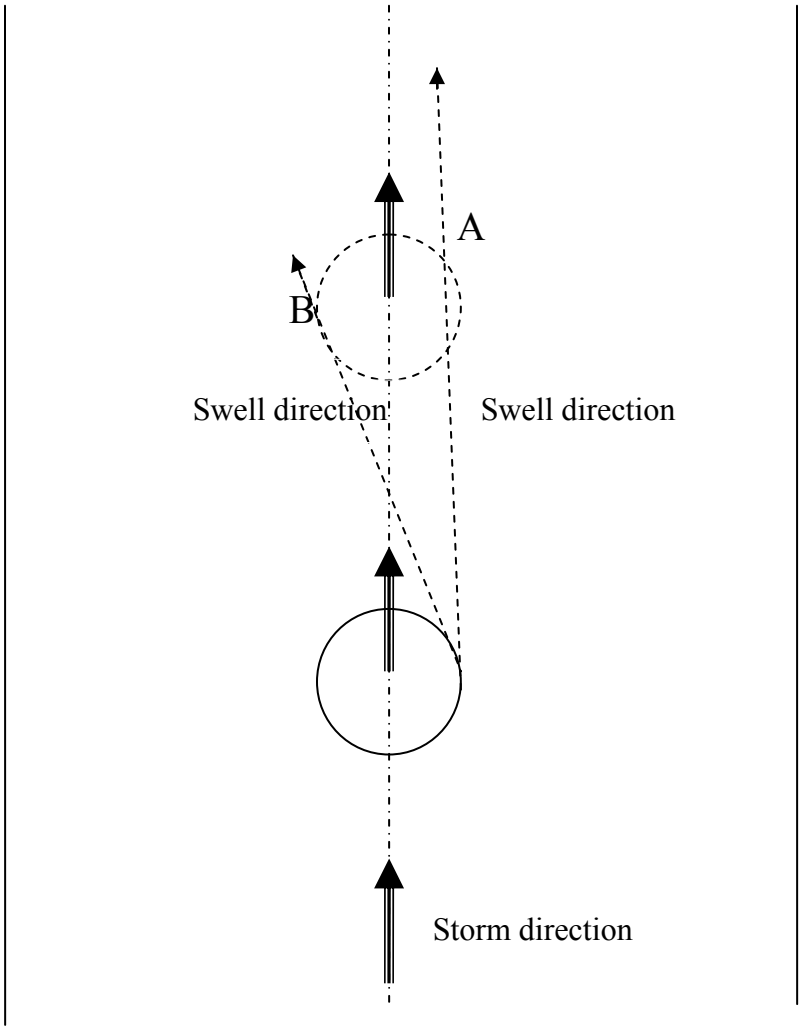

Figure 4.6 Schematic picture of swell (of Point A and Point B) propagating in the direction tangential to the circle defined by the RMW at an earlier position of the storm.

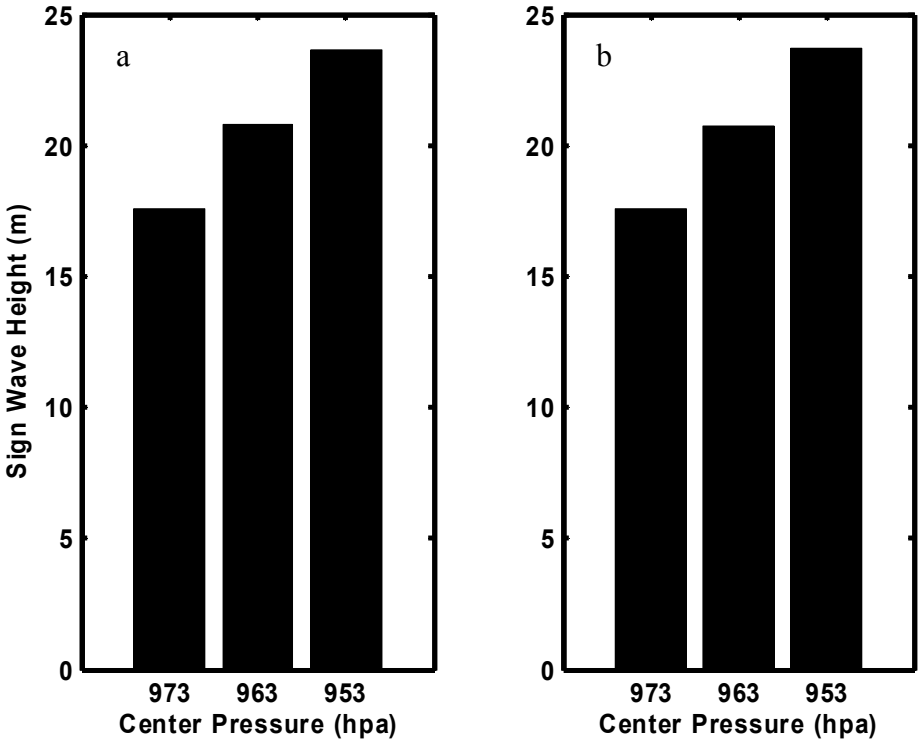

Figure 4.7 SWH values of waves generated by static and symmetric hurricanes with different intensity of location ‘A’ a) and location ‘B’ b) (shown in Figure 2) at MWRs.

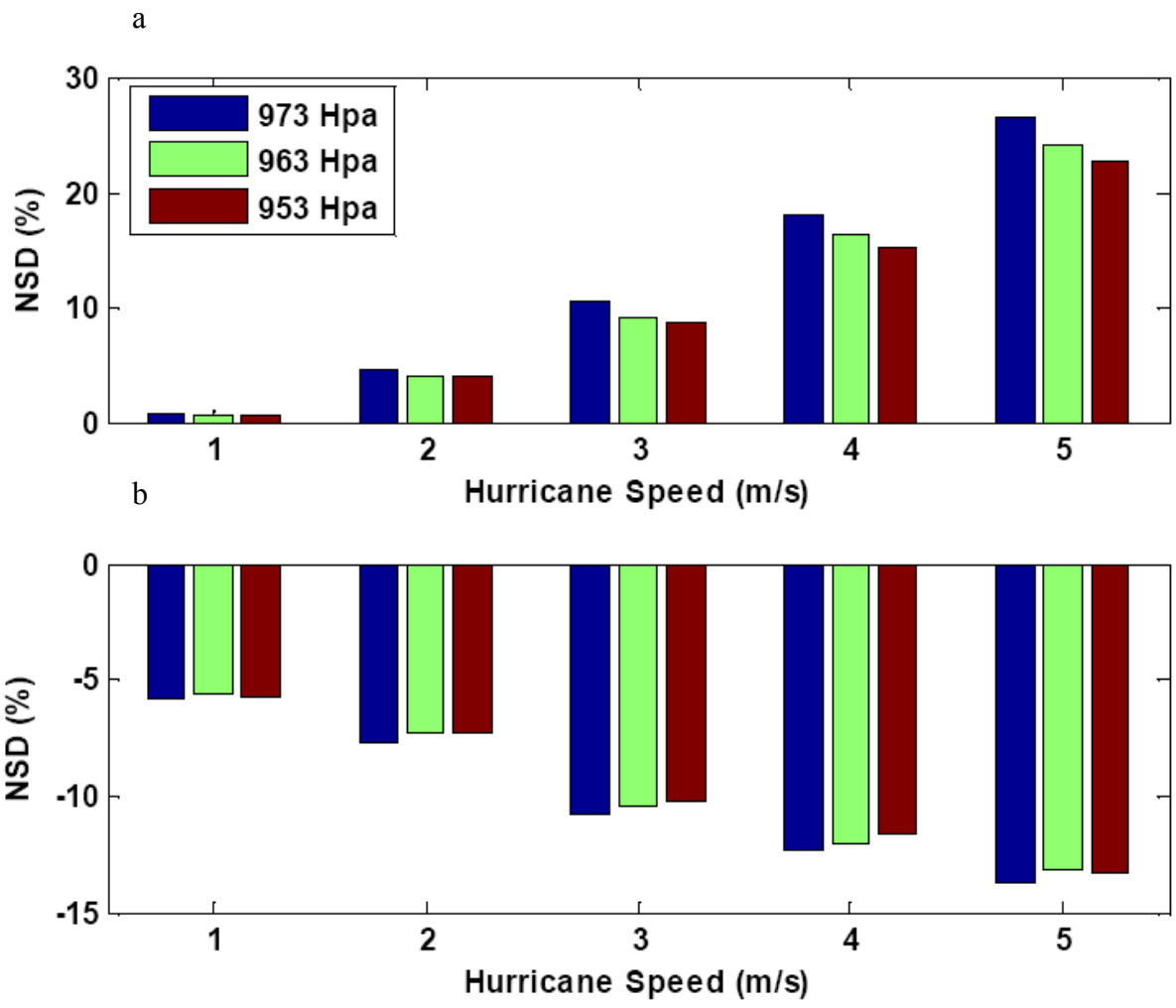

Figure 4.8 Normalized SWH difference (NSD) at location 'A' a) and location 'B' b) (shown in Figure 4.2).

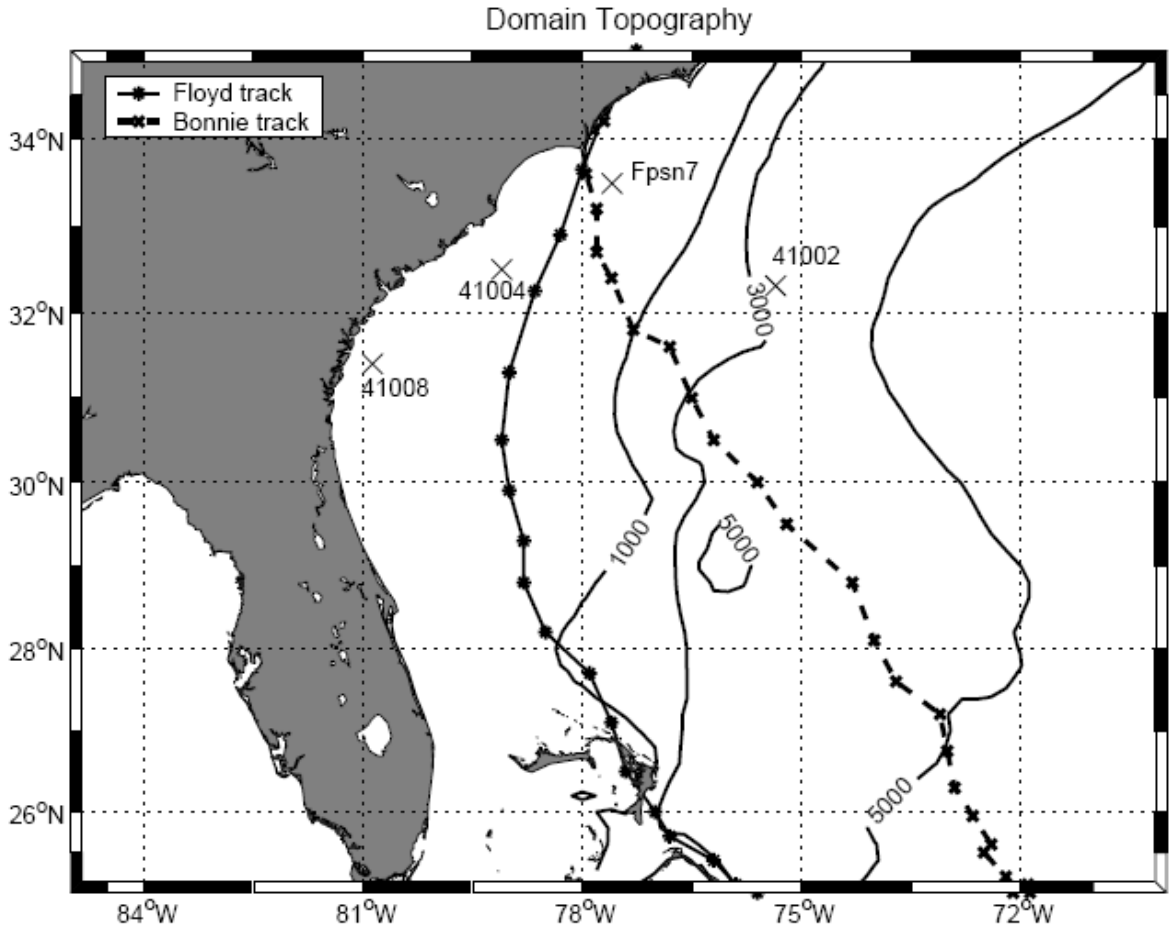

Figure 4.9 The model topography and domain used in experiment D, extends latitudinally from 25o to 35o north and longitudinally from 85o to 70o west. Dashed-X line and solid-point line are the best tracks of Bonnie and Floyd respectively. The X-mark is the distribution of the buoy stations.

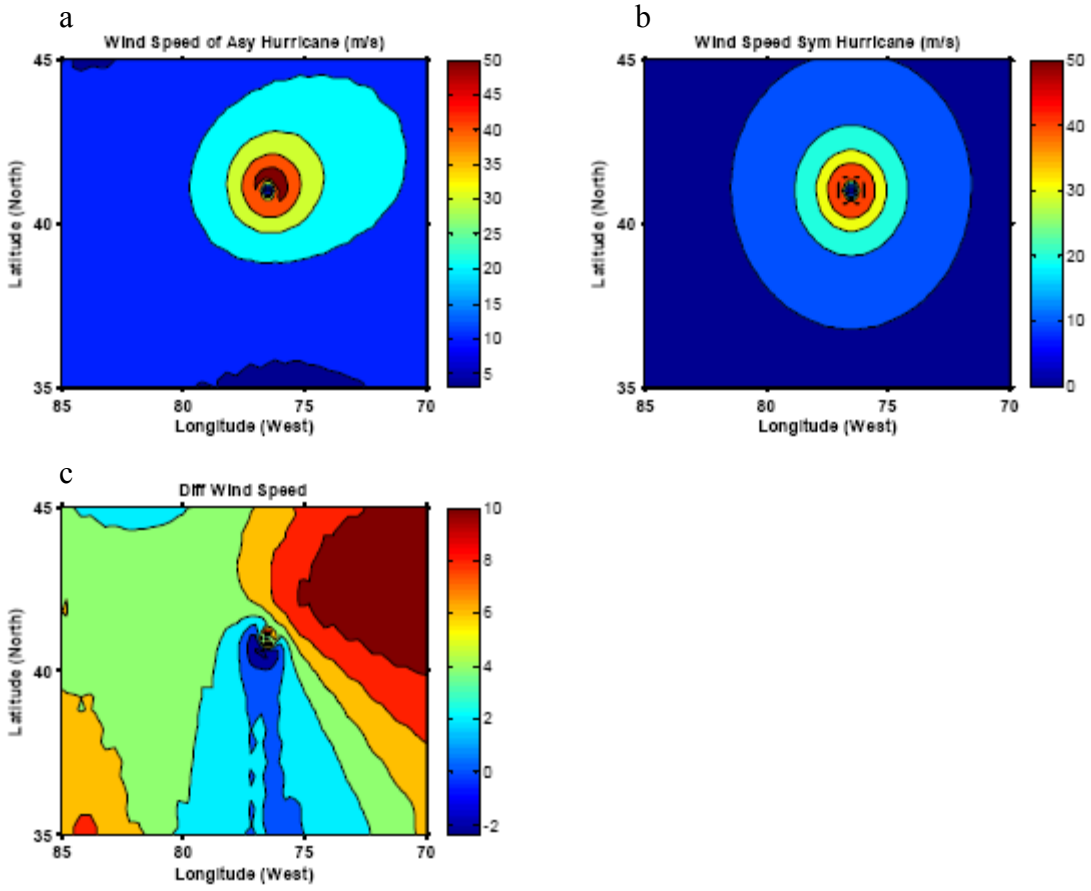

Figure 4.10 a) The distribution of symmetric hurricane wind fields (Bonnie) at 18:00 of Aug 25, 1998; b) Same as a) but for asymmetric hurricane wind and c) The difference between these two wind fields.

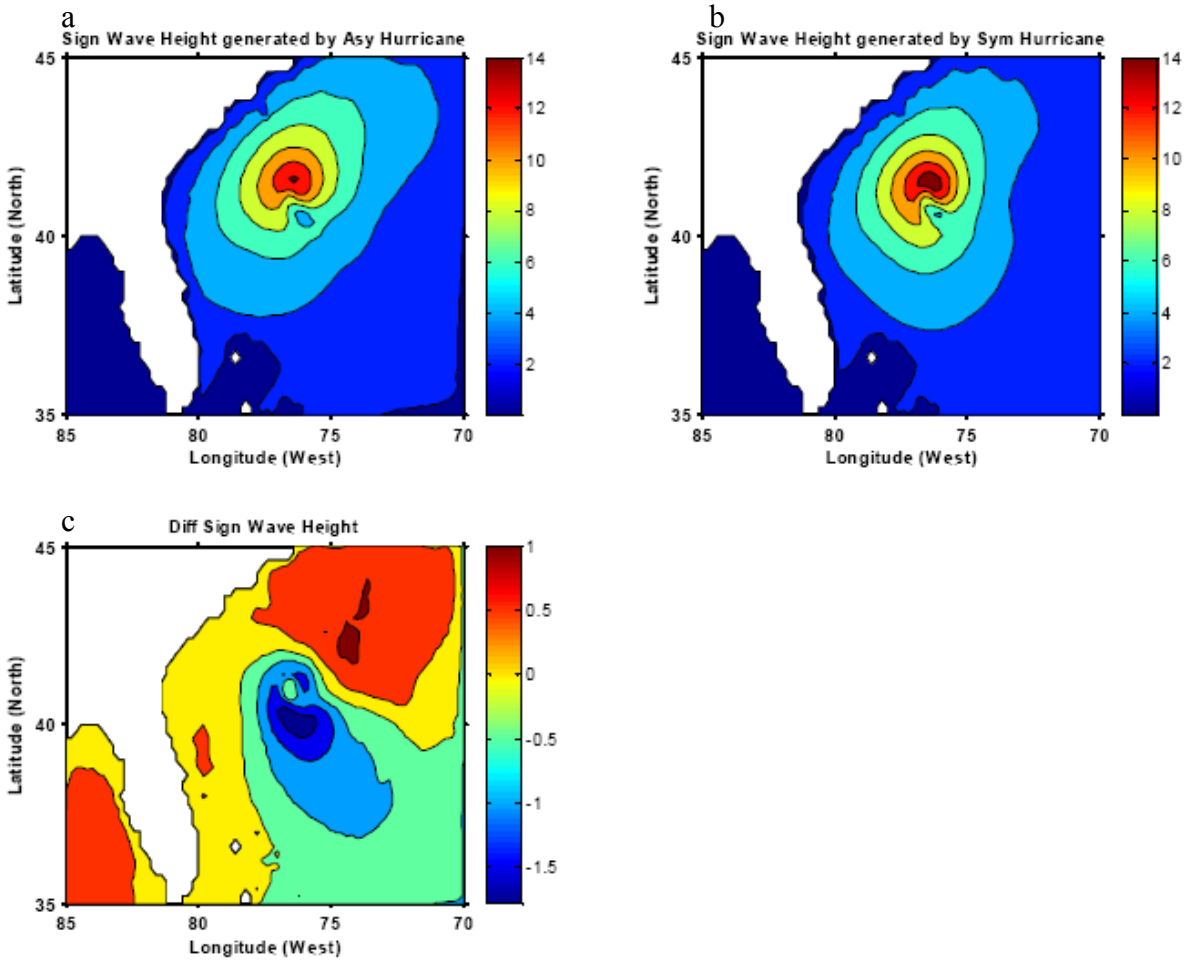

Figure 4.11 a) The distribution of SWH generated by symmetric hurricane wind (Bonnie) at 18:00 of Aug 25, 1998; b) Same as a) but driven by asymmetric hurricane wind and c) The difference between these two SWH fields.

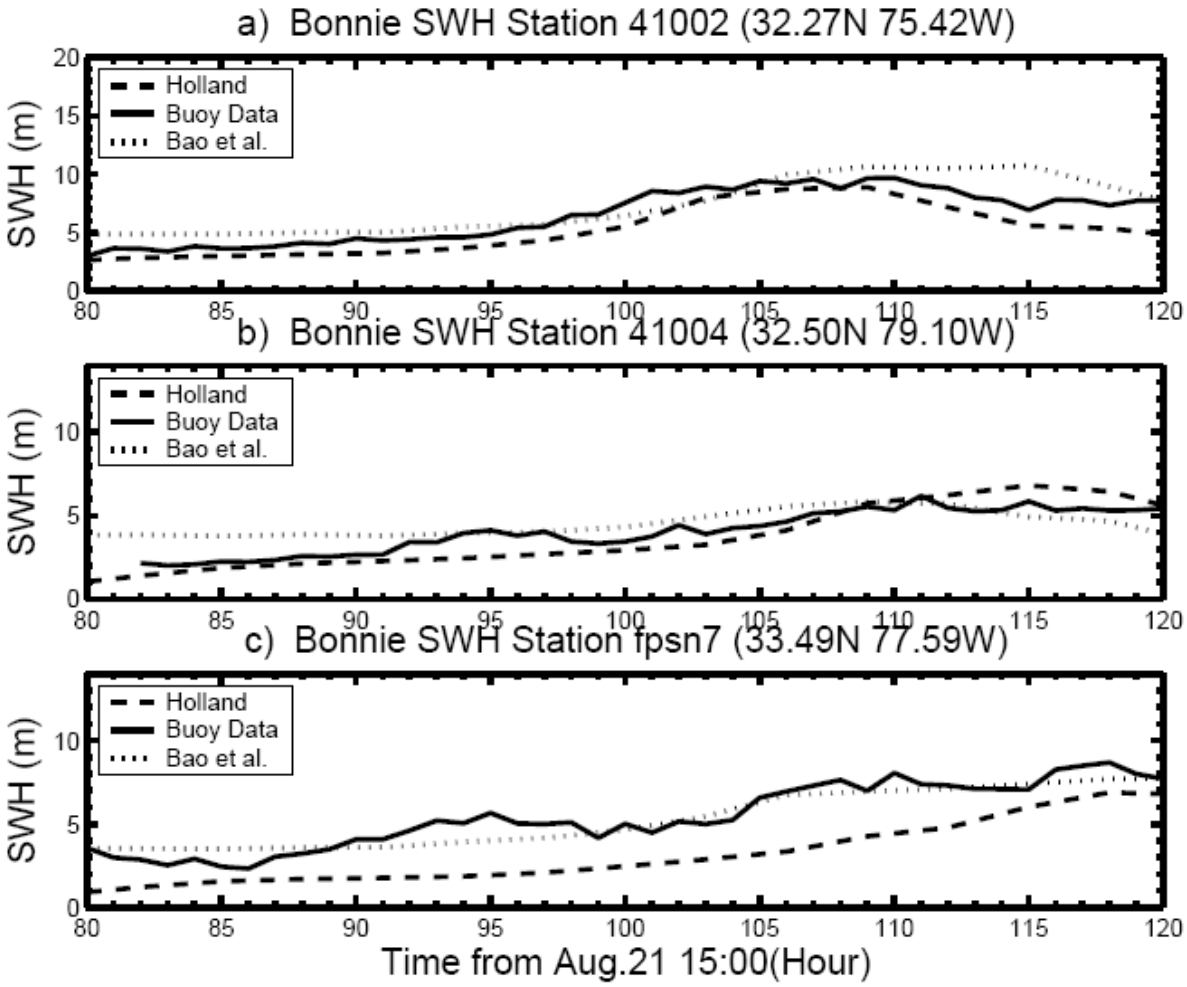

Figure 4.12 SWH values during hurricane Bonnie at buoy station a) 41002; b) 41004 and c) Fpsn7. Solid line is buoy data, dashed line is model results driven by symmetric hurricane and dotted line is model results driven by asymmetric hurricane wind.

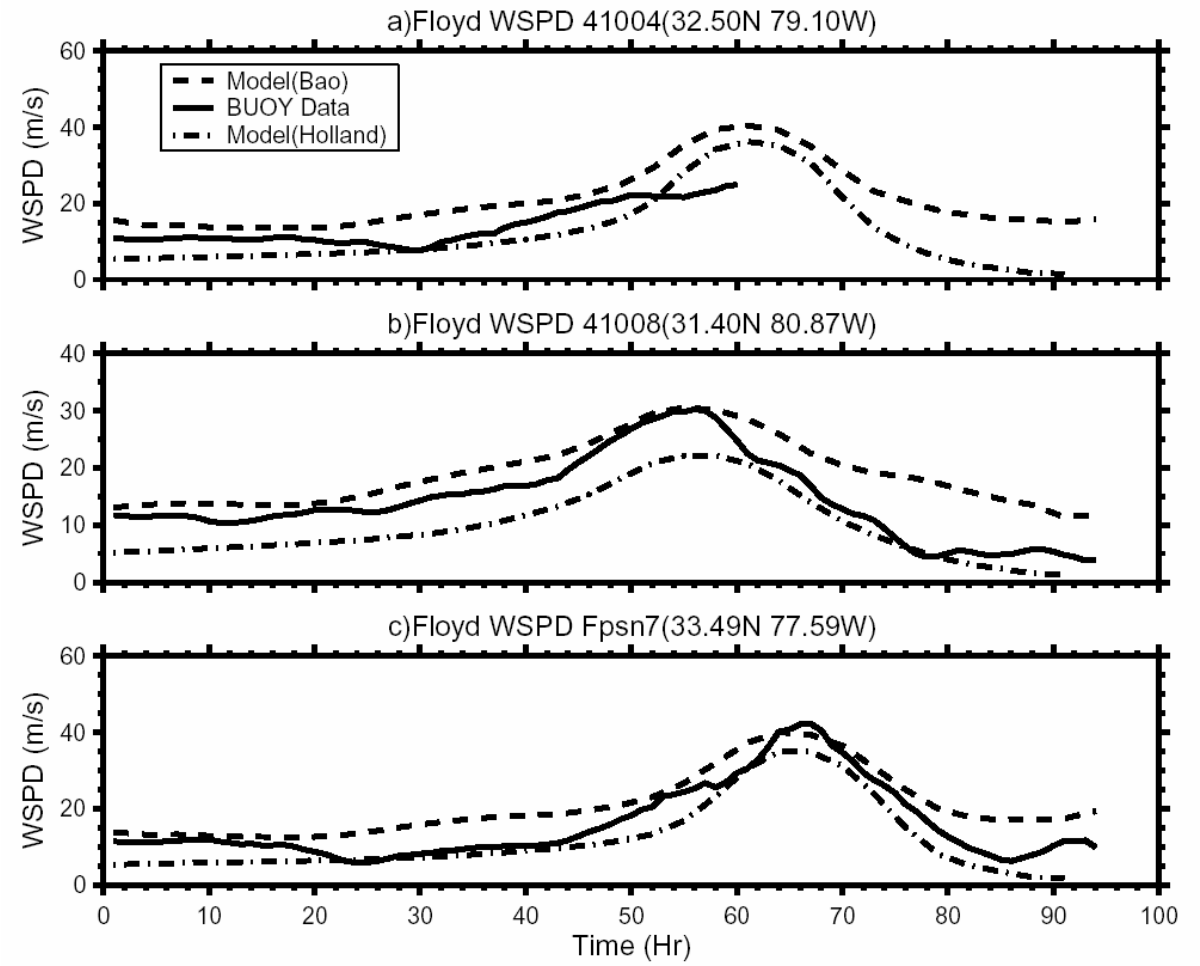

Figure 4.13 Wind speed during hurricane Floyd at buoy station a) 41004; b) 41008 and c) Fpsn7. Solid line is buoy data, dashed line is the result of asymmetric hurricane model and dot-dashed line is the result of symmetric hurricane model.

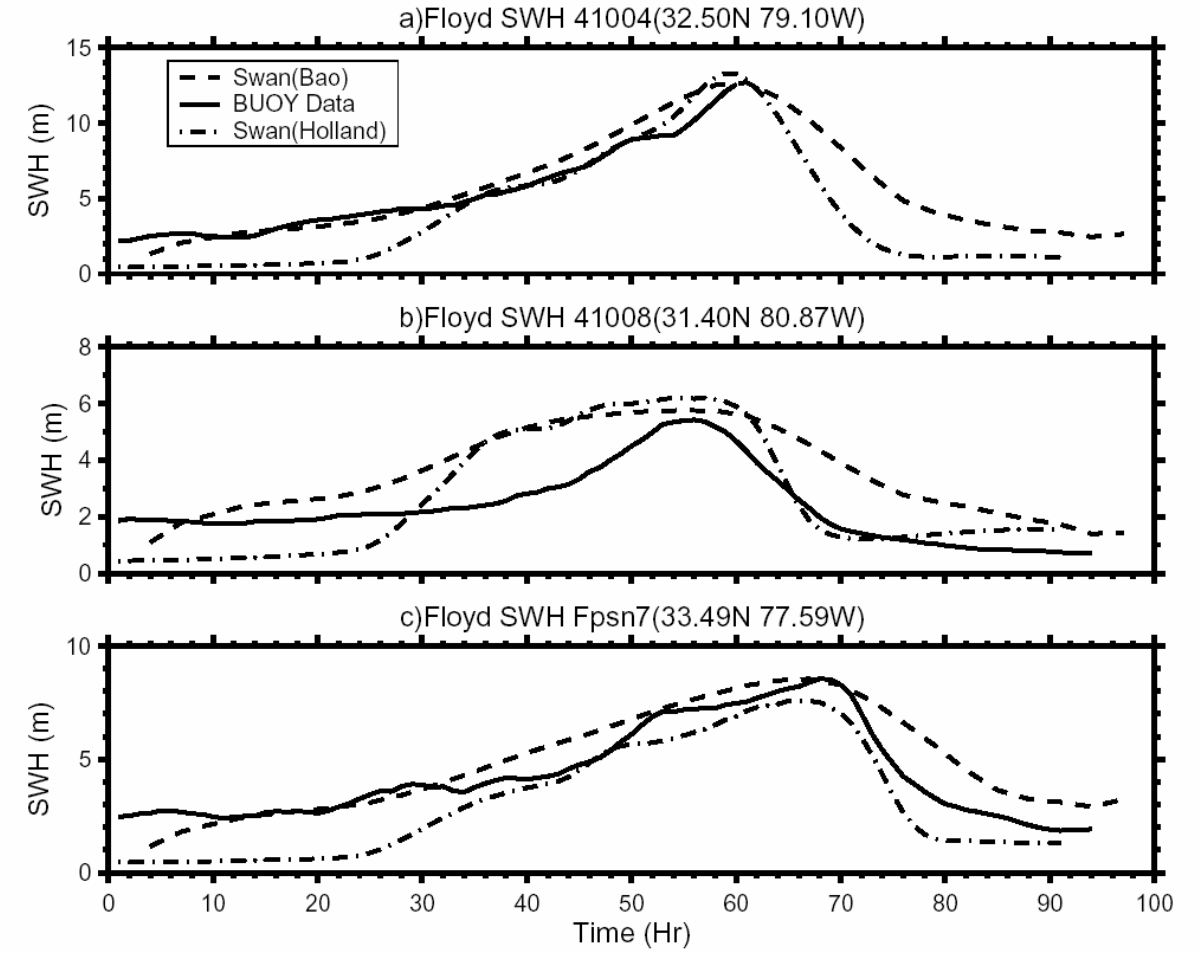

Figure 4.14 Same as Figure 4.13 but for SWH field.

References

Bao, S., L. Xie, L.J. Pietrafesa, 2006. A Numerical Study of the Effect of Hurricane Wind Asymmetry on Storm Surge and Inundation (Submitted to Monthly Weather Review, in review)

Booij, N., R. C. Ris and L. H. Holthuijsen, 1999. A third-generation wave model for coastal regions, 1. Model description and validation, *J. Geophys. Res.* **104** (C4), 7,649-7,666.

Bowyer, P.J. and A.W. MacAfee, 2000. The theory of trapped-fetch waves with tropical cyclones - An operational perspective, *Weather Forecasting*, **20**, 229-244.

Holland, G. J., 1980. An analytic Model of the wind and pressure profiles in Hurricanes. *Mon. Wea. Rev.,* 108, 121-1218.

King, D.B. and O.H. Shemdin, 1978. Radar observations of hurricane wave directions, paper presented at 16th International Conference on Coastal Engineering, Hamburg, Germany.

Komen, G. J., L. Cavaleri, M. Donelan, K. Hasselmann, S. Hasselmann, and P. A. E. M. Janssen, Dynamics and Modelling of Ocean Waves, 532 pp., Cambridge Univ. Press, New York, 1994.

Kurihara, Y., M. A. Bender, and R. J. Ross, 1993. An initialization scheme of hurricane models by vortex specification. *Mon. Wea. Rev.*, 121, 2030-2045.

Miles, J. W., 1957. On the generation of surface waves by shear flows, *J. Fluid Mech.*, **3**, 185-204.

Moon, I. J., I. Ginis, T. Hara, H. L., Tolman, C. W. Wright and E. J. Walsh, 2003. Numerical simulation of sea surface directional wave spectra under hurricane wind forcing, *J. Phys. Ocean*. **33**, 1,680-1,760.

Moon, I. J., I. Ginis and T. Hara, 2004. Effect of surface waves on air-sea momentum exchange. Part II: Behavior of drag coefficient under tropical cyclones, *J. of the Atm. Sci.*, **61**, 2,334-2,348.

Ou, Shan-Hwei, Jian-Ming Liau, Tai-Wen Hsu and Shiaw-Yih Tzang, 2002. Simulating typhoon waves by SWAN wave model in coastal waters of Taiwan, *Ocean Eng.*, **29**, 947-971.

Phillips, O.M., 1957. On the generation of waves by turbulent wind, *J. Fluid Mech*., **27**, 4,815-4,827.

Ris, R. C., L. H. Holthuijsen and N. Booij, 1999. A third-generation wave model for coastal regions, 2. Verification, *J. Geophys. Res.* **104** (C4), 7,667-7,681.

Tolman, H.L., 1991, A third-generation model for wind waves on slowly varying, unsteady and inhomogeneous depths and currents. *J. Phys. Oceanogr.*, 21, 782-797.

Xie, L., K. Wu, L. J. Pietrafesa and C. Zhang, 2001. A numerical study of wave-current interaction through surface and bottom stresses: Wind-driven circulation in the South Atlantic Bight under uniform winds, *J. Geophys. Res.* **106** (C8), 16,841-16,855.

Xie, L., S. Bao, L. J. Pietrafesa, K. Foley and M. Fuentes, 2006. A real-time hurricane surface wind forcasting model: Formulation and verification, *Mon. Wea. Rev.* **134,** 1355–1370**.**

Young, I.R., 1988. Parametric hurricane wave prediction model**,** *J. Waterway, Port, Coastal Ocean Eng.***, 114,** 637-652**.**

Young, I. R., 2006. Directional spectra of hurricane wind waves, *J. Geophys. Res.*, **111** (C8), C08020, doi:10.1029/2006JC003540.

Walsh, E.J., C.W. Wright, D. Vandemark, W.B. Krabil, A.W. Garcia, S.H. Houston, S.T. Murillo, M.D. Powell, P.G. Black and F.D. Marks, 2002. Hurricane directional wave spectrum spatial variation at landfall, *J. Phys. Oceanogr*., **32**, 1667-1684.

WAMDI Group, A third-generation model for wind waves on slowing varying, unsteady and inhomogeneous depths and currents, J. Phys. Oceanogr., 21, 782– 797, 1988.

Wang, D.W., D.A. Mitchell, W.J. Teague, E. Jarosz and M.S. Hulbert, 2005. Extrem waves under Hurricane Ivan, Science, 309, 896-896.

Wright, C.W., E.J. Walsh, D. Vandemark, W.B. Krabil, A.W. Garcia, S.H. Houston, M.D. Powell, P.G. Black and F.D. Marks, 2001. Hurricane directional wave spectrum spatial variation in the open ocean, *J. Phys. Oceanogr*., **31**, 2472-2488.

CHAPTER 5. THE EFFECT OF WAVE-CURRENT INTERACTIONS ON THE STORM SURGE AND INUNDATION IN CHARLESTON HARBOR DURING HURRICANE HUGO 1989

5.1 Introduction

Wind waves, storm surges and ocean circulation are important, mutually interacting physical processes in coastal waters. Over the past two decades, there have been a number of studies focusing on wave-current interactions [Tolman, 1990, Zhang and Li 1996, Xie et al. 2001, 2003]. Wind waves can indirectly affect the coastal ocean circulation by enhancing the wind stress [Mastenbroek et al., 1993] and by influencing the bed friction coefficients [Signell et al., 1990, Davies and Lawrence, 1995]. More recently, Xie et al. [2001, 2003] showed that wave-current interactions through surface and bottom stresses can significantly affect coastal ocean currents and storm surge.

The key questions here must address are how surface waves and currents affect one another and how they can be properly coupled in numerical models. In general, these processes influence one another in several ways: 1) wind stress, which is a function of the drag coefficient which is strongly tied to wave parameters [Donelan et al., 1993]; 2) radiation stress, which is considered to be an additional mechanical force in storm surge models [Xie et al., 2001, Mellor, 2003, Xia et al., 2004] and can be incorporated into wave models by

invoking wave-action conservation [Komen et al., 1994, Lin and Huang, 1996]; 3) bottom stress, which is a function of wave-current interaction in the near bottom layer when the water depth is sufficiently shallow for wave effects to penetrate to the bottom [Signell et al., 1990]; 4) water depth variation and current conditions, which are input parameters for the wave models [Tolman, 1991]; 5) the Stokes' drift current induced by the non-linearity of surface waves [Huang, 1979]; and 6) wave run-up, which impacts on storm surge and inundation prediction [Holman et al., 1985 and 1986, Hedges, 2004].

Because of the importance of these interactions, there have been several studies which have attempted to incorporate these separate but important and linked effects into coupled models. Tolman [1991] described the effects of astronomical tides and storm surges on wave modeling via the consideration of unsteady currents and varying topography. Tolman's results suggest that the effects of tides and storm surges should be considered in modeling wind waves in shelf seas. Tolman's study, however, did not consider the feedback effect of wind waves on storm surge. Signell et al. [1990] and Davis and Lawrence [1995] studied the effect of waves on bottom shear stress and showed that wind waves could play an important role in determining surface and near bottom currents as well as water level variations over and along a coastal region. In these modeling studies, surface waves were considered as an external input into the ocean circulation model, a one-way effect.

Xie et al. [2001, 2003] investigated the dynamic coupling between waves and currents and found that it was important to incorporate the surface wave effects into coastal circulation and storm surge modeling. The results of their study showed an improved storm

surge prediction capability. However, they did not consider depth variations in their wave model, which limited the more complete application of their results. Moon [2005] also developed a wave-tide-circulation coupled system, in which the effects of wave-current interactions on surface stress, a wave breaking parameterization, and depth variations in their wave model were included. However, the effects of wave-current interaction on the bottom shear stress were not included. Moreover, all of the above mentioned storm surge models did not include the three-dimensional radiation stress in their coupled system as pointed out by Mellor [2003] and Xia et al. [2004]. Furthermore, none of the studies cited above discussed the effect of wave-current interaction on inundation.

Flooding caused by coastal storms is an increasing threat to people living in coastal regions. The focus of this study is on investigating the effect of wave-current interaction on storm surge and inundation induced by coastal atmospheric storms via the inclusions of wave-dependent surface wind stress, wave-current-dependent bottom shear stress, and time-dependent sea surface elevation in the wave model, and three-dimensional radiation stress. This study extends that of Xie et al. [2001, 2003] by including wave-current interactions in the presence of both wave-induced surface and bottom shear stresses in an interactively coupled system. The basic wave model employed is the SWAN or Simulating WAves Nearshore model [Booij et al. 1999] and the storm surge model is based on the Princeton Ocean Model (POM) [Mellor, 1996]. An inundation scheme, developed in Xie et al [2004], is included in this chapter. A brief description of the models used in the coupled system, and the coupling procedure are provided in section 5.2. Section 5.3 introduces model parameterizations and numerical experiments performed. The effects of the wave-current

interaction on the resulting storm surge and inundation are investigated in section 5.4. Discussion and conclusions are presented in section 5.5.

5.2 Coupled wave-current system

5.2.1 Model description

The coupled wave-current system is based on the well known POM [Mellor, 1996] and a third generation wave model (SWAN) [Booij et al. 1999]. POM is a three-dimensional, primitive-equation model that uses a sigma coordinate in the vertical, a curvilinear orthogonal coordinate and an "Arakawa C" grid scheme in the horizontal with previous applications described in Xie et al. [2001]. Albeit, there are two differences between the versions of POM used in this study and the POM versions described in Xie et al. [2001]. First, the radiation stresses due to direct wave-current interactions are three-dimensional, following the formulation described in Xia et al., [2004]. Xia et al. [2004] extended the traditionally used (2-D) model of radiation stress by introducing a vertical profile to the stress. The equations used in their study are:

$$
\begin{aligned}
S_{xx}(\sigma) &= E\frac{k}{\sinh 2kD}[\cosh 2k(1+\sigma)D+1]\cos^2\theta \\
&- E\frac{k}{\sinh 2kD}[\cosh 2k(1+\sigma)D-1]-\frac{E\sigma}{D} \\
&+ E\frac{k(1+\sigma)\sinh k(1+\sigma)D}{\cosh kD} \\
&- \frac{E}{D}[1-\frac{\cosh k(1+\sigma)D}{\cosh KD}],
\end{aligned}
\tag{5.1}
$$

$$
\begin{aligned}
S_{yy}(\sigma) &= E\frac{k}{\sinh 2kD}[\cosh 2k(1+\sigma)D+1]\sin^2\theta \\
&- E\frac{k}{\sinh 2kD}[\cosh 2k(1+\sigma)D-1]-\frac{E\sigma}{D} \\
&+ E\frac{k(1+\sigma)\sinh k(1+\sigma)D}{\cosh kD} \\
&- \frac{E}{D}[1-\frac{\cosh k(1+\sigma)D}{\cosh KD}],
\end{aligned}
\tag{5.2}
$$

$$
S_{xy}(\sigma) = E\frac{k}{\sinh 2kD}[\cosh 2k(1+\sigma)D+1]\sin\theta\cos\theta, \tag{5.3}
$$

$$
S_{xy}(\sigma) = S_{yx}(\sigma) \tag{5.4}
$$

where E is wave energy density, K is wave number, θ is the angle between the x axis and the propagation direction of the waves, D is the total water depth (H+η) including surface water level fluctuations, and σ (σ = (z-η)/D) is the vertical coordinate. All above formulae are obtained from monochromic wave theory. Here these formulae will be used to calculate the radiation "force" included in the POM nonlinear momentum equations [Xie et al. 2001], in which there is an assumption that these formulae are suitable for the component waves in the wave directional spectrum described by linear random wave theory.

The other difference is that an inundation and draining (or wetting and drying) grid scheme was added to POM in Xie et al. [2004], so that the inundation process accompanying coastal storms, especially tropical storms, can be handled. Peng et al. [2004] used this integrated storm surge and inundation model to successfully simulate hurricane-induced the storm surge and inundation in and around the Croatan- Albemarle-Pamlico Estuary system of North Carolina.

SWAN is a third generation wave model developed by Booij et al. [1999] in the spirit of the WAM wave model [WAMDI Group, 1988]. The model is based on an Eulerian formulation of the discrete spectral balance of action density that accounts for refractive propagation over arbitrary bathymetry and current fields. It is driven by boundary conditions and local winds. As in other third-generation wave models, the processes of wind wave generation, wave white capping, quadruplet wave-wave interactions, and bottom dissipation are represented explicitly. In SWAN, the depth-induced wave breaking process is included, which implies that the computations are more realistic in shallow water. Moreover the surface elevation can be added to the water depth in SWAN, so that the effect of storm surge on waves can be included. The evolution of the wave spectrum in SWAN is described by the spectral action balance equation, which for Cartesian coordinates is:

$$\frac{\partial}{\partial t}N + \frac{\partial}{\partial x}C_x N + \frac{\partial}{\partial y}C_y N + \frac{\partial}{\partial \sigma}C_\sigma N + \frac{\partial}{\partial \theta}C_\theta N = \frac{S}{\sigma} \tag{5.5}$$

where N is the wave action density ($N(\sigma, \theta) = E(\sigma, \theta) / \sigma$), E is the energy density spectrum and σ is the relative frequency. C_x, C_y and C_σ are propagation velocity components in x-, y-, σ- and θ-space respectively. S is the source term that represents the effects of generation, dissipation and nonlinear wave-wave interactions.

5.2.2. The coupling procedure

In this study, three types of wave effects are incorporated into the POM model: 1) surface wind stress; 2) bottom stress; and 3) 3-D radiation stress. Contemporaneously, current fields and water surface elevation outputs, fed back from POM model, are provided to the SWAN

wave model. In other words, the coupling procedure in the present study is two-way and dynamic. So, values of currents and water elevation computed from POM are used in SWAN to compute the wave parameters. Then the wave parameters are used to compute new surface wind stress, bottom stress and 3-D radiation stress, which are, in turn used in POM to compute the currents and surface water level at the next time step, and so on. Through this iterative process, the two models are dynamically coupled. This coupling procedure is illustrated in **Fig. 5.1**.

5.3. Model settings and experiments

5.3.1. Model domain and nesting windows

In this study, the wave-current coupling system is configured for Charleston Harbor, its coastline and its adjacent shelf. In order to resolve the hydrodynamics of the relatively small harbor and its surrounding water, three nested domains (**Fig. 5.2**) with the smallest imbedded into a middle-sized domain, in turn imbedded into a larger one, are employed for the study. The outermost domain is 78.0-82.5°W, 31.0-34.5°N with a 1 minute spatial grid size for both latitude and longitude. The middle domain spans 79.7-80.1°W, 32.5-33.0°N, with a 12 second spatial grid size. The innermost domain, resolving more detailed geographic features in and around Charleston Harbor, covers 79.75 -80.00°W, 32.70-32.90°N, with a 3 second spatial grid size. Four uniformly spaced sigma levels are used in the vertical for all domains. The bottom topography for all three domains is obtained from GEODAS, version 4.0.7 (available online from http://www.ngdc.noaa.gov/mgg/gdas). A minimum depth of 1m was

given to grid cells where the mean water depth is less than 1m. As we are principally interested in investigating the coupled effects of waves and currents on storm surge, inundation and retreat, the coupled modeling system was only used in the innermost domain. In other words, in the middle and outermost two domains, the wave and storm surge models are not coupled and are computationally run separately to provide lateral boundary conditions.

5.3.2. Experiments

Hurricane Hugo impacted the Charleston region, South Carolina (SC) from September 10 to September 22, 1989. The National Hurricane Center's (NHC) best track for the event near and at land fall (09/21/22Z to 09/23/08Z) is shown in **Fig. 5.2**. Based on reconnaissance aircraft reports, Hurricane Hugo had sustained winds of around 135 mph when the cyclone's eye crossed the SC coast. Hurricane Hugo made landfall in SC, causing extensive damage throughout the state and continued to North Carolina where it hit Charlotte, the largest city in that state. Damage estimates for SC alone reached $5 billion, while total storm damage for the Southeastern United States (US) and Caribbean exceeded $9 billion, making Hugo one of the top 5 costliest hurricanes to ever hit the US.

Hurricane Hugo is chosen as the actual event around which to focus the numerical experiment to examine the effect of wave-current interaction on storm surge and inundation. The Hugo wind field is calculated from the theoretical hurricane wind model of Holland [1980], which also provides a distribution of sea level pressure and the gradient wind within a tropical cyclone: $P = P_c + (P_n - P_c)\exp(-A/r^B)$, where P is the atmospheric pressure at

radius r. The Holland hurricane wind model computes hurricane wind speed as a function of radial distance from the center of the storm as described by,

$$V_a = [AB(P_n - P_c)\exp(-A/r^B)/\rho_a r^B]^{1/2} \quad (5.6)$$

where V_a is wind speed at radius r, P_c is the central pressure, P_n the ambient pressure, and A, B are scaling parameters ($A = (R_{\max})^B$). Wind field parameters used in equation (5.6) were obtained from the NHC.

In order to investigate the effects of waves on storm surge and inundations, five experiments (**Table 5.1**) are conducted in this study. The storm surge and inundation model run without wave-current interaction is referred to as Case NN. Cases YN, NY and NNR assume wave-current coupling mechanism through changing only surface stress, bottom stress and radiation stress, respectively. The coupled system including all three wave-current interaction mechanisms is conducted in Case YYR. In all cases, the vertically integrated current and surface elevation, as calculated from the storm surge model, are provided as input into the wave model.

5.4. Results of experiments

5.4.1. The impact of wave-current interaction on storm surge

Consider first the effect of wave-current interaction on storm surge. To quantify the effects of surface waves on storm surge, the difference between the peak surges computed by

the wave-surge coupled model and the stand alone surge model at nineteen locations in the Charleston Harbor region (**Fig. 5.3a**) were calculated. The simulated peak storm surges from the stand-alone surge model (case NN) and the wave-surge coupled model (case YYR) are shown in **Fig. 5.3b**. The impact of waves on the peak surge is evident, but varies from location to location. The largest differences (~0.25-0.7 m or 1-2.5 ft) occurred in the river estuaries (locations 11-14), while smaller effects (less than 0.5 ft differences) were felt at the southern Atlantic coast (locations 1 and 2) as well as along the southern water-front of downtown Charleston (locations 7-9). During Hurricane Hugo, the wave effects led to significant increases in storm surge in western (locations 5 and 6) and northern regions (locations 11-14), whereas decreases along the Atlantic Coast to the northeast of the harbor (locations 17-19). As we will show in the next section, these differences in storm surge led to significant differences in coastal flooding around the Charleston Harbor.

5.4.2. The impact of wave-current interaction on inundation

In this section, the effect of wave-current interaction on inundation is analyzed from a set of model experiments: Cases NN, YN, NY, NNR and YYR, as described in **Table 5.1**.

First, consider the simulated inundation generated by Hurricane Hugo using the stand-alone surge model (case NN). The areas flooded by the storm surge in the Charleston region during the passage of Hurricane Hugo are shown in **Fig. 5.4a**. There are two main inundation areas, one located in the Atlantic coastal region of the study area to the northeast of the Charleston Harbor, and the other in the southwestern region of the study area, both along the

Atlantic coast and the southern bank of the Charleston Harbor. Significant flooding also occurred along the southern and northeastern coasts of downtown Charleston, as well as along parts of the river banks further north (**Fig. 5.4**).

Next, examine the effect of wave-induced surface stress on the inundation caused by Hurricane Hugo. Wind stress is one of the most important factors in storm surge prediction [Xie et al., 2001, 2003]. In this study the effect of surface waves on the surface shear stress applied to the storm surge model is computed as in Xie et al. [2001].

Figure 5.5a depicts the accumulated flooding area from Case YN which included the effect of waves on the surface shear stress. The difference of the flooding areas between Case YN and Case NN is computed by subtracting the land (0) and water (1) mask functions in Case NN from that in Case YN. A difference value of 0 means no change, stands for switching from land to water (flooding), and 1 for switching from water to land (drying). The results are depicted in **Fig. 5.5b**. The flooding areas were evidently impacted in three regions. One was in the northeast coastal region, where the flooding area was reduced (yellow color in **Fig. 5.5b**), another in the area southwest of the Charleston Harbor, where the flooding area increased (purple color in **Fig. 5.5b**), and the third was in the northern section of the study area, mainly showing as a drying effect. **Table 5.2** shows the flooding areas and the percentage changes of the flooding areas in different cases. The percentage change is computed as the absolute total difference value (sum of the absolute difference value over the entire model domain) divided by the original flooding area in Case NN. Flooding and drying in Case YN showed a 19% difference from that in Case NN as measured by the absolute total

difference value. The difference varies from region to region as shown in **Table 5.3**. The regions are defined in **Fig. 5.6**. The region to the north of the harbor (labeled North Region) showed the largest percentage difference (68%), followed by the region to the east of the harbor (labeled as East Region) (22%) and then the southwest (labeled as Southwest Region) (15%). Note that the Southwest Region covers most of the Charleston Harbor, where a large area was flooded during Hurricane Hugo. The East Region covers mainly the coastal area to the north of the harbor where there was also significant flooding. The North Region includes mainly river and river banks, and the area of flooding is relatively small compared to the other two regions.

Next, focus on Case NY, in which only the effect of wave-induced bottom stress was considered in the surge model. The effect of waves on the bottom stress has been studied by Davis and Lawrence [1995] and Signell et al. [1990]. Xie et al. [2001] gave a detailed description of the method used to incorporate wave-induced bottom stress into the wave-current coupled system. This same approach is followed in this study.

Figure 5.7a shows the flooding area simulated in Case NY. **Figure 5.7b** depicts the difference of the flooding areas between Cases NY and NN, computed the same way as those shown in **Fig. 5.5b** (i.e., the wet/dry index of Case NY minus that of Case NN). Clearly wave-induced bottom stress did not affect inundation as much as it did through the surface stress. Flooding and drying in Case NY showed only a 5% difference from that in Case NN, as measured by the absolute total difference value (**Table 5.2**). The only obvious difference lies in the North Region, in which the accumulated flooding area in Case NY was 26% larger

than in Case NN (**Table 5.3**). Note, however, that the total area of flooding is small in the North Region. In the East Region, the effect of wave-induced bottom stress on inundation slightly increased the flooding area there, whereas wave-induced surface shear stress led to a decrease in flooding area in this region (**Fig. 5.5b**).

Consider now the effect of radiation stress. The radiation stress was first introduced by Longuet-Higgins and Stewart [1962], and they used this concept to analyze wave set-up and set-down. Following their study, the issue on how to incorporate the wave radiation stress into an ocean circulation model became topical. Recently the concept of a 3-D radiation stress was defined by Mellor [2003], which suggested that an expression for a vertically-dependent radiation stress would be appropriate for three-dimensional ocean models. Xia et al. [2004] extended the traditional 2-D radiation stress via the introduction of vertical dependence using a simpler approach. In the simulated examples presented in Xia et al. [2004], the vertical structure of wave-induced currents both inside and outside the surf zone was quite realistic.

In Case NNR, 3-D radiation stress is incorporated into the wave-surge coupled modeling system using the approach described by Xia et al. [2004]. The flooding area simulated by Case NNR and the difference between Case NNR and Case NN (wet/dry index in Case NNR minus that in Case NN) are shown in **Fig. 5.8a** and **5.8b**, respectively. Overall the effect of radiation stress resulted in a 14% difference in inundation which is slightly less than that caused by the wave-induced surface stress, but more than that due to wave-induced bottom stress (**Table 5.2**). In the three sub-regions, the North Region showed a large (214%)

difference, but the net flooding area itself is small there (about 5 km2) (**Fig. 5.8b**). The percentage changes in the East and Southwest regions were 10% and 8%, respectively. Note that the maximum flooding area is decreased in Case NNR in these two regions (**Fig. 5.8b**).

Finally, let's examine the combined effect of wave-induced surface, bottom, and radiation stresses on inundation (Case YYR). The accumulated flood area for Case YYR is presented in **Fig. 5.9a**. **Figure 5.9b** shows the difference of the flooding area between Case YYR and Case NN (Case YYR minus Case NN). It appears that the wave-induced wind stress played the most important role in determining the inundation, since **Figure 5.9a** is quite similar to **Figure 5.5b**. However, there is still some difference between Case YYR and Case YN, in all regions, as seen by comparing **Figure 5.9b** to **Figure 5.5b**. Case YYR showed a new flooding area in the North Region. Moreover, the reduced flooding area in the East Region is larger in Case YYR than that in case YN. Overall, the combined wave effects produced a 29% difference in the flooding/drying areas over the whole domain (**Table 5.2**). Regionally, the percentage differences were 237%, 38% and 15% in the North, East and Southwest regions, respectively (**Table 5.3**).

5.5. Discussions and conclusions

Previous studies have shown that wave-current interactions can significantly influence water level and currents [Xie et al., 2001, 2003]. These prior studies suggested that the inclusion of wave-current interactions in coastal ocean circulation modeling and in particular storm surge and inundation prediction was desirable, especially during impending storms.

The results from the study presented within show that the combined effects of wave and currents on the inundation caused by a tropical cyclone (a Category 4 Hurricane, Hugo in 1989) are significant and furthermore the effects are non-uniform across the model domain.

Comparing the three effects of wave-current interactions (Cases YN, NY and NNR), wave-induced wind stress played a more significant role in determining the inundation area than the effects of the wave-induced bottom stress and the surface radiation stress. We note that although the effects of wave-induced bottom stress and radiation stress are smaller comparing with the effect of wave-induced surface shear stress, none of the processes should be arbitrarily neglected in the wave-current coupling, since these dynamical processes are a part of the physics of the system and the effect can become significant locally in certain regions.

The experimental results and discussions presented in the above sections indicate that wave-current interaction effects should be taken into account not only in storm surge simulations, but also, and very importantly, in inundation simulations. As shown within, wave-induced wind stress in storm surge and inundation models can significantly affect inundation predictions. Incorporating wave-induced bottom stress and surface radiation stress should further improve inundation predictions.

Table 5.1. List of Experiments

Experiments	Cases	Wave induced surface Stress	Wave induced bottom Stress	Radiation Stress
1	NN	no	no	no
2	YN	yes	no	no
3	NY	no	yes	no
4	NNR	no	no	yes
5	YYR	yes	yes	yes

Table 5.2. Difference of flooding areas (total) among experiments

Experiments	Cases	Flooding areas (km^2)	Difference flooding areas (%)
1	NN	58.76	
2	YN	56.47	18.58
3	NY	61.03	4.65
4	NNR	61.48	14.21
5	YYR	61.91	28.98

Table 5.3. Difference of flooding areas (Regional) among experiments

	North Region		East Region		Southwest Region	
	Flooding areas (km^2)	Diff flooding areas (%)	Flooding areas (km^2)	Diff flooding areas (%)	Flooding areas (km^2)	Diff flooding areas (%)
NN	1.65		19.53		37.58	
YN	0.54	68.26	15.21	22.20	40.72	14.51
NY	2.07	25.65	20.12	5.40	38.84	3.34
NNR	5.04	214.34	20.24	9.99	36.20	7.62
YYR	5.57	237.39	14.40	38.29	41.94	14.99

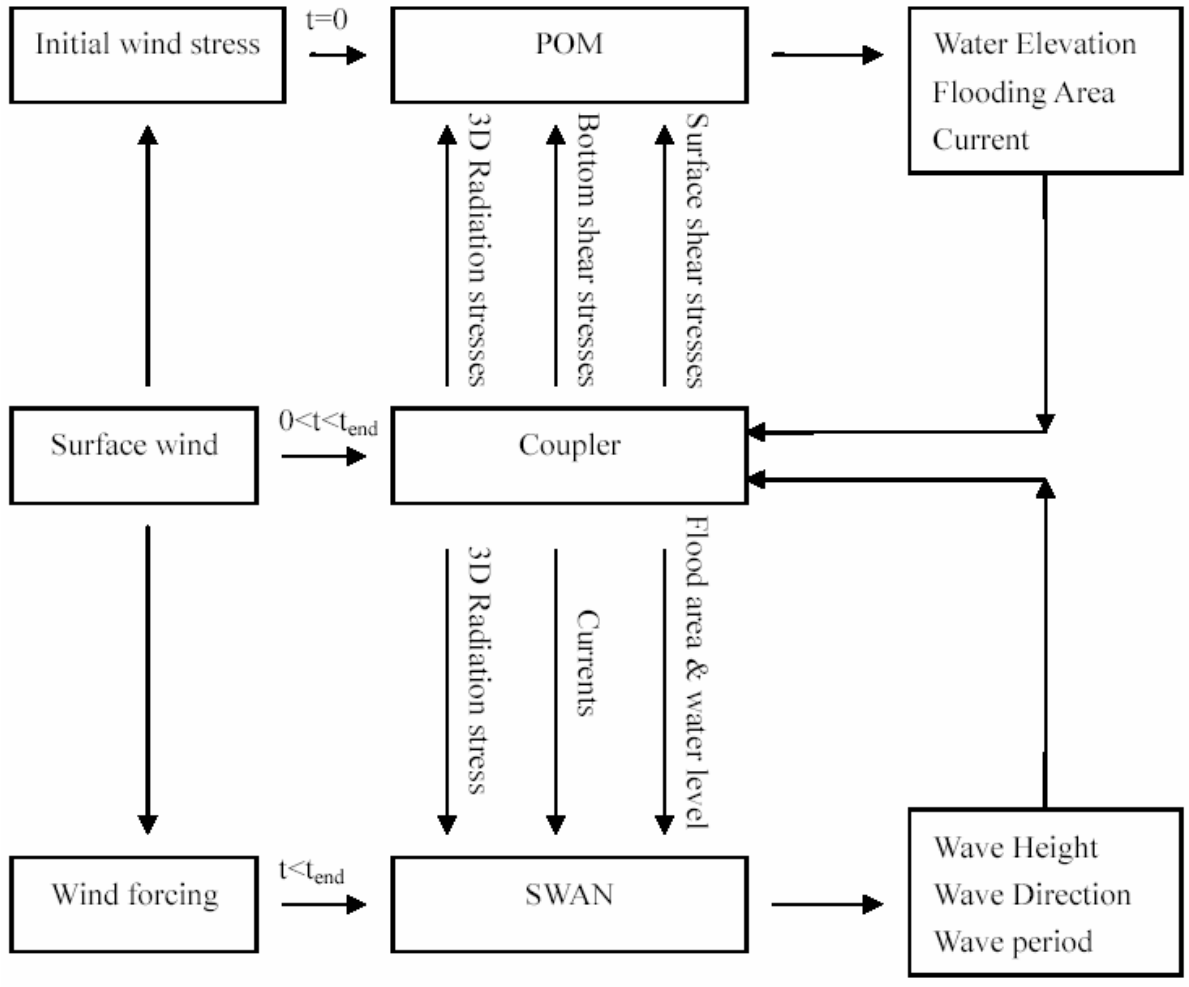

Figure 5.1 Flow diagram illustrating the coupling process between the wave and current model.

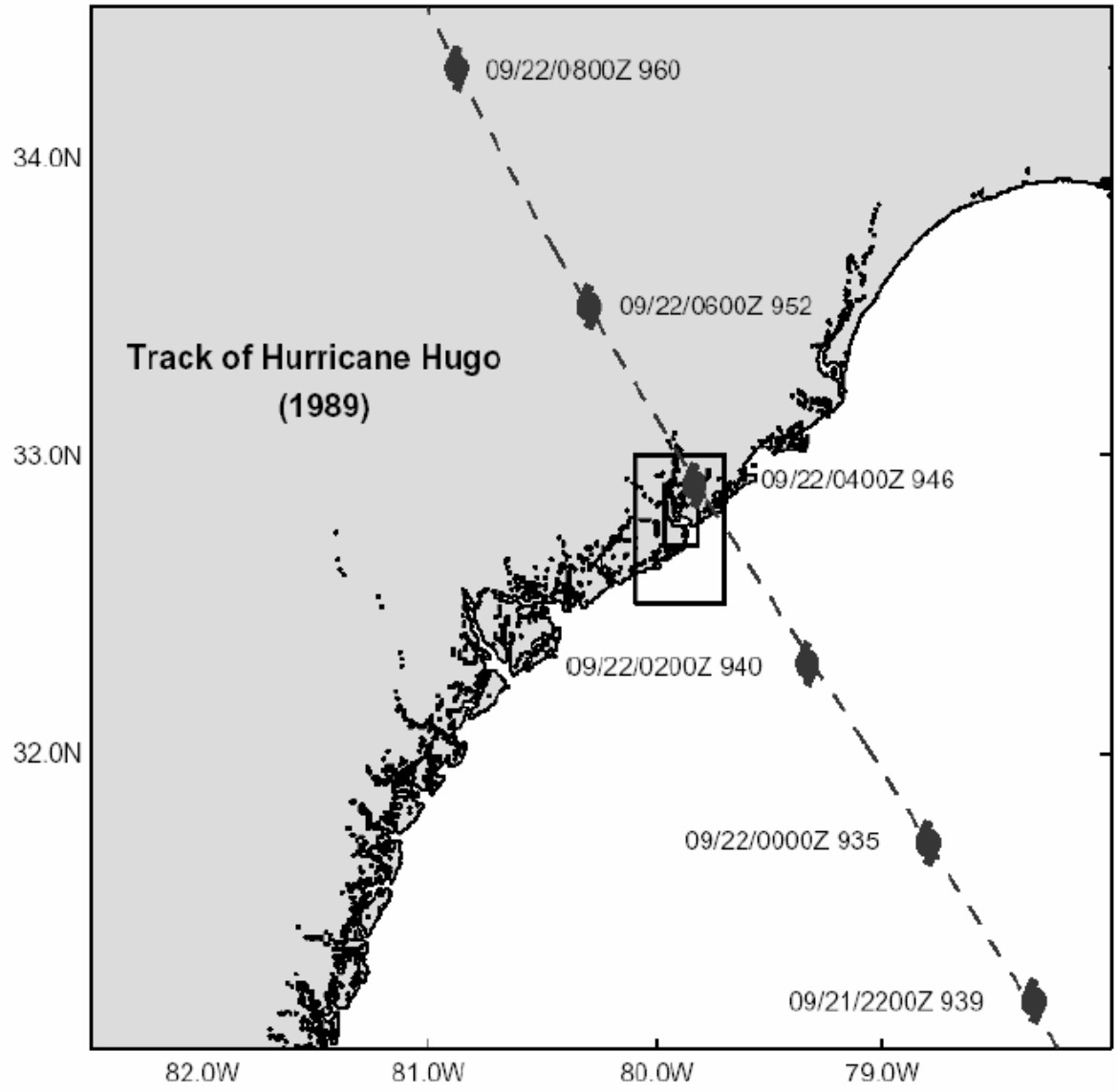

Figure 5.2 The setup of nesting domain and the best track of hurricane Hugo.

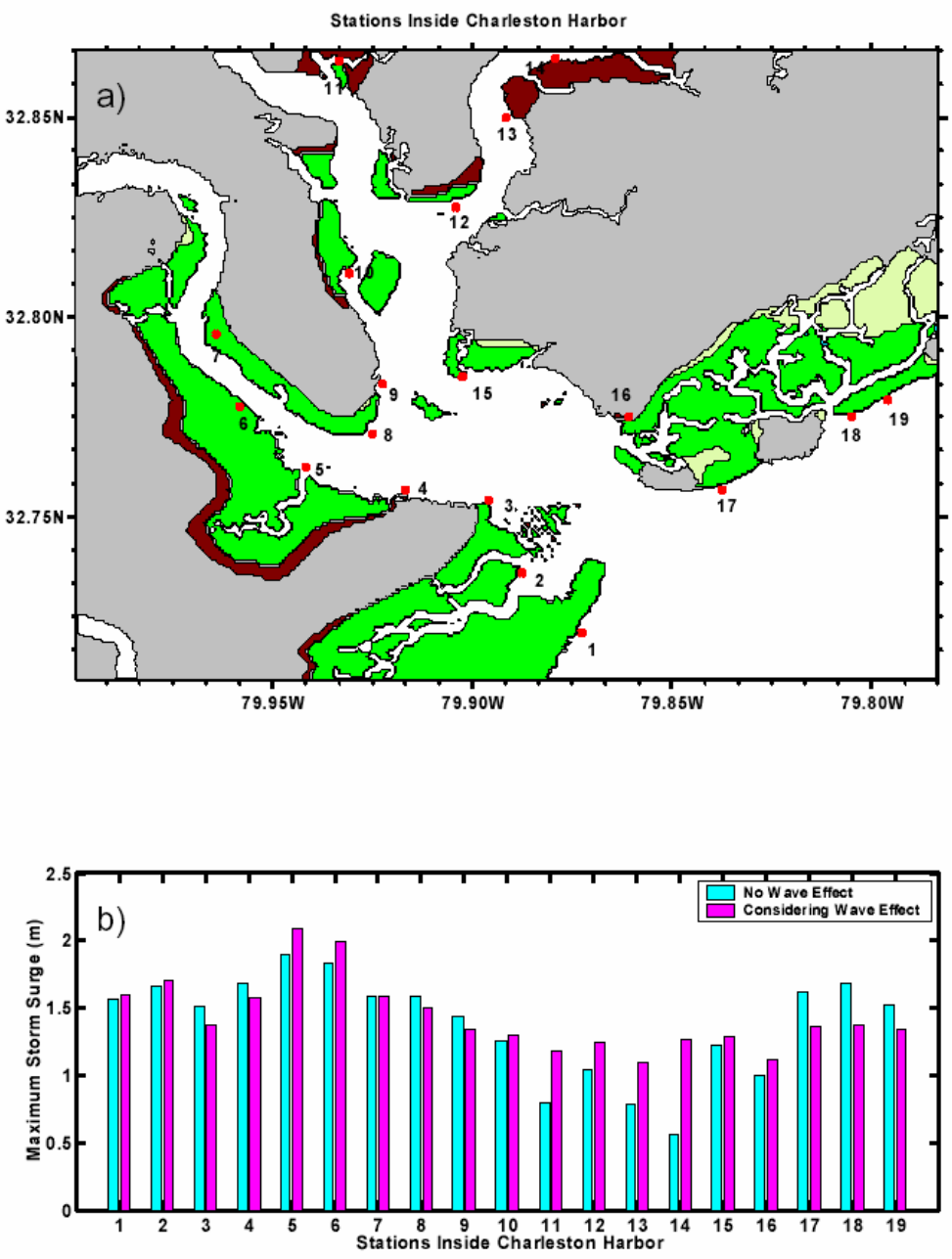

Figure 5.3 a) Locations in the study area where data are used to plot the peak surges in panel b). b) Peak storm surges at the locations shown in a) for Case NN (green), YYR (red) and observational water level (asterisk).

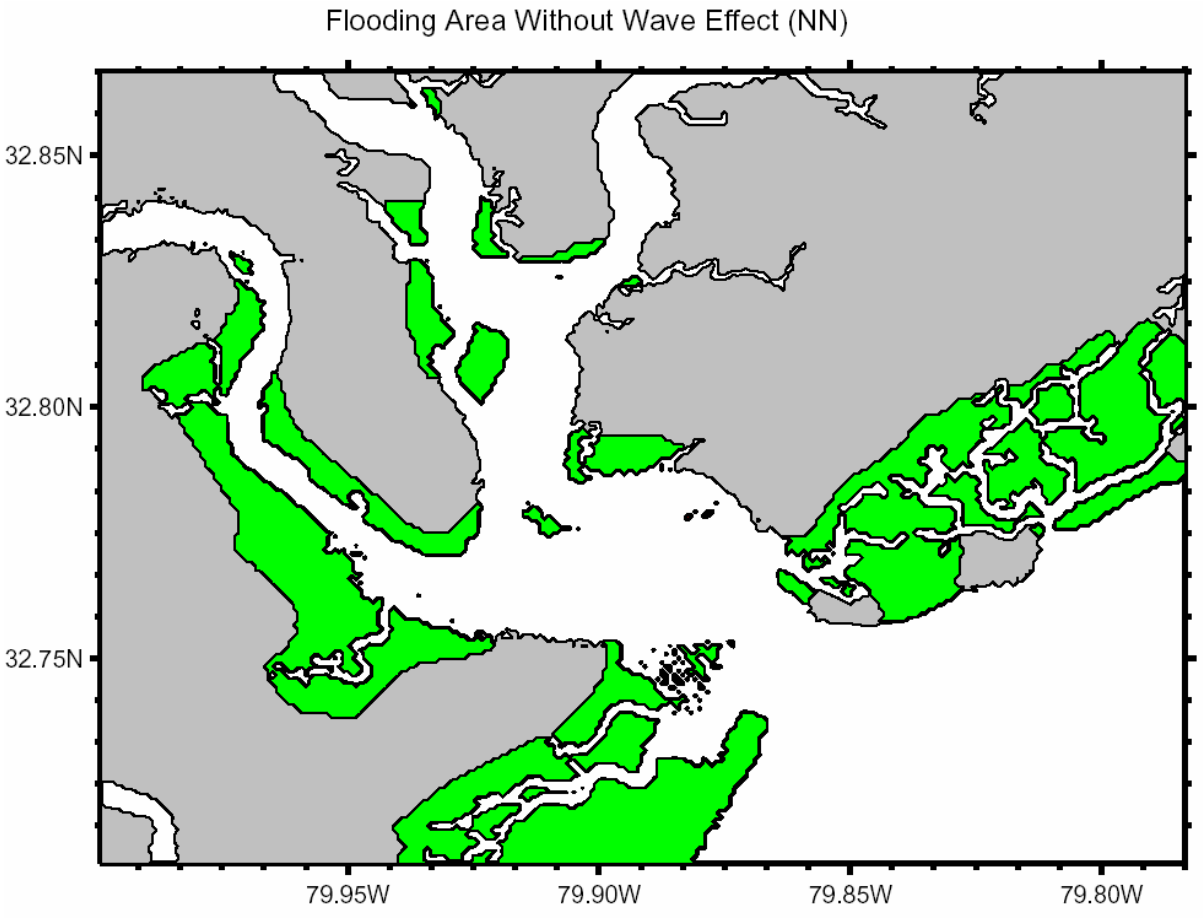

Figure 5.4 Simulated accumulated flooding areas in Case NN. The green color represents the flooding areas.

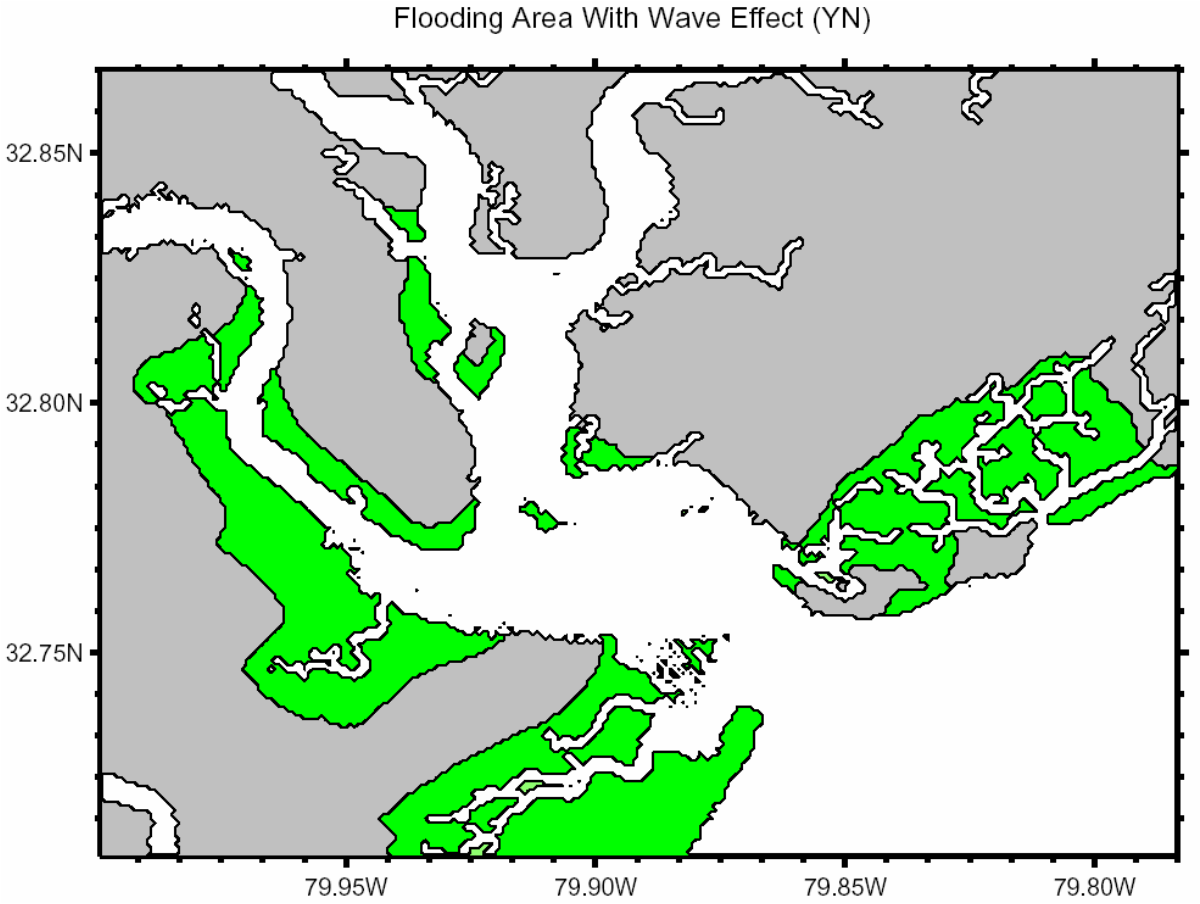

Figure 5.5 a) Simulated accumulated flooding areas in Case YN.

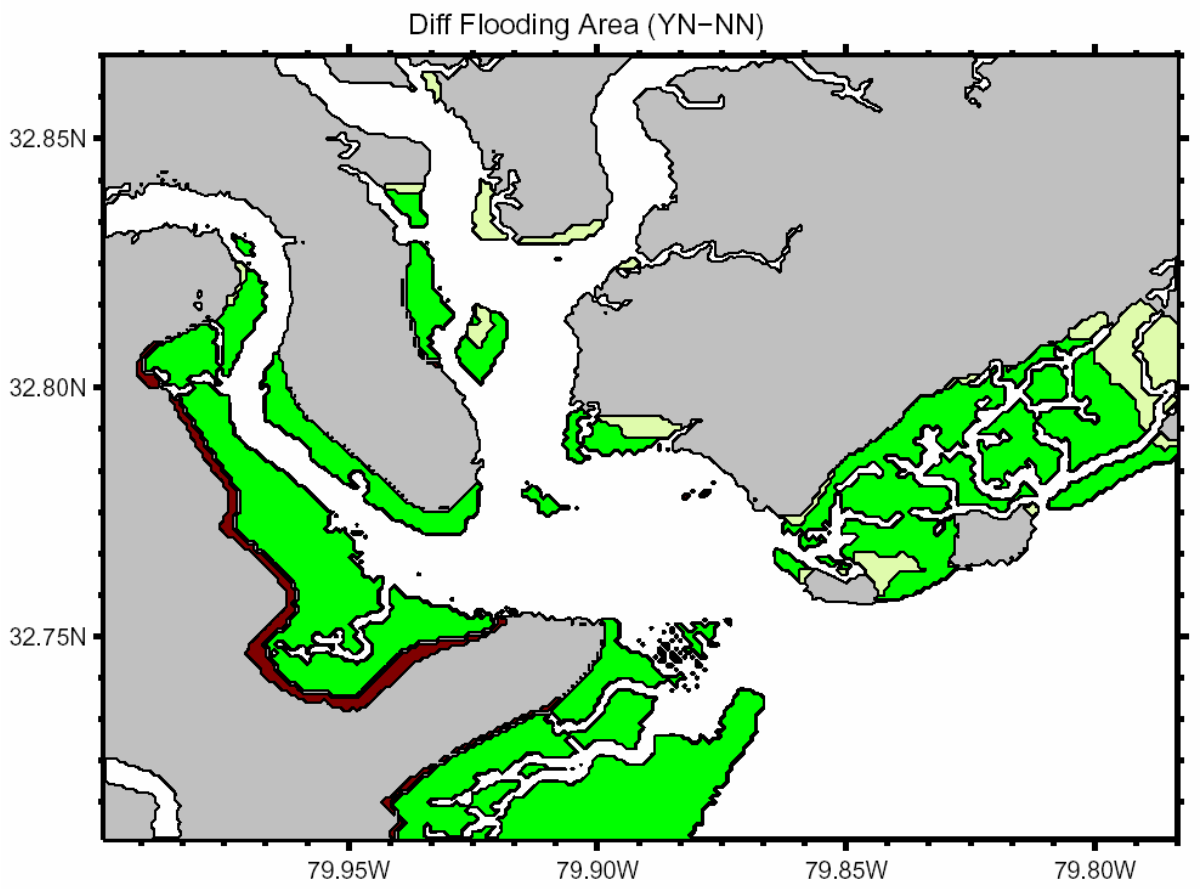

Figure 5.5 b) The difference of flooding areas between Case YN and Case NN computed as the sum of the absolute values of the differences between the land-water mask functions in Case YN and Case NN. The dark red color represents increased flooding areas and the light green color represents reduced flooding areas.

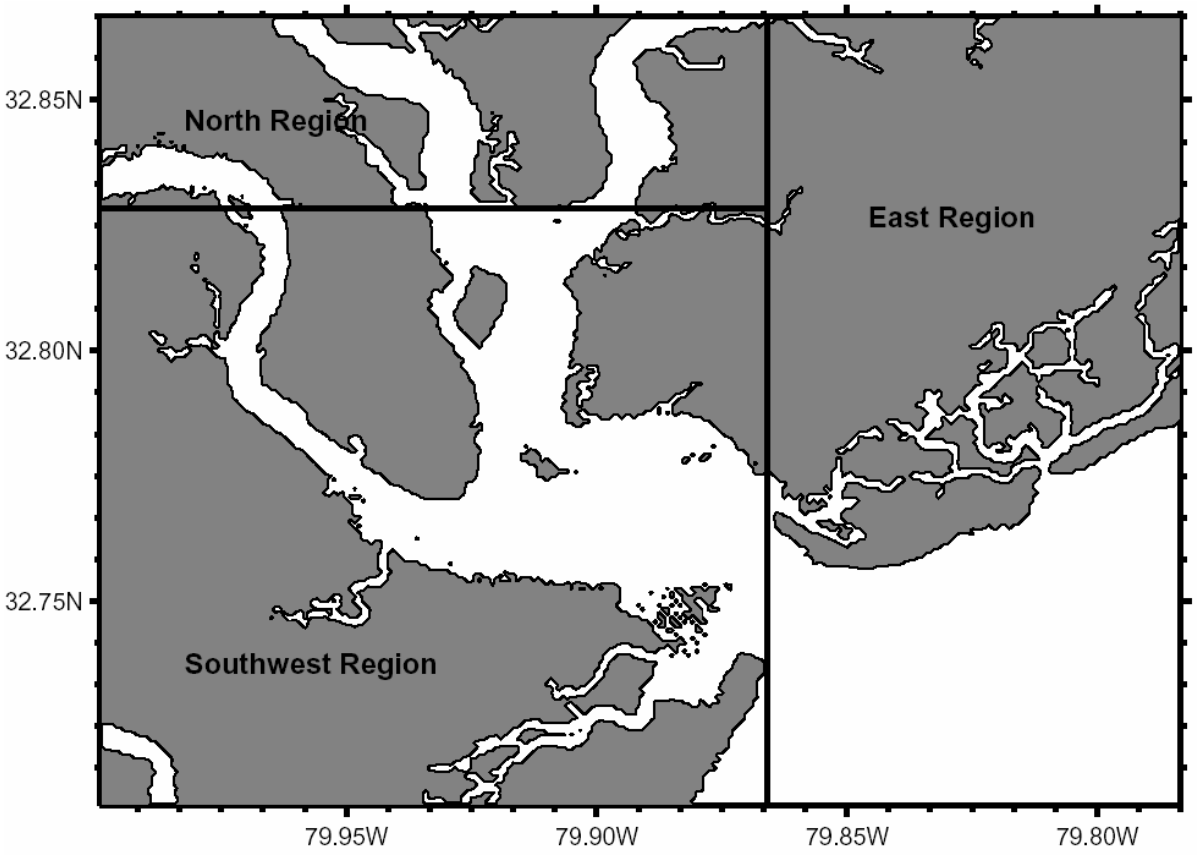

Figure 5.6 The definition of North, East and Southwest regions.

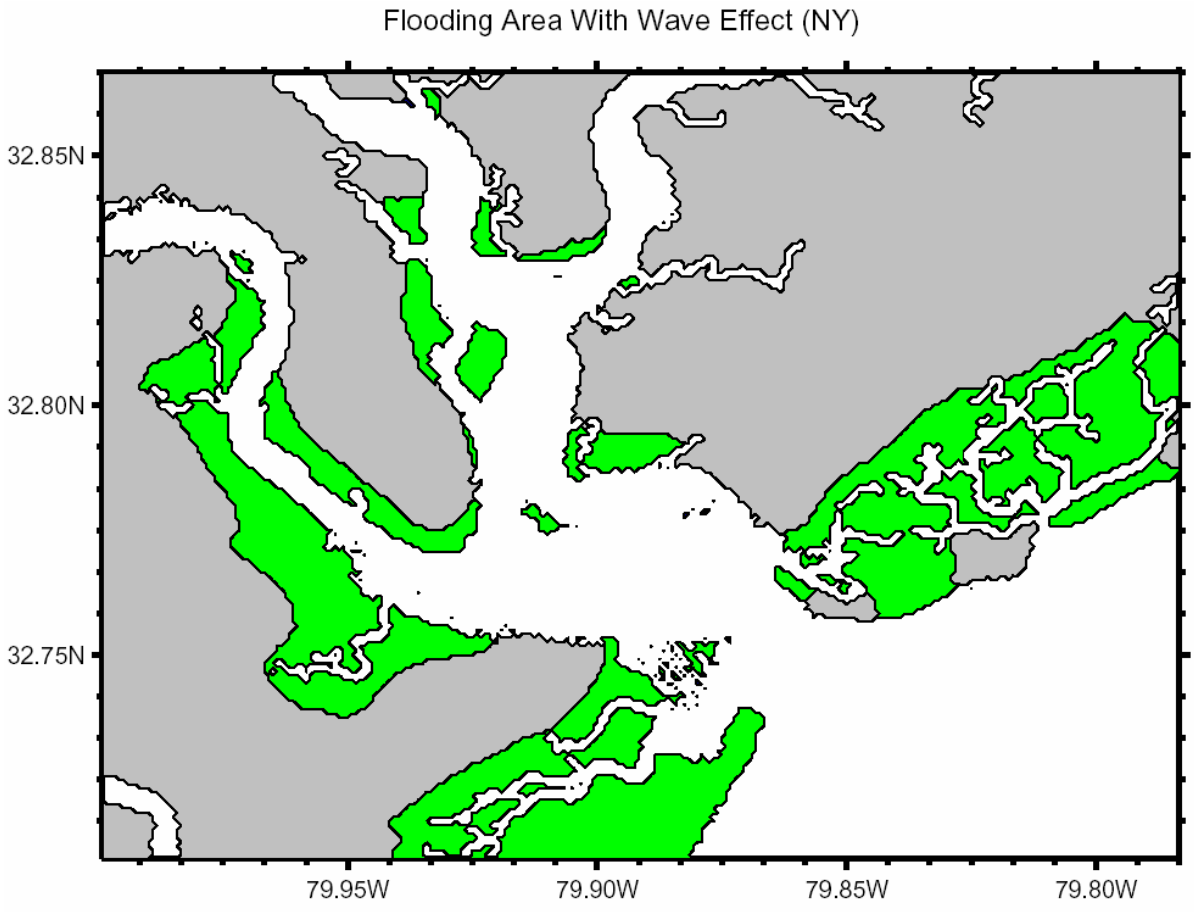

Figure 5.7 a) Same as Figure 5a, but for case NY.

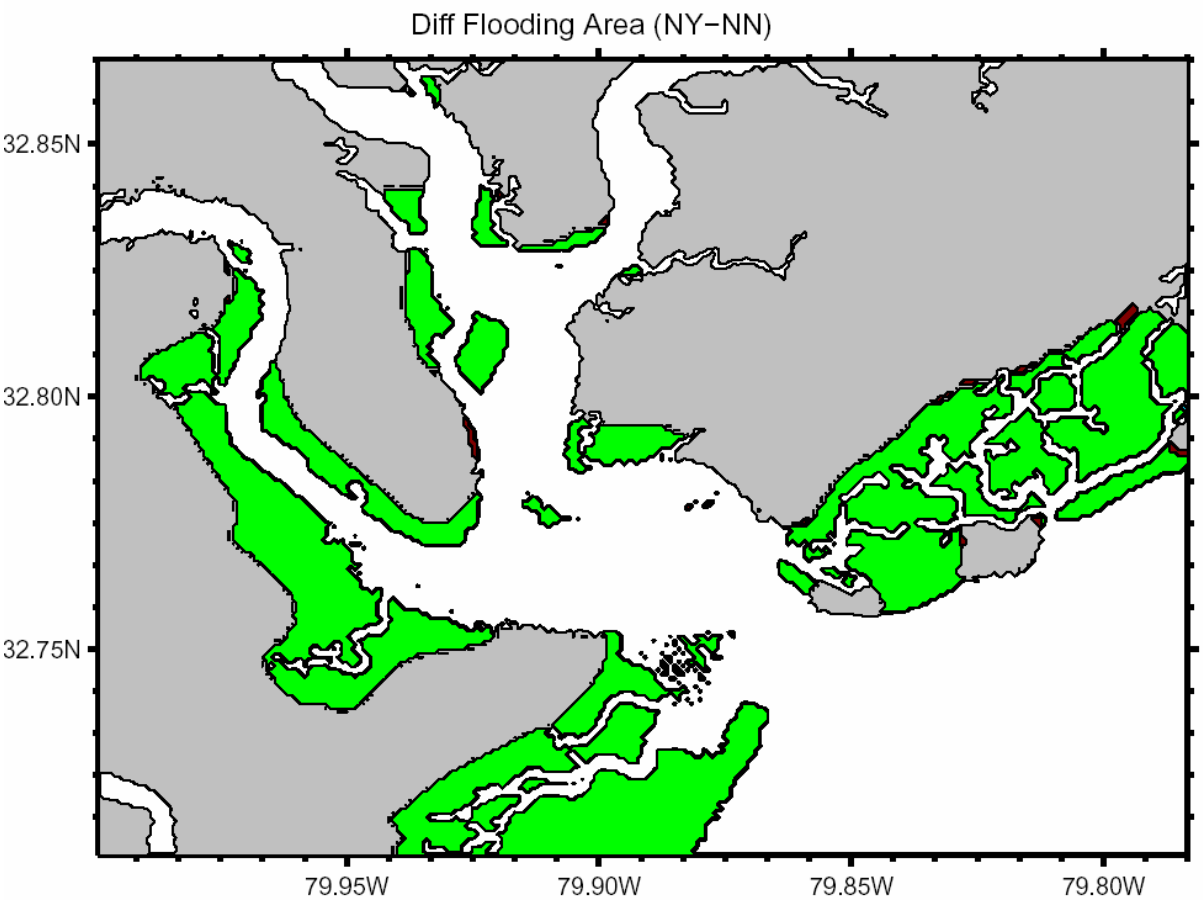

Figure 5.7 b) Same as Figure 5b, but for case NY.

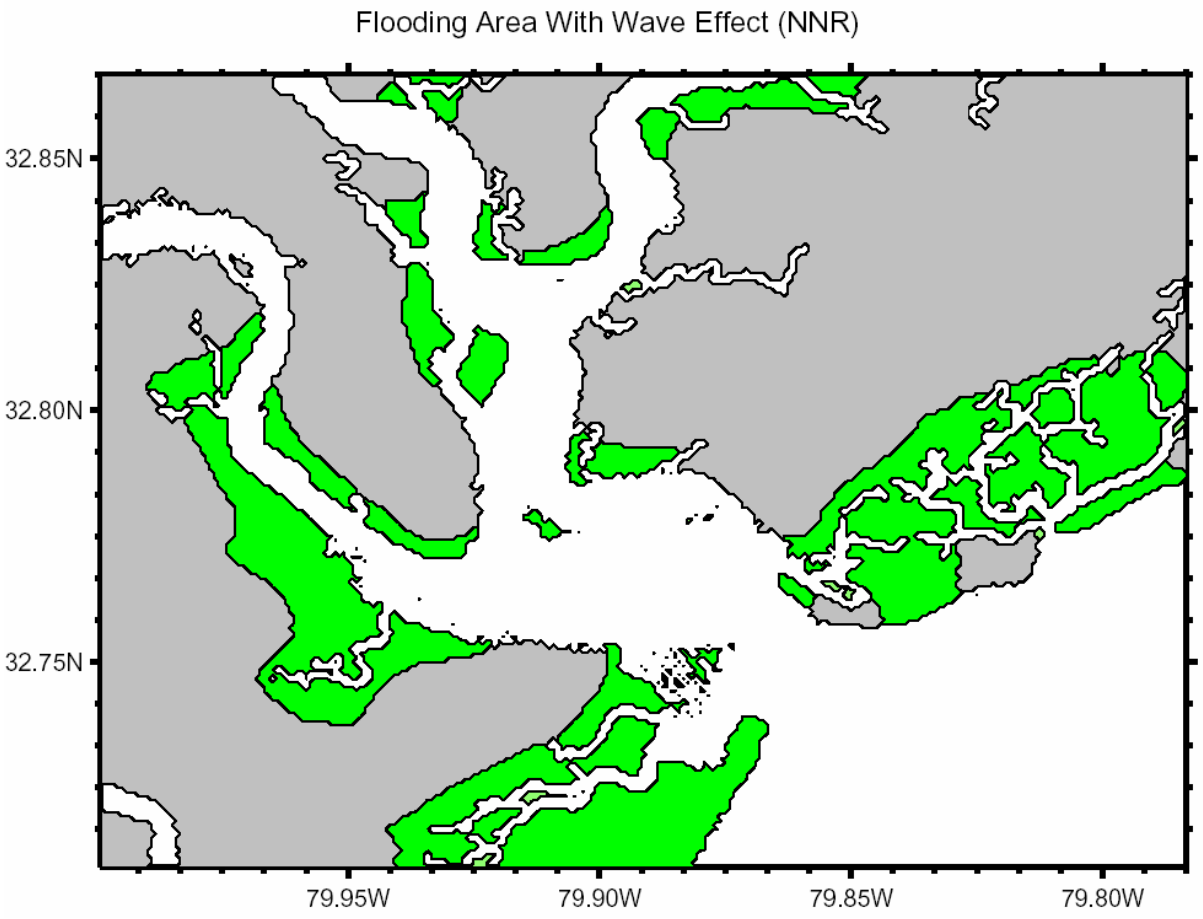

Figure 5.8 a) Same as Figure 5a, but for case NNR.

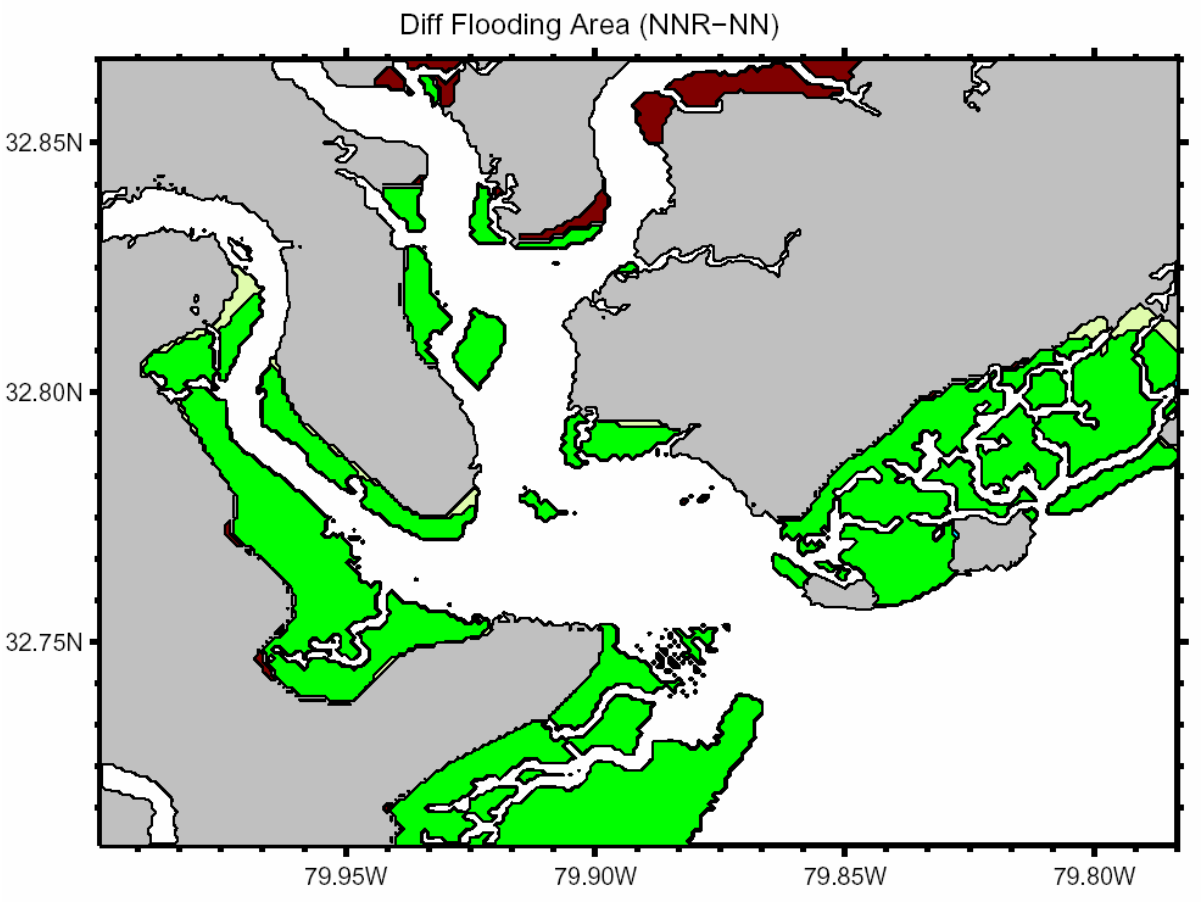

Figure 5.8 b) Same as Figure 5b, but for case NNR.

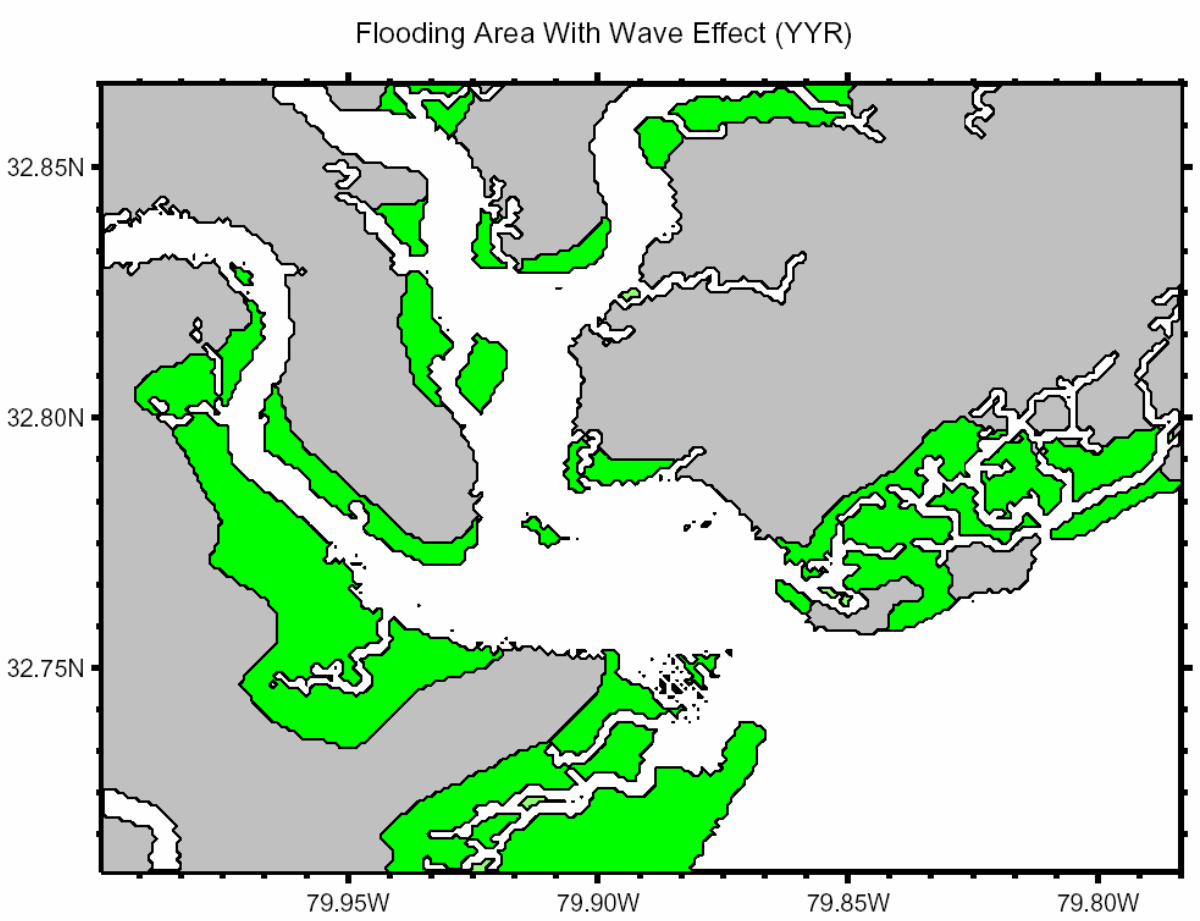

Figure 5.9 a) Same as Figure 5a, but for case YYR.

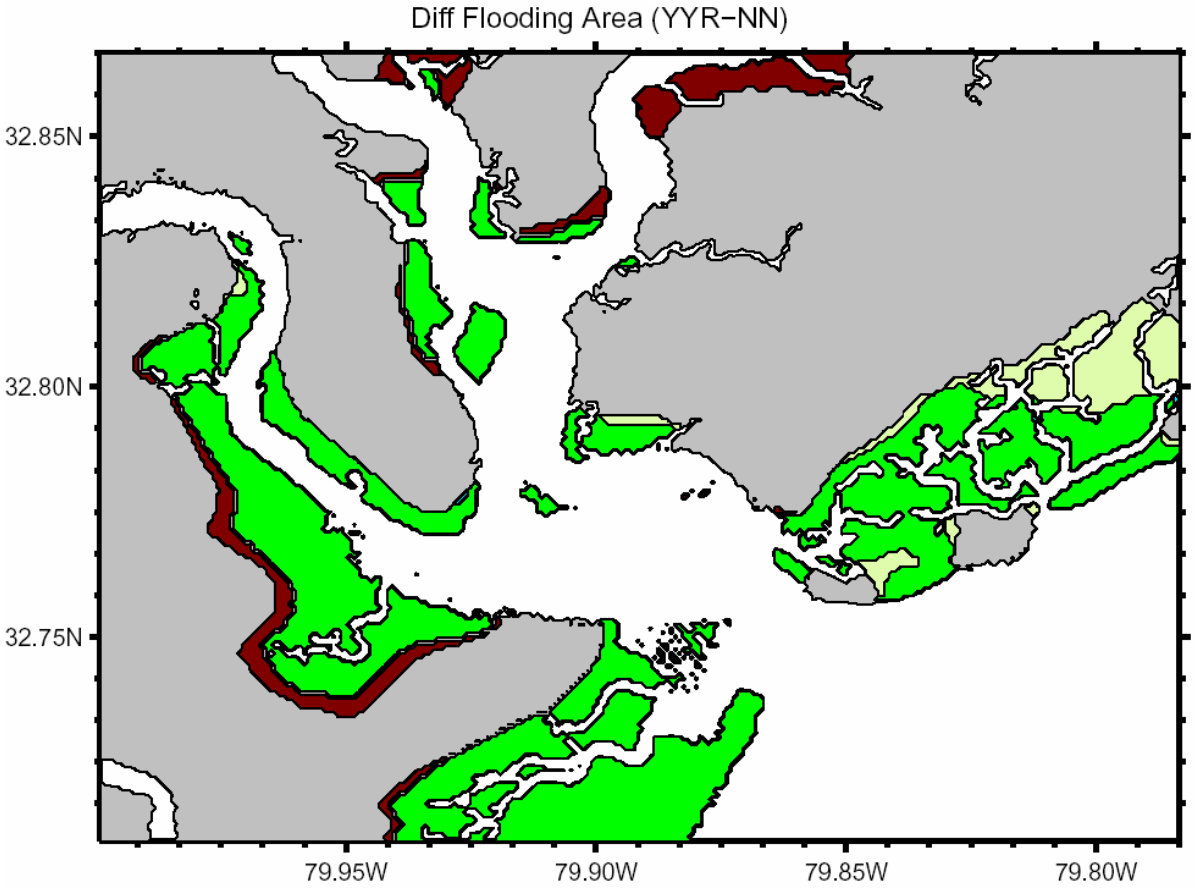

Figure 5.9 b) Same as Figure 5b, but for case YYR.

References

Booij, N., R.C. Ris and L.H. Holthuijsen, 1999, A third-generation wave model for coastal regions, Part I, Model description and validation, *J. Geoph. Res.*, 104, C4, 7649-7666.

Davies, A. M., and J. Lawrence, Modeling the effect of wave-current interaction on the three-dimensional wind-driven circulation of the Eastern Irish Sea, *J. Phys. Oceanogr., 25*, 29–45, 1995.

Donelan, W. A., F. W. Dobson, and S. D. Smith, On the dependence of sea surface roughness on wave development, *J. Phys. Oceanogr., 23*, 2143–2149, 1993.

Hedges, T.S., and H. Mase, Modified Hunt's Equation Incorporating Wave Setup. *J. Waterway, Port, Coastal and Ocean Engineering, 130*, 109-113, 2004.

Holland, G. J., An analytic model of the wind and pressure profiles in hurricanes, *Mon. Weather Rev., 108*, 1212–1218, 1980.

Holman, R.A. and Sallenger, JR.A.H., Setup and swash on a natural beach, 90, *J. Geoph. Res.*, No. C1, 945-943, 1985.

Holman, R.A., Extreme Value statistics for wave run-up on a natural beach. *Coastal Eng., 9*, 527-544, 1986.

Huang, N. E., On surface drift currents in the ocean, *J. Fluid Mech.*, 91, 191– 208, 1979.

Komen, G. J., L. Cavaleri, M. Donelan, K. Hasselmann, S. Hasselmann, and P. A. E. M. Janssen, Dynamics and Modelling of Ocean Waves, 532 pp., Cambridge Univ. Press, New York, 1994.

Lin, R. Q., and N. E. Huang, The Goddard coastal wave model, 1, Numerical method., *J. Phys. Oceanogr., 26*, 833– 847, 1996.

Longuet-Higgins, M. S., and R. W. Stewart, Radiation stress and mass transport in gravity waves, with application to ‘‘surf-beats’’, *J. Fluid Mech., 10*, 529– 549, 1962.

Mastenbroek, C., G. Burgers, and P. A. E. M. Janssen, The dynamical coupling of a wave model and a storm surge model through the atmospheric boundary layer, *J. Phys. Oceanogr., 23*, 1856– 1866, 1993.

Mellor, G. L., The three-dimensional current and surface wave equations, *J. Phys. Oceanogr., 33*, 1978–1989, 2003.

Mellor, G. L., Users Guide for a Three Dimensional, Primitive Equation Numerical Ocean Mode, 39 pp., Princeton Univ. Press, Princeton, NJ,1996.

Moon, I.J, Imapct of a coupled ocean wave-tide-circulation system on coastal modeling,

Ocean Modeling, 8, 203-236, 2005.

Moon, I.J., T. Hara, and I. Ginis, Effects of surface waves on air-sea momtum exchange. Part I: Effect of mature and growing seas, *J. Atmos. Sci., 61*, 2321-2333, 2004a.

Moon, I.J., I. Ginis, and T. Hara, Effects of surface waves on air-sea momtum exchange. Part II: Behavior of drag coefficient under tropical cyclones, *J. Atmos. Sci., 61*, 2321-2333, 2004b.

Peng, M., L. Xie, and L.J. Pietrafesa, A numerical study of storm surge and inundation in the Croatan-Albemarle-Pamlico estuary system, *Estuarine, Coastal and Shelf Science*, *59*, 121-137, 2004.

Signell, R. P., et al., Effect of wave-current interaction on wind-driven circulation in narrow shallow embayments, *J. Geophys. Res., 95*, 9671– 9678, 1990.

Tolman, H.L, Effects of tides and storm surges on North Sea wind waves, *J. Phys. Oceanogr., 21*, 766-781, 1991.

Tolman, H.L, The influence of unsteady, depths and currents of tides on wind-wave propagation in shelf seas, *J. Phys. Oceanogr., 21*, 782-789, 1990.

WAMDI Group, A third-generation model for wind waves on slowing varying, unsteady and inhomogeneous depths and currents, J. Phys. Oceanogr., 21, 782– 797, 1988.

Xia, H., Z. Xia, and L. Zhu, Vertical variation in radiation stress and wave-induced current, *Coastal Eng., 51*, 309-321, 2004.

Xie, L., K. Wu, L.J. Pietrafesa, and C. Zhang, A numerical study of wave-current interaction through surface and bottom stresses: Wind-driven circulation in the South Atlantic Bight under uniform winds, *J. Geophys. Res., 106*, 16,841– 16,855, 2001.

Xie, L., L. J. Pietrafesa, and M. Peng, Incorporation of a mass-conserving inundation scheme into a three dimensional storm surge model, *J. Coastal Res.*, *20*, 1209-1223, 2004.

Xie, L., L.J. Pietrafesa, and K. Wu, A numerical study of wave-current interaction through surface and bottom stresses: Coastal ocean response to Hurricane Fran of 1996, *J. Geophys. Res., 108*, NO. C2, 3049, doi:10.1029/2001JC001078, 2003.

Zhang, M. Y., and Y.S., Li, The synchronous coupling of a third-generation wave model and a two-dimensional storm surge model, *Ocean Eng. 6*, 533-543.

CHAPTER 6. FINAL REMARKS

6.1 Parameterization of Drag Coefficient and Roughness

Drag coefficient (Cd) and surface roughness (z0) are important parameters for qualifying air-sea momentum and energy exchanges. Present, most ocean and atmospheric models just use a simple bulk parameterization to estimate Cd or z0. As mentioned in above section, surface waves play a significant role in determining the z0 (or Cd) [Donelan et al., 1993; Moon et al., 2004]. However, Jones and Toba [2001] suggested that the influence of surface waves on the z0 is still far from conclusive after reviewing previous studies. Especially at extreme wind conditions, Cd will level off as wind speeds increase above hurricane force according the measurement of Powell et al. [2003]. It is necessary to set up a new set parameterization of z0 (or Cd) into the coupling system by considering surface waves effect in order to be consistent with the observational data at high wind speeds.

6.2 The effect of wave-current on waves (e.g. the effect of storm surge on waves)

So far, the most work in this study focuses on analyzing the influence of wave-current effect on current models (e.g. circulation, storm surge and inundation). However, wave-current interaction effect is two-way and it has impact on waves as well. In order to make the study (the analysis of wave-current interaction) complete, the effect of wave-current on

waves should be included in this study (e.g. effect storm surge on waves). Hence, some experiments will be designed to examine the effect of wave-current on waves. The major part of wave-current interaction on waves is governed by storm surge and current induced changes in wave height, wave direction and some other wave statistic parameters. This part of study aims to assess the importance of the storm surge and currents on waves driven by tropical storms in coastal areas.

6.3 Turbulence Closure

Surface water temperature (SST) is an essential factor to be considered in air–sea coupling systems. SST is an important energy source for the tropical cyclone (TC). Emanuel [1986] suggested that the TC maximum potential intensity is primarily determined by underlying SST. Therefore, it is important to consider variation of water temperature and salinity in the coupling system. The equations for momentum, temperature and salinity contain the vertical turbulent exchange coefficients that are determined by a turbulence closure scheme (M-Y). However, traditional M-Y closure model (e.g. POM) does not consider the effect of breaking waves. Therefore it is important for simulating reasonable SST to introduce the impact of breaking waves into M-Y turbulence closure scheme in the coupling system.

6.4 Coupling With Atmospheric model

As mentioned above section, SST is an important factor for predicting TC intensity. At the same time TC has a significant effect on SST forecasting. Actually, there is an important positive and negative feedback mechanism that exists in the TC-ocean system. As the tropical cyclone intensifies, the evaporation rate increases due to the larger wind speeds, leading to an increase in the latent energy supply that drives the circulation of the tropical cyclone. This represents a positive feedback process. Strong turbulent mixing also develops in the upper ocean in response to the increasing wind stress. This causes a decrease in the SST due to entrainment of the cooler waters from the thermocline into the mixed layer representing a negative feedback mechanism. Therefore, the last proposed work is to setup a fully air-ocean-wave coupling system.

References

Donelan, W. A., F. W. Dobson, and S. D. Smith, On the dependence of sea surface roughness on wave development, *J. Phys. Oceanogr., 23*, 2143–2149, 1993.

Emanuel, K. A., An air–sea interaction theory for tropical cyclones. Part I: Steady-state maintenance. *J. Atmos. Sci.,* 43**,** 585-604, 1986.

Jones, I.S.F. and Y. Toba, Wind stress over the ocean, Cambridge University Press, 307 pp, 2001.

Moon, I.J., I. Ginis and T. Hara, Effect of surface waves on charnock coefficient under tropical cyclones, *Geophys. Res. Lett.,* 31, doi:10.1029/2004GL020988, 2004.

Powell, M., P. J. Vickery and T. A. Reinhold, Reduced drag coefficient for high wind speeds in tropical cyclones, *Nature*, 422, 279-283, 2003.